INVESTIGATION OF THE FEASIBILITY OF THE ELECTRON BEAM-EXCITED, HIGH-PRESSURE RECOMBINATION LASER

TEXAS UNIVERSITY

PREPARED FOR
OFFICE OF NAVAL RESEARCH

21 MARCH 1974

AD-778033

Security Classification

DOCUMENT CONTROL DATA - R & D

(Security classification of title, body of abstract and indexing annotation must be entered when the overall report is classified)

1. ORIGINATING ACTIVITY *(Corporate author)*
The University of Texas at Dallas
P. O. Box 688
Richardson, Texas 75080

2a. REPORT SECURITY CLASSIFICATION
UNCLASSIFIED

2b. GROUP

3. REPORT TITLE
INVESTIGATION OF THE FEASIBILITY OF THE ELECTRON BEAM-EXCITED, HIGH-PRESSURE RECOMBINATION LASER

4. DESCRIPTIVE NOTES *(Type of report and inclusive dates)*
Fourth Semi-Annual Technical Report (period covered by this report 9/1/73-2/28/74)

5. AUTHOR(S) *(First name, middle initial, last name)*
Carl B. Collins
Austin J. Cunningham

6. REPORT DATE	7a. TOTAL NO. OF PAGES	7b. NO. OF REFS
21, March 1974	118	16

8a. CONTRACT OR GRANT NO.	9a. ORIGINATOR'S REPORT NUMBER(S)
N00014-67-A-0310-0007	
b. PROJECT NO. ARPA Order No. 1807	UTDP A002-4
c. Program Code 2E90	9b. OTHER REPORT NO(S) *(Any other numbers that may be assigned this report)*
d.	

10. DISTRIBUTION STATEMENT
Distribution of this document is unlimited

11. SUPPLEMENTARY NOTES	12. SPONSORING MILITARY ACTIVITY
	Office of Naval Research

13. ABSTRACT

This report describes research applied toward the determination of the feasibility of developing a recombining, electron beam-excited plasma into a pulsed laser of exceptionally high peak power.

DD FORM 1 NOV 65 1473

Security Classification

14. KEY WORDS	LINK A		LINK B		LINK C	
	ROLE	WT	ROLE	WT	ROLE	WT
Recombination Laser						
Laser						

Fourth Semi-Annual Technical Report

Item A002

Period Ending 1, March, 1974

Short Title: RECOMBINATION LASER

ARPA Order Number 1807

Program Code Number 2E90

Contract Number N00014-67-A0310-0007

Principal Investigator: C. B. Collins
The University of Texas at Dallas
P. O. Box 688
Richardson, Texas 75080
(214) 690-2885

Contractor: The Board of Regents of
The University of Texas System

Scientific Officer: Director
Physics Programs
Physical Sciences Division
Office of Naval Research
Department of the Navy
800 N. Quincy Street
Arlington, Virginia 22217

Effective Date of Contract : 21 March 1972

Expiration Date of Contract: 31 December 1973

Amount of Contract :	$ 99,990.00
Amount of Modification #1 :	91,400.00
Amount of Modification #2 :	100,000.00
Total Amount :	$291,390.00

Sponsored by

Advanced Research Projects Agency

ARPA Order No. 1807

Form Approved Budget Bureau No. 22-R0293

CONTENTS

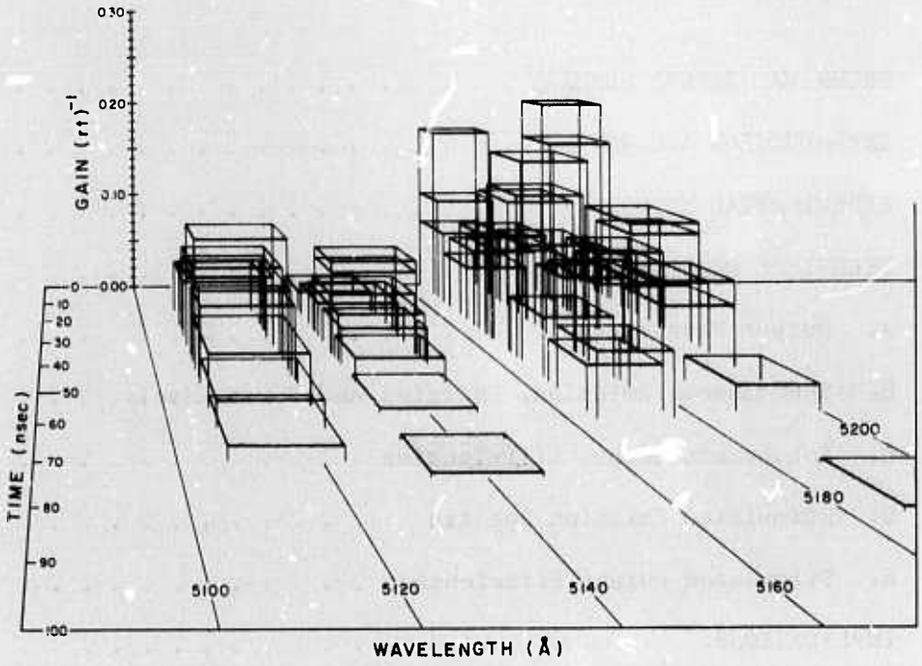

Figure 1

Time resolved stimulated emission spectrum for the 5100 - 5200 Å wavelength region of the afterglow of a 3 atmosphere helium plasma. Data is plotted in units of fractional gain per round trip transit as directly measured from the amplification or attenuation of a dye laser beam reflected through the afterglow. Time resolution was a uniform 10 nanoseconds and shaded data planes appearing anomalously long result from the overlap of contiguous measurements. The observed gain maximum corresponds to the peak of the P-branch of the $3p^1\Pi_g \rightarrow 2s^1\Sigma_u^+$ transition of He_2.

I. TECHNICAL REPORT SUMMARY

The objective of the research described in this report is to determine the feasibility of developing a recombining electron beam-excited plasma into a pulsed laser of exceptionally high peak power. Currently accepted theory supported by the results of this contract research to date indicates this should be possible. Stimulated emission in 3 atmospheres of helium was first reported[1,2] at 6400 Å and research during the most recent contract period has provided a more detailed spectrum of this band and extended these results to a second band at 5170 Å. As seen in the facing figure, gains of the order of 0.03 cm^{-1} have been found in the new band by directly measuring the time-resolved amplification of a tunable dye laser beam used to probe the plasma. Power extractions of the order of a megawatt/liter have been accomplished with no evidence of saturation of the medium, and indications are encouraging for the prospect of similar activity in related bands of He_2 at 4400 and 4000 Å. These results confirm the importance of the collisionally-stabilized recombination mechanism as a source of population inversion of significance to the development of new types of high energy lasers depending upon electron beam excitation at high gas densities.

Although a wide variety of recombination processes are known to occur in gaseous plasmas, it is this relatively complex and unfamiliar collisionally-stabilized one which appears to hold outstanding promise as a lasing medium. As discussed in Section II, this process is optimized at high charge densities and relatively low energies but is almost completely quenched in atomic and molecular systems which can participate in dissociative recombination. Theory predicts that, in helium at charge densities of the order of $10^{16} cm^{-3}$, collisionally-stabilized recombination should produce large inverted populations of the resulting neutrals which would tend to radiate in the 2.0μ to 0.3μ wavelength region, provided the temperature of the electron swarm is kept low. It is this requirement which suggests that, unlike conventional visible and UV lasers

excited by electron beams in hydrogen and nitrogen, the lasing action from recombination would be optimized in the afterglow period following the termination of the beam. There is a considerable advantage in this from the viewpoint of fundamental collision cross-sections. In the conventional, directly-excited visible and UV systems, over 95% of the beam energy is lost to the production of ionization not contributing to the laser output. In contrast and as detailed in Section II, theory has predicted that the subsequent collisionally-stabilized recombination of the ions with electrons could provide a mechanism for recovering some of this ionization energy with a resulting order of magnitude increase in the optical output. In this respect, the present system resembles the excimer lasers such as the xenon laser in that high total efficiencies are expected. Unlike those systems, the recombination step is collisionally stabilized thereby introducing an additional dependence on electron temperature and density which offers the prospect of controlling the time-dependent radiative economy through these parameters.

Since both the available output energy and pulse duration depend strongly on the electron density, the high values which only become available from e-beam excitation at high neutral gas pressures are needed. In this requirement lay the basic uncertainty in the approach since previous investigations of this type of charge neutralization had centered on neutral gas densities some 200 times less than the 20 atmosphere values which theory requires for significant radiative output.

The research effort reported here and in previous technical reports[1,3,4] has focused upon this recombination approach, and the intent of the initial considerations had been to first provide additional tests of theory in helium at intermediate pressures around three atmospheres. From there could be directly determined the amount of light output, the lifetime of the recombination process, and whether or not population inversions were developed.

During previous reporting periods, an electron beam-excited helium afterglow system, operating routinely at 5 atmospheres and capable of modification to 20, was instrumented so that spectroscopic observation of transient emissions, both spontaneous and stimulated, in the visible and near IR region could be made with 10 nanosecond resolution. A tunable dye laser was incorporated into the experimental system for the direct measurement of gain through observation of the time-dependent amplification or attenuation of the dye laser beam when passed through the discharge afterglow. Construction details and system performance are presented in Section III.

Technical results reported previously and extended during the most recent reporting period, as discussed in Section IV, appear highly encouraging from the perspective of the contract objective. In particular, it was determined that:

1. In the absence of lasing, incoherent emissions of the order of 0.1 to 1.0 milli-Joules/liter per pulse occurred in the afterglow of the 3 atmospheres of helium at 6400 and 5875 Å, respectively. System efficiencies ran as high as 0.04% even without laser action. The efficiency of the recombination process relative to direct excitation of excited states by either primary or energetic secondary electrons was suggested by observation at 3 atmospheres pressure of 0.1 milli-Joule $liter^{-1}$ of spontaneous emission at 6400 Å from the former and less than 0.003 milli-Joules $liter^{-1}$ from the latter.
2. Both the detailed functional forms and effective lifetimes of the spectral transients were consistent with the theory of collisionally-stabilized recombination as applied to an electron swarm at 1000°K effective temperature. Characteristic lifetimes for the recombination source of the radiating populations of He_2 were found to range from 160 nanoseconds at 1 atmosphere of

helium to 26 nanoseconds at 7 atmospheres. The corresponding peak power radiated inccherently at 6400 Å was of the order of 1 KW/liter.

3. Optical gains were examined with two techniques: a) a qualitative survey inferring gain from measurements of time-resolved enhancement ratios of axial intensity emitted from a resonant cavity containing the afterglow and b) by direct measurement of the amplification or attenuation of a pulsed dye laser beam tuned to the wavelength of the transition and transiting the plasma. From the first technique, positive gain was indicated for all transitions examined not terminating on metastable levels. Favorable indications were obtained for bands at 6400, 5130, 4450, and 4000 Å. Use of the tunable laser afforded a resolution of both spectral and temporal behavior of the gain parameters. Detailed study of the $(3s^3\Sigma_u^+ \rightarrow 2p^2\Pi_g)$ band at 6400 Å showed gain reaching 0.23 per round trip transit for the low members of the P-branch with a time-dependence similar to that of the spontaneous emission. Somewhat smaller gain of the order of 0.15 per round trip was found at 5170 Å for the peak of the P-branch of the $3p^1\pi_g \rightarrow 2s^1\Sigma_u^+$ band of He_2.

4. The first estimates of the economy of energy extraction indicated that the energy normally lost during the recombination to non-radiative channels of stabilizations can, in fact, be returned to an induced radiative channel. Energy of the order of 30 milli-Joules/liter and power densities of 5 MW/liter were extracted from the afterglow in preliminary measurements at 6400 Å with the tunable laser without evidence of saturation of the transition. This value approaches 20% of the maximum energy available theoretically to this transition assuming one

photon per ion and reflects favorably upon the feasibility of extracting the energy of one photon from the stimulated transition for each recombination event. Lower dye laser powers prevented examination of the 5170 Å emission for stimulated emission at energies above 2 milli-Joules/liter, but to that level no evidence of saturation was observed.

Should theory continue to be validated, the feasibility of the recombination laser would, in fact, be established. In that case, the consequent advantages inherent in the use of the collisionally-stabilized recombination process would be expected to be:

1) Visible to near-UV operating wavelengths. The principal molecular Rydberg series in He_2 extends from 6400 Å to 3680 Å.
2) One output photon per ion. Most of the excitation energy in inert gases goes into ionization and overall efficiencies of 8% should be attained.
3) Lifetimes for the source of population proportional to the inverse cube of the electron density. At 20 atmospheres pressure and an electron density of the order of $10^{16} cm^{-3}$, lifetimes of the order of 1.0 nanosecond should be realized.
4) Scalable output energies. Approximately 5 Joules/liter could be expected at electron densities of $10^{16} cm^{-3}$. At electron densities of $10^{17} cm^{-3}$ which are characteristic of 200 atmospheres pressures, 50 Joules/liter would be expected in a picosecond if the same electron temperature were maintained.
5) Control of the precise temporal form of the output pulse. This can be controlled in principle by heating the recombining electrons and thus varying the rate of the population supply through its expected $T_e^{-9/2}$ dependence.

Evidently, the critical point in the course of this research has been successfully attained in that stimulated emission has been obtained in both the 6400 Å and 5170 Å bands of He_2 with the consequent extraction of significant energy from the afterglow. The task for the immediate future lies in the further confirmation of these results and their extension to other related bands of He_2. With the projected construction of 100 GW electron beam device (APEX) lasing action should be realized in one or more of the bands. Subsequent optimization would then be dependent upon further extensive research into the detailed steps and thermal economy of the recombination process

II. INTRODUCTION AND REVIEW

Theory[5,6,7,8,9] predicts the occurrence of extremely large inversions of populations in certain recombining high pressure plasmas. However, prior to the commencement of the research contracted in this project, such inversions had only been examined in low pressure helium afterglows. Indications based on those studies of collisionally-stabilized recombination were that it could, in fact, form the basis for a new type of laser of high power. In such a device, the inversion of population would be produced as a consequence of particular ion-electron recombination processes in which the excited atomic or molecular states are sequentially populated, energetically speaking, from the top down. Although theory had predicted substantial consequent pair inversion ratios for almost a decade[9], the difficulties in obtaining recombination controlled plasmas of large volume, which at the same time were free from the competing effects of dissociative recombination, generally prevented the actual observation of such inversions.

The process of collisionally stabilized recombination is a complex one occurring in two composite steps, 1) capture of an electron by an ion and 2) subsequent stabilization. For example, in helium the sequences are the following:

Capture processes	Stabilization processes	
$He^+ + 2e \rightleftarrows He^*(p) + e$	$He^*(p) + e \rightleftarrows He^*(q) + e$	$p > q$
$He^+ + He + e \rightleftarrows He^*(p) + He$	$He^*(p) + He \rightleftarrows He^*(q) + He$	$p > q$
$He^+ + e \rightarrow He^*(p) + h\nu$	$He^*(p) \rightarrow He^*(q) + h\nu$	$p > q$

where He*(p) denotes an excited helium atom with principal quantum number, p.

The net result of the initial capture sequence is the establishment of a quasi-equilibrium distribution of population among the bound states whose ionization potential is less than a few KT for the electron gas. However, the total population within such states is usually small compared to the ion density and does not represent a significant portion of the loss of ionization due to recombination. Subsequent stabilization can occur by successive collisional or radiative processes which tend to move population to states of greater ionization potential. When an element of population has been moved to a level of sufficiently high ionization potential, the rates for the inverse excitation processes are negligible, and the stabilization is complete. It is during the course of this latter sequence of steps that substantial inversions of population should be produced.

Of first importance to the evaluation of collisional radiative recombination as a process for populating inversions in a practical laser medium are its potential in terms of a) output wavelength and pulse energy, b) pulse duration, and c) efficiency. Consideration of each is reviewed in the following subsections:

a) Output wavelength and pulse energy -- an estimate for these parameters can be made by recognizing that first for a sufficiently high upper state the nearly degenerate sublevels are in thermal equilibrium at the electron temperature, and secondly that most collision-induced changes of energy level result in only a unit change in principal quantum level.[6] In other words, there is no effective mechanism by which the recombining electrons can avoid the upper state of the stimulated transition. Consequently, the least upper boundary on

the number of transitions per pulse which can be stimulated to emit is the number of recombination events occurring in the afterglow period following each ionizing pulse and plasma. Assuming competing losses of ionization can be suppressed, one photon could be obtained for each electron originally produced. Optimization of the energy available would occur by selecting a transition in a Rydberg series of the atom or molecule with principal quantum number as large as possible without elevating the energy into the "quasi-equilibrium group" of levels mentioned above. In principal, this means a photon of energy a few KT less than the greatest ionization energy found in the class of states having transitions to states with very short radiative lifetimes. Examples are found in Figures 2 and 3 which shows excited state energies for He and He_2, respectively. In the former the most suitable series would be the $n^3F \rightarrow 3^3D$ commencing at 1.87μ and converging at ~8190 Å. In the latter species, He_2, the more favorable series, $np^1\Pi_g \rightarrow 2s^1\Sigma_u$, ranging from 5130Å to 3130Å and $ns^3\Sigma_u^+ \rightarrow 2p^3\Pi_g$ ranging from 6400Å to the convergence limit at 3680Å could be attempted. In these cases, Table I summarizes the consequent peak pulsed energy available in a recombining helium afterglow of 10^{16} electron-ion pairs/cm^3.

Figure 2

Energy level diagram of He. Energies of the excited states have been plotted relative to the ground state which is off-scale to the bottom. Wavelengths of the principal transitions have been indicated.

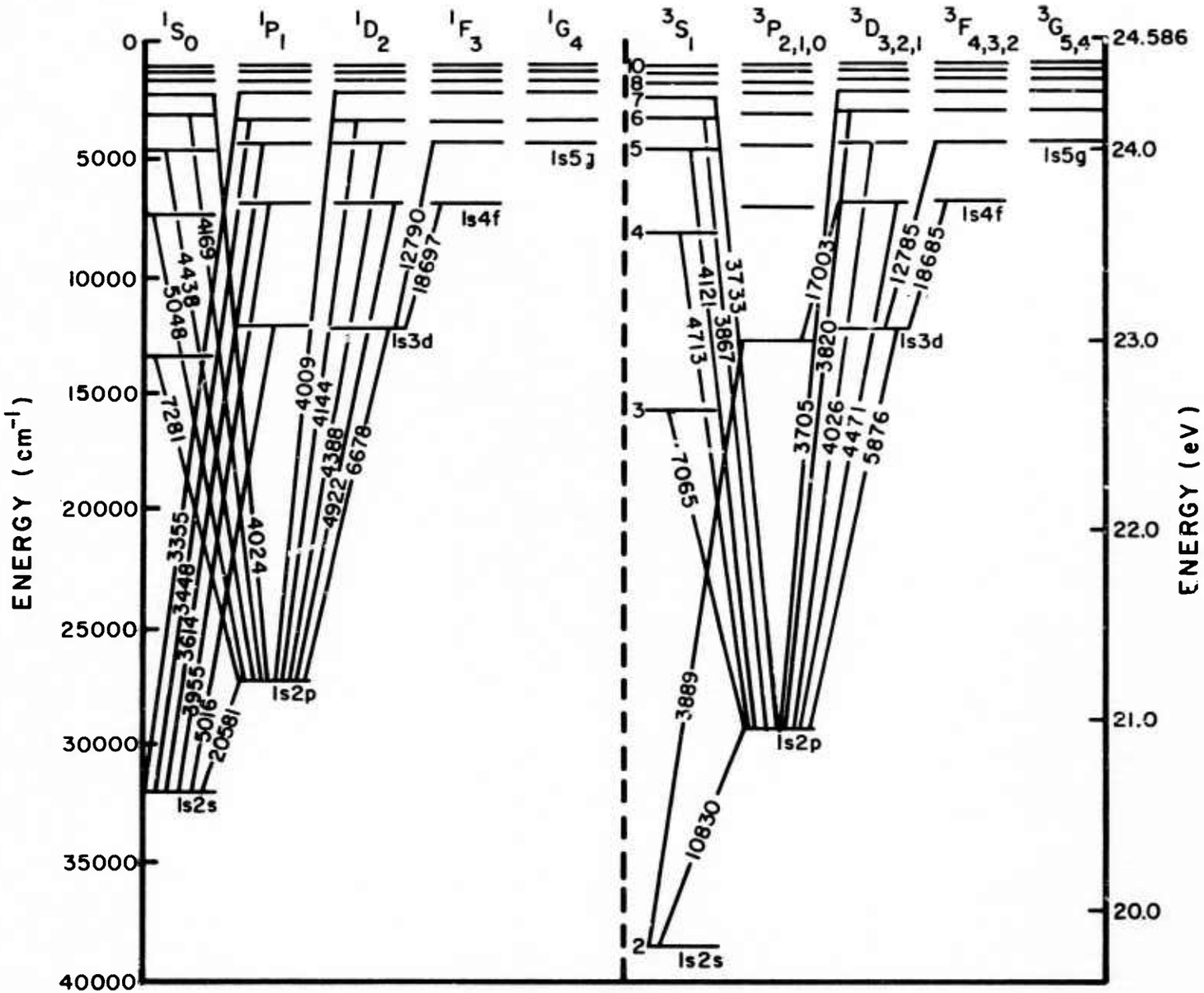

ENERGY LEVELS OF He

Figure 3

Energy level diagram of He_2. Values of energy characteristic of the equilibrium internuclear separation have been plotted relative to the lowest metastable $2s^3\Sigma_u^+$ state. The ground state is $1s\sigma^2 2s\sigma^2$ and strongly repulsive at these internuclear separations. Wavelengths of the band origins of principal transitions have been indicated.

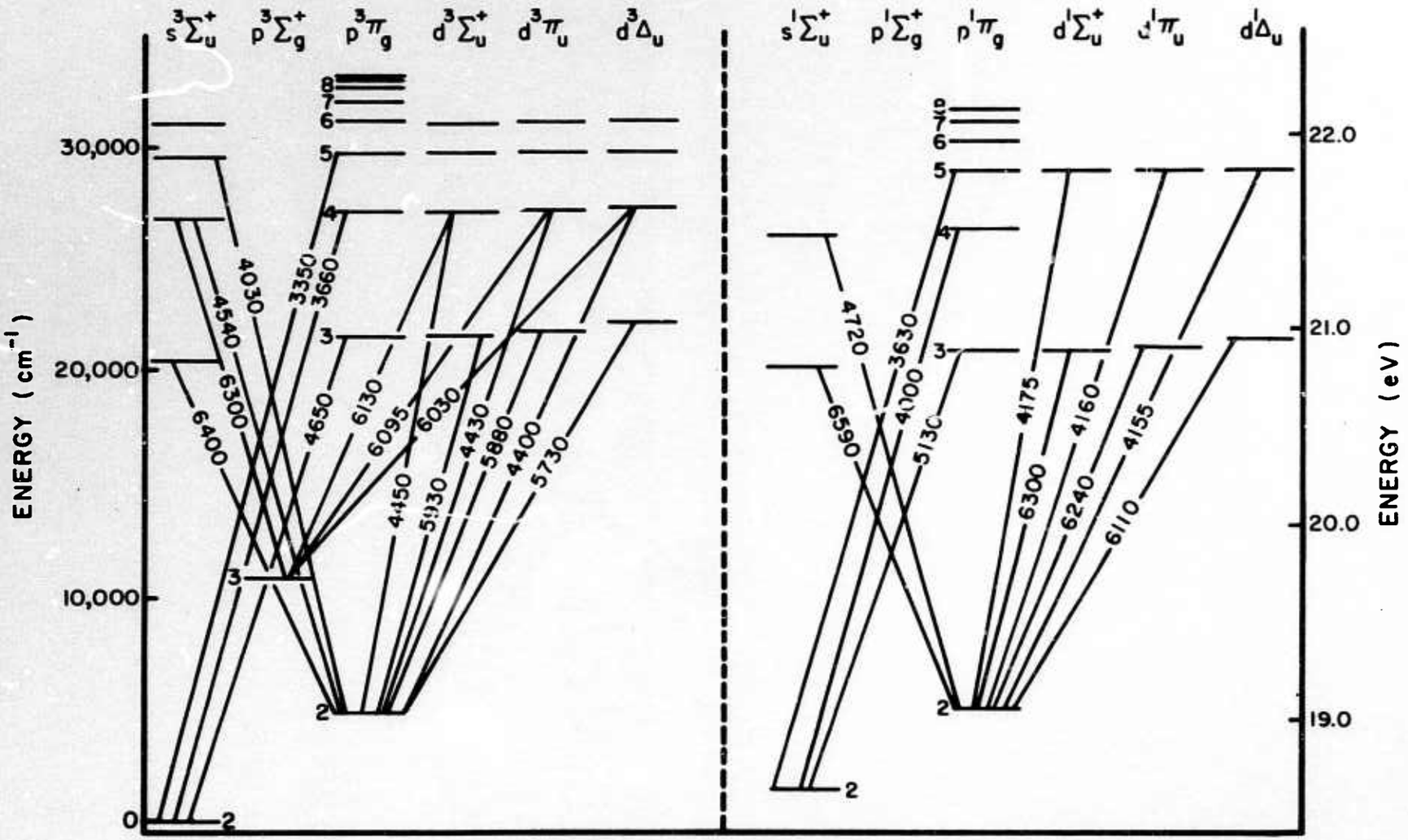

ENERGY LEVELS OF He_2

Table I

Peak Pulsed Energies Available in Listed Transitions

Wavelength	Species	State	Quantum Efficiency	Energy (Joule/liter)
18700Å	He	$4^3F \rightarrow 3^3D$	2.7%	1.1
8190Å	He	$\lim n^3F \rightarrow 3^3D$	6.2%	2.4
6400Å	He_2	$3s^3\Sigma_u^+ \rightarrow 2p^3\Pi_g$	8.6%	3.1
5130Å	He_2	$3p^1\Pi_g \rightarrow 2s^1\Sigma_u$	10.8%	3.8
3680Å	He_2	$\lim ns^3\Sigma_u^+ \rightarrow 2p^3\Pi_g$	15.0%	5.4
3130Å	He_2	$\lim np^1\Pi_g \rightarrow 2s^1\Sigma_u^+$	17.7%	6.3

b) Pulse duration -- The pulse duration is more difficult to estimate from theory. In the first approximation, the entire energy available to the lasing transition can be assumed to be emitted in a time comparable to the inverse of the recombination rate. Initially, problems resulted from the paucity of measurements of this rate for collisionally-stabilized recombination. For theoretical reasons, the effective two-body recombination rate coefficient, defined for the ion X^+ by

$$\frac{\partial}{\partial t}[X^+] = -\alpha[X^+][e] \quad , \qquad (1)$$

was expected[6,10] to have the form

$$\alpha = K_e[e]\,(T_e/300)^{-9/2} + K_N[X]\,(T_e/300)^a \qquad (2)$$

where [e] and [X] denote the concentrations of free electrons and neutral atoms respectively, T_e, the electron temperature, and a is a coefficient which is still undetermined at the present time.

Values in the literature[10,11,12] had been somewhat scattered and entirely confined to values of electron and neutral particle densities several orders of magnitude below those now obtainable with beam-excited discharges. In the absence of more appropriate values, the best estimates for He^+ from the literature had seemed to be

$$\alpha \simeq 7 \times 10^{-20}[e](T_e/300)^{-9/2} + 10^{-27}[He] \quad , \qquad (3)$$

and for He_2^+

$$\alpha \simeq 1.5 \times 10^{-20}[e](T_e/300)^{-9/2} + 1.5 \times 10^{-27}[He] \quad . \qquad (4)$$

However, there was some evidence[13] that a more generalized model was necessary and best characterized by

$$\alpha = K[e]^{\eta}(T_e/300)^{-9/2} \qquad (5)$$

where η is a function of pressure and $0 \leq \eta \leq 1$. At 44.6 Torr prior measurements over the range, 10^{10} to 10^{12} cm^{-3}, of electron densities for He_2^+ indicated a value of

$$\alpha \simeq 2.8 \times 10^{-11}[e]^{0.185} \qquad (6)$$

where [e] is again the electron density in units of cm^{-3}.

In either case, an equivalent exponential lifetime against recombination, τ, could be defined to be

$$\tau^{-1} \equiv \frac{1}{[X^+]} \frac{\partial}{\partial t} [X^+] = -\alpha[e] \quad . \qquad (7)$$

The resulting expected lifetimes are summarized in Table II.

Table II

Lifetimes Against Recombination

Species	[e] (cm^{-3})	T_e (°K)	τ (sec)
He^+	10^{16}	300	0.14×10^{-12}
		3000	0.44×10^{-8}
He_2^+	10^{16}	300	1.0×10^{-12}
		3000	3.0×10^{-8}

Superficially, it appears that any lifetime, hence pulse duration could be attained provided 1) the ionization could be produced in a time short compared to the output pulse and 2) the electron temperature could be adjusted to a sufficiently low value in the same time. Unfortunately, the electron temperature is not a free parameter, but had been predicted[14,15] to be controlled by the feedback of energy to the electron gas during the stabilizing collisions between excited states and the free electrons. Current theory[14] had originally indicated that a value in the range 1500°-1800°K would be appropriate for the 10^{16} cm^{-3} electrons in helium at STP. Nevertheless, it must be recognized that such an estimate had been based upon extrapolation of parameters over so many orders of magnitude from measured values as to render the nine-halves power of the result to be of questionable value.

These questions were largely resolved[3,4,16] during the first contract year of this project through the measurement and parametric representation of the functional dependence on time of the intensity of the spontaneous emission. The relevant model for that radiation is obtained by starting from the more general expression for the collisional recombination rate coefficient, equation (5), substituting it into the continuity equation for ion density, neglecting diffusion at these pressures, as well as competing reactions, assuming $[He_2^+] = [e]$, and a

constant $T_e \sim 300°$; then

$$[He_2^+ (t)]^{-(1+\eta)} - [He_2^+ (0)]^{-1+\eta} = (1+\eta)Kt \quad . \qquad (8)$$

Now it is expected[12] that the rate of spontaneous photon emission in any particular band during the course of the stabilization of the recombination should approximately equal some constant fraction, f, of the recombination rate of the ions which, allowing for geometric collection factors and sensitivities, implies that

$$I(t) = C\,K\,[He_2^+ (t)]^{2+\eta} \quad , \qquad (9)$$

where C represents all collected scale factors. Substituting (9) into (8) gives:

$$\frac{I(t)^{-\frac{1+\eta}{2+\eta}} - I(0)^{-\frac{1+\eta}{2+\eta}}}{t} = K(1+\eta)(CK)^{-\frac{1+\eta}{2+\eta}} \quad . \qquad (10)$$

This implies that a plot of intensity to the $-(1+\eta)/(2+\eta)$ power would be a linear function of time and that the slope, S, of such a curve would be simply the right-hand side of (10). Defining then

$$S = K(1+\eta)(CK)^{-\frac{1+\eta}{2+\eta}} \qquad (11)$$

enables the effective lifetime of the collisional recombination defined by equation (7) to be written in terms of experimentally measured parameters as

$$\tau_0^{-1} = \alpha[He_2^+(0)] = S(1+\eta)^{-1} I_0^{\frac{1+\eta}{2+\eta}} \quad . \qquad (12)$$

Examination of this equation in comparison with (11) shows τ_0^{-1} to be independent of the scaling of the intensity as would be expected.

These results suggested the procedure of plotting the inverse intensity to the $(1+\eta)/(2+\eta)$ power for various trial values of η between 0 and 1, determining the best straight line slope, if any, and then obtaining the recombination lifetime from (12). This was accomplished experimentally in an extensive series of measurements recently reported[1,4,16] and briefly reviewed below for convenience.

In practice, these measurements were greatly facilitated in both speed and accuracy by interfacing a Biomation 8100 transient recorder to the on-line date acquisition computer serving the University's Atomic Physics group. A digital image of each decay curve of spontaneous intensity could be stored and the required inverse intensity to the various fractional powers plotted. The resulting data is typified by that of the principal spectral features of He_2 at 6400 Å for an afterglow at 3 atmospheres pressure in the HPAC-1b system, as shown in Figure 4 together with the resulting computer analyses and plots.

Lifetimes of the molecular features showed reasonable agreement over the range of pressures examined and suggested the validity of the assumption summarized in equation (9) that the emitted intensity is a constant fraction of the energy released by the recombining He_2^+ ions.

The converse behavior was found for the recombination portion of the decay of the atomic lines examined. Lifetimes deduced did not agree with the recombination rates for the molecular bands or even with each other. The most extreme divergence was shown by the $3^3D \rightarrow 2^3P$ transition at 5875 Å which is reproduced in Figure5 .

The lifetime is anamolously long as can be seen upon inspection, and consists of two slopes as shown in the corresponding analyses which present the inverse intensities for various η. Other atomic lines did not show the two lifetime behavior but did show scattered lifetimes.

Figure 4

Data plots showing the time evolution and its analyses of the 6400 Å emission in the afterglow from single discharges of the e-beam at 3 atmospheres pressure in the HPAC-1b system. Shown counter-clockwise from the upper left,

a) Photograph of the refreshed oscilloscope trace of the analog reconstruction of the stored transient.
b) Plot of the digital image of the stored transient.
c) Plot of the inverse intensity to the M-power as a function of decay time for $\eta=0$, neutrally stabilized recombination.
d) Plot of the inverse intensity to the M-power as a function of decay time for $\eta=1$, electronically stabilized recombination.

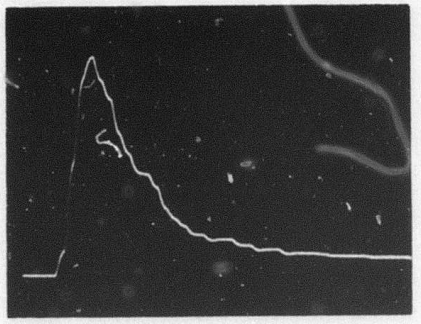

Scale: 40 nanoseconds per horizontal division
0.05 Volts per vertical division

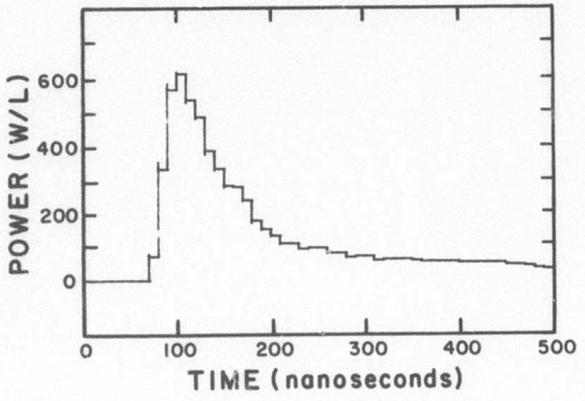

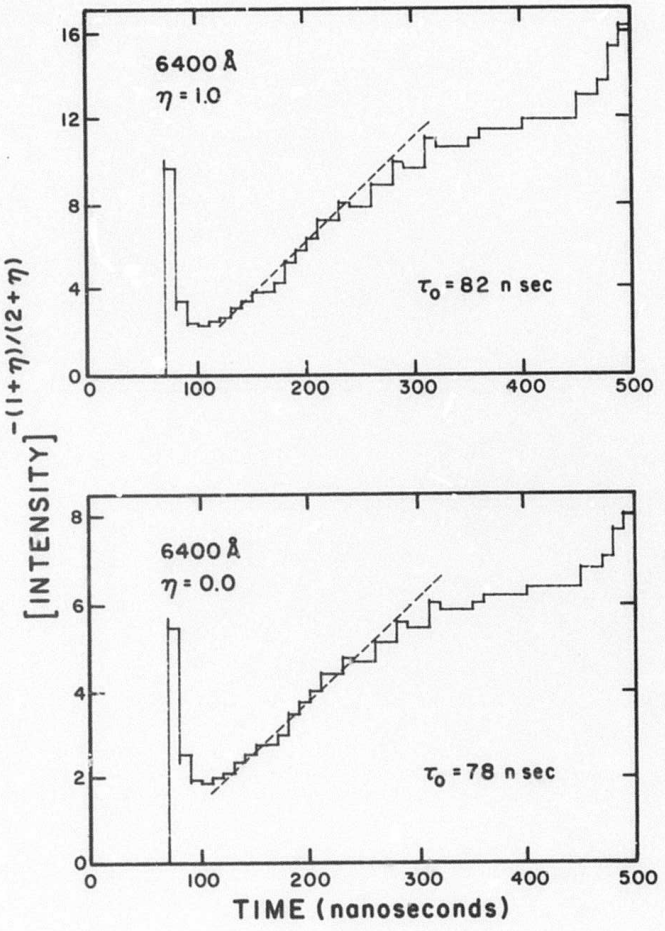

Figures 5

Data plots showing the time evolution and its analyses of the 5875 Å emission in the afterglow from a single discharge of the e-beam at 3 atmospheres pressure in the HPAC-1b system. Shown counter-clockwise from the upper left,

a) Photograph of the refreshed oscilloscope trace of the analog reconstruction of the stored transient.
b) Plot of the digital image of the stored transient.
c) Plot of the inverse intensity to the M-power as a function of decay time for $\eta=0$, neutrally stabilized recombination.
d) Plot of the inverse intensity to the M-power as a function of decay time for $\eta=1$, electronically stabilized recombination.

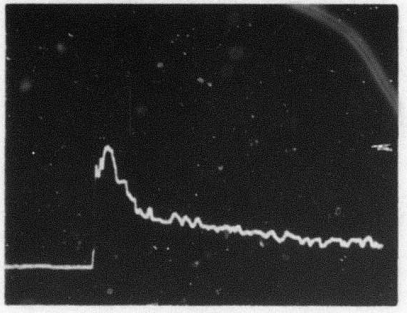

Scale: 200 nanoseconds per horizontal division
0.025 Volts per vertical division

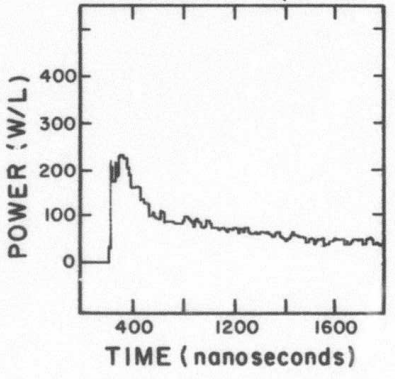

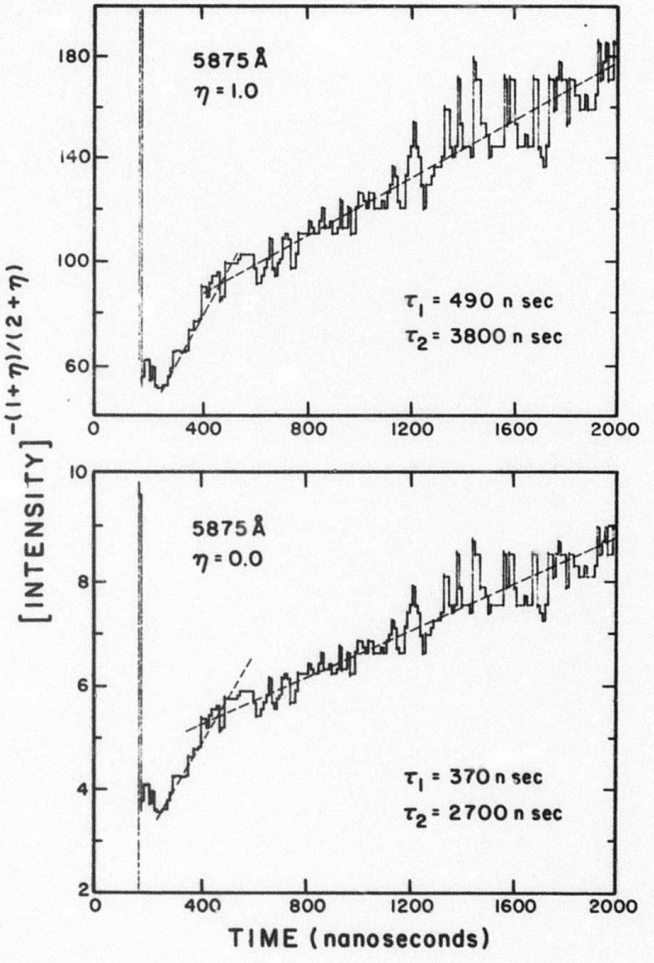

The rather extreme variation of atomic recombination lifetimes strongly indicates that, for the production of excited atoms, the assumption expressed by (9) does not hold and that the relative importance of the various stabilizing channels is a changing function of electron density and hence, time. This is in general agreement with the results of 0.1 atmosphere work which has demonstrated that the molecular bands tend to have the same time decays[13] in agreement with (9) while the atomic lines do not[12].

Results for the He_2^+ recombination lifetimes are collected in Table III and presented graphically in Figure 6.

Table III

Summary of Lifetimes of the Principal Spectral Features

Wavelength	Lifetime η=1 (nanoseconds)			
Pressure (atm)	1	3	4.2	7
He_2				
6400 Å	160	82	59	26*
4650 Å	126	82.5	53	34*
He				
7065 Å	-	267	350*	93*
6678 Å	208*	100*	45*	29*
5875 Å early	880	490	425	300*
late	2800	3800	2700	2320*

*HPAC-2 system

These results evidently agree with expression (4) for an electron temperature which is a weak function of pressure and has a value around 1000°K at 3 atmospheres.

Figure 6

Lifetimes of the sources of population of states resulting from the collisionally stabilized recombination of helium ions produced by the e-beam. Experimental values at different pressures are shown by open circles and theoretical values by solid bars. Values are marked on the bars which correspond to the electron temperatures indicated.

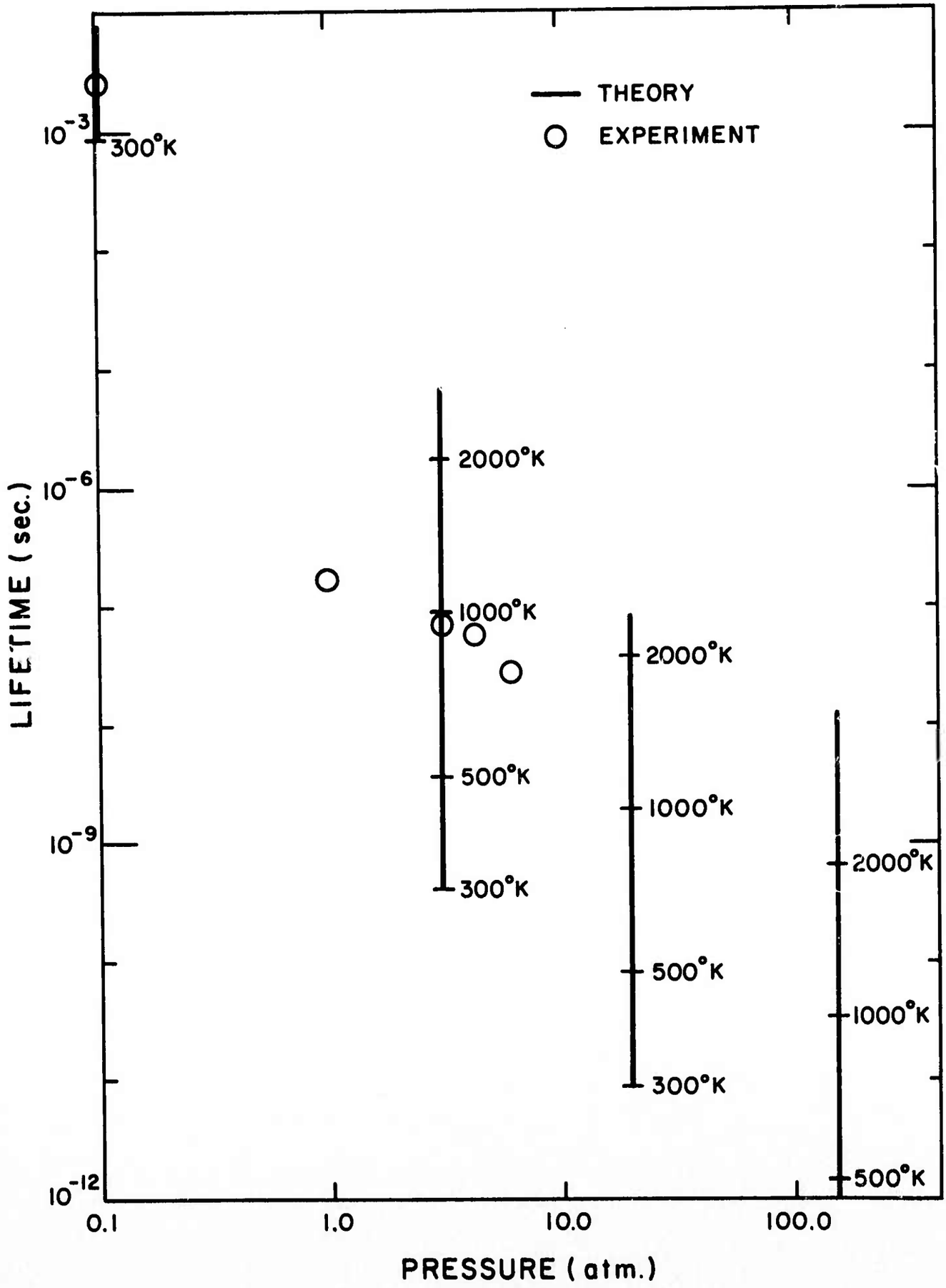
THEORY
EXPERIMENT
10^{-3}
300°K
10^{-6}
10^{-9}
10^{-12}
LIFETIME (sec.)
2000°K
1000°K
500°K
300°K
2000°K
1000°K
500°K
300°K
2000°K
1000°K
500°K
0.1
1.0
10.0
100.0
PRESSURE (atm.)

c) Efficiency -- Although the quantum efficiencies summarized previously in Table I are not extremely impressive, the system efficiencies expected for a recombination laser should be limited primarily by these quantum efficiencies. This results from an exceedingly effective use of electron beam energy. Whereas in many e-beam excited laser systems, including N_2 and H_2, waste of over 90% of beam energy lost in inelastic collisions occurs in the production of ionization as opposed to excitation, in the recombination scheme use is directly made of that ionization. Considering that about 42.3eV of beam energy is expended in the production of a 24.5eV He^+ ion or 22.4eV He_2^+ ion, system efficiencies of 58% and 53%, respectively, of the quantum efficiencies should be attainable. This implies that recombination lasers should achieve overall efficiencies of 5 to 10 percent. Preliminary measurements discussed in Section IV on the economy of energy extraction tend to support this estimate.

III. EXPERIMENTAL METHOD

The objective of this program has been stated to be the evaluation of the potential utility to laser development of recombining high pressure helium plasmas. Although there are several ways in which this could have been done, the paucity of data existing prior to the initiation of this contract research necessitated an initial survey and characterization of the afterglow properties in order to develop a model to guide understanding. As discussed in the previous section, even theory provided little assistance, being extrapolated to parameter values over two orders of magnitude beyond prior experimental verifications.

The initial approach consisted of three steps. First, a survey of the spectrum of spontaneous emission was planned to identify which excited species and states could be found under the various experimental conditions of pressure and electron density. Second, an investigation of the time-resolved decay of spontaneous emission was intended to determine the relevant rate coefficients for recombination and de-excitation. Finally, measurements of the potential gain of the various promising transitions were planned to guide the study of any stimulation emissions which might be expected and prepare the way for quantative measurement of the resulting radiative economy. It has been essentially this course which has been followed, as reported in this and previous technical reports.[1,3,4]

To support this research, a sophisticated ultra-high vacuum and gas handling system was constructed and used to prepare and fill several different designs of high-pressure afterglow chambers (HPAC's). System integrity was found to be of great importance because of the high ionization potential of the helium ions and their large cross-sections for charge transfer to impurity gas atoms and molecules. Figure 7 schematically outlines the functions of the gas handling system. All standard components were Varian 2 in. UHV grade.

Figure 7

Schematic representation of the UHV vacuum and associated gas handling systems. The dotted lines enclose portions bakeable to 400°C. The dashed lines enclose additions to the system which were implemented when HPAC-2 was installed and used subsequently with HPAC-1b.

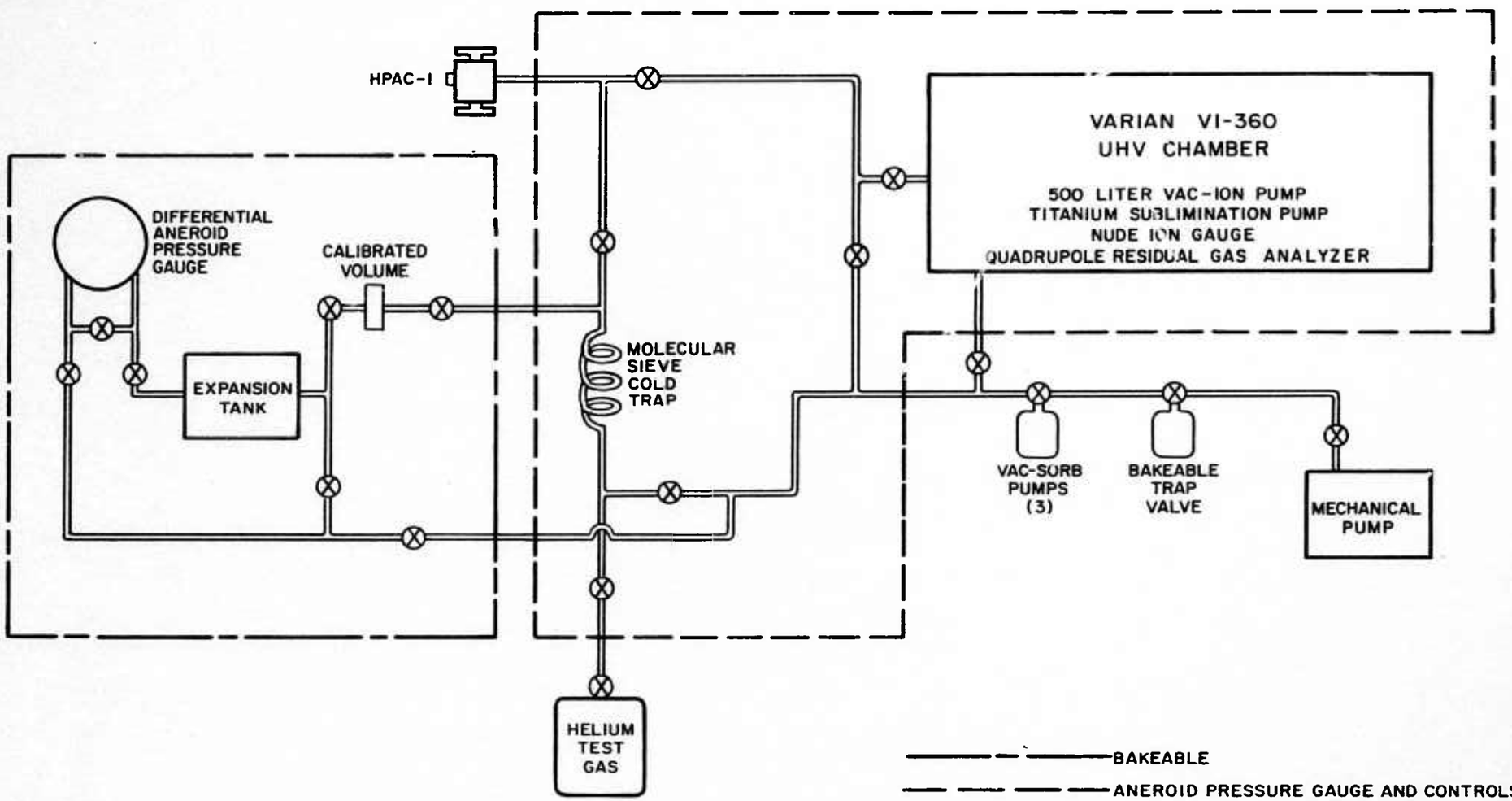
HPAC-1
VARIAN VI-360
UHV CHAMBER
500 LITER VAC-ION PUMP
TITANIUM SUBLIMINATION PUMP
NUDE ION GAUGE
QUADRUPOLE RESIDUAL GAS ANALYZER
DIFFERENTIAL ANEROID PRESSURE GAUGE
CALIBRATED VOLUME
EXPANSION TANK
MOLECULAR SIEVE COLD TRAP
VAC-SORB PUMPS (3)
BAKEABLE TRAP VALVE
MECHANICAL PUMP
HELIUM TEST GAS
BAKEABLE
ANEROID PRESSURE GAUGE AND CONTROLS

The portion enclosed in dotted lines was bakeable to 400°C while the part in dashed lines was an addition implemented with HPAC-1b to provide accurate pressure measurement without contamination.

System integrity was such that, after a mild bakeout with heating tapes, a pressure of 3×10^{-11} Torr could be maintained in the dump tank while the valve to HPAC-1b was open. Final verification was obtained with a commercial helium leak detector which failed to show any detectable leaks.

Figure 8 shows a drawing of the afterglow chamber HPAC-1b. It is basically a welded stainless steel box having the schematic form of a horizontal cross with an additional downward leg serving as an inlet port. One pair of opposed arms is terminated by copper gasketed windows and the other pair contains the pumping port opposite to the e-beam window. Dimensions and construction details are found in the figure. Windows were either quartz fused through graded seals to Varian flanges, or sapphire directly mounted in Varian flanges.

Residual gas analysis was performed after each evacuation and showed only traces of contaminant. A typical mass spectrum is shown in Figure 9a.

After evacuation, the chamber was valved off from the pump and filled through the inlet port with helium of high initial purity, further conditioned by passing it at the fill pressure through a molecular sieve trap cooled to liquid nitrogen temperatures. Bureau of Mines analyses of cylinders of similar grade have shown one or two ppm non-condensable, inert (neon) impurity, and it is believed that this figure represents the ultimate purity attainable with this system. As will be discussed in the following section, this treatment sufficed to reduce all impurities below the threshold of spectroscopic detection by optical means. Typical mass spectrometric analysis of the cell contents at the completion of an experimental sequence is shown in Figure 10b. No evidence of leakage or gas evolution can be detected.

Figure 8

Drawing of the High Pressure Afterglow Chamber, Version 1b (HPAC-1b) showing construction details.

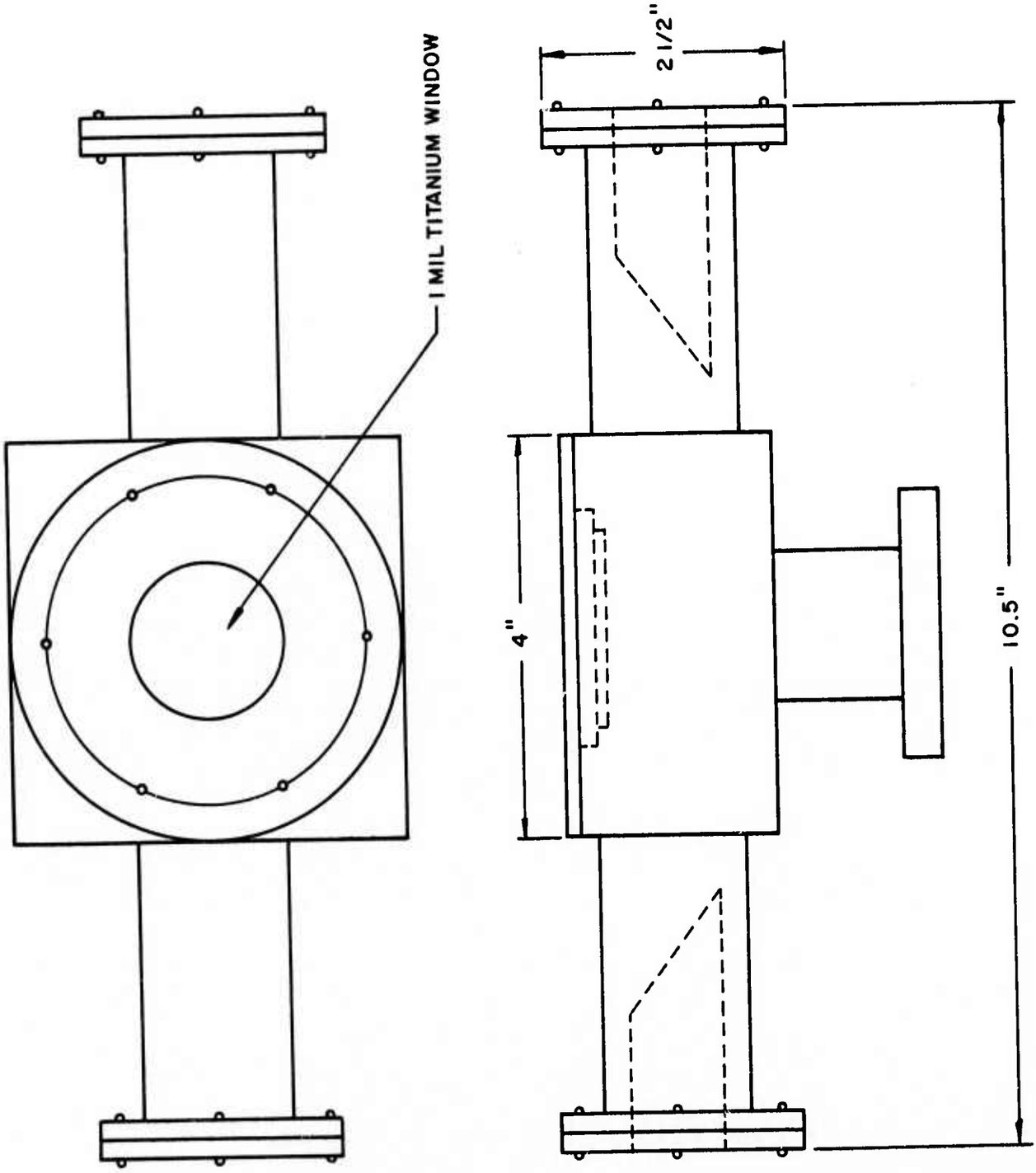
1 MIL TITANIUM WINDOW
2 1/2"
4"
10.5"

Figures 9

Residual gas analysis obtained after evacuation of HPAC-1b

a) Mass spectrum of steady state evacuation, initial condition before filling with helium.

b) Mass spectrum of cell contents after an experimental cycle of the order of 4 hours and 50 e-beam discharge pulses.

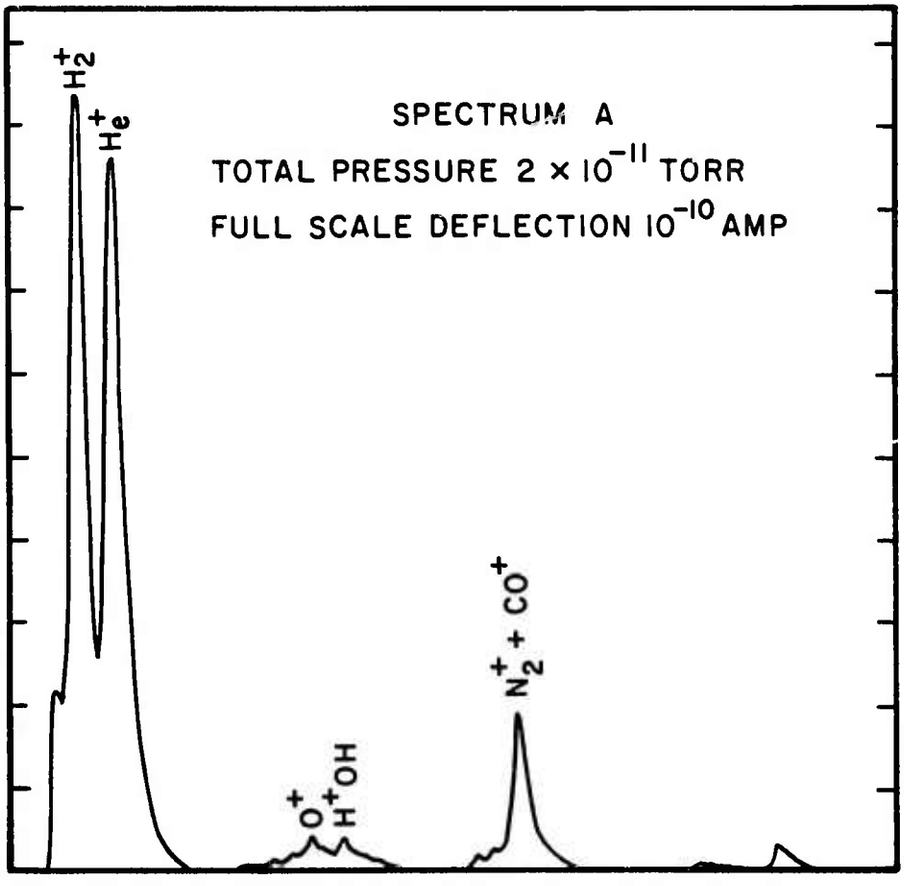
SPECTRUM A
TOTAL PRESSURE 2 × 10⁻¹¹ TORR
FULL SCALE DEFLECTION 10⁻¹⁰ AMP
H2+
He+
O+
H+OH
N2+ + CO+

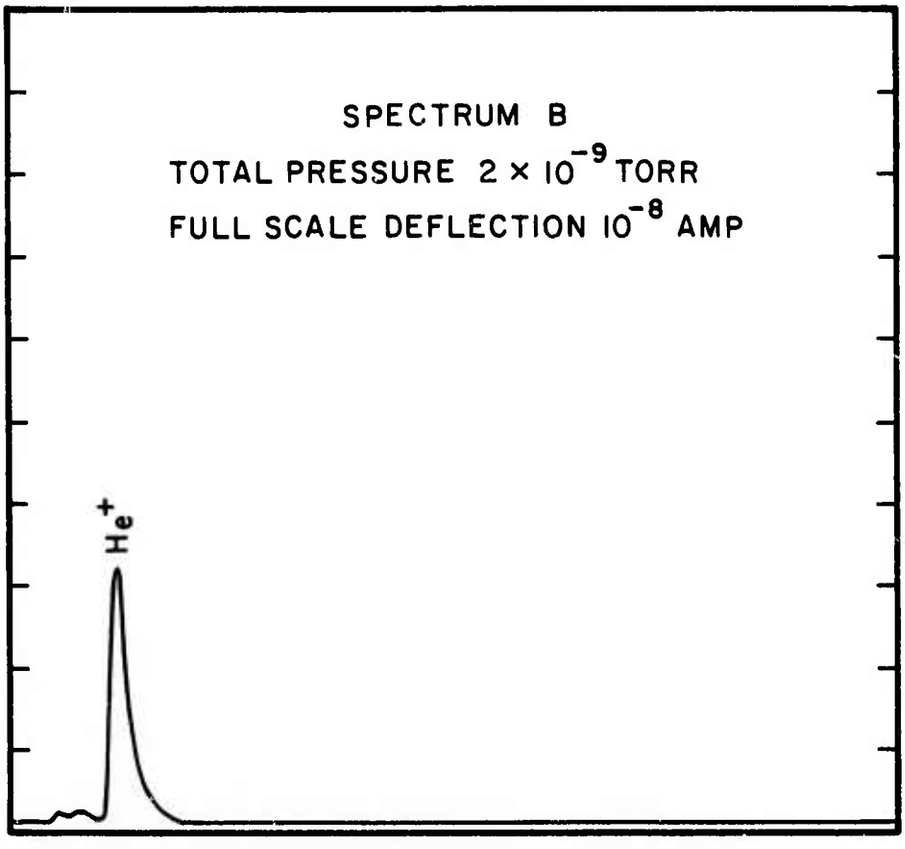
SPECTRUM B
TOTAL PRESSURE 2 × 10⁻⁹ TORR
FULL SCALE DEFLECTION 10⁻⁸ AMP
He+

In the cell, the primary ionization is produced by a nominal 0.5 MeV electron beam entering the HPAC through a 0.001 inch thick titanium foil. The beam is produced by a Field Emission Corp. 706 e-beam gun which can emit 2×10^{14} electrons per 3-nanosecond pulse. Divergence of the beam is reported to be 30° so that, at a distance ℓ, normal to the window, there can be expected to be

$$N_p = 1.5 \times 10^{14}[1 + 0.81\ell + 0.165\ell^2]^{-1} \quad , \quad (13)$$

primary electrons per cm^2 incident upon the HPAC beam window. From values of average range, energy expended per ion-electron pair, and gas density, an average charge multiplication factor in helium of

$$M = 15.6 \text{ cm}^{-1}\text{atm}^{-1} \quad , \quad (14)$$

can be computed.

The preliminary diagnostic data obtained with HPAC-1 and discussed in the following section was obtained at a helium pressure of 3 atm. with the e-beam gun located a distance of 7 cm from the afterglow chamber. For these parameters, the initial helium ion concentration should be

$$[+] \sim 5 \times 10^{14} \text{ cm}^{-3} \qquad \text{HPAC-1} \quad . \quad (15a)$$

Closer proximity to the e-beam gun was obtained with HPAC-1b and corresponded to an initial ion concentration at 3 atmospheres of

$$[+] \sim 1.7 \times 10^{15} \text{ cm}^{-3} \qquad \text{HPAC-1b} \quad (15b)$$

For purposes of the subsequent calculation of efficiencies, an expression for the input energy to the afterglow from the beam is useful. Considering the specified beam energy of 4.8 Joules and range of 450 cm/atm at the 60% power of 300 KeV, the average beam energy deposited in the plasma is

$$E_b = 7.8 \times [1 + 0.81\ell + 0.165\ell^2]^{-1} \quad \text{J/liter} \qquad . \qquad (16)$$

Better values for these parameters are contingent upon calibration of beam current and divergence, but it is believed that the interim use of these approximations is consonant with the current allocation of priorities in this project, as well as consistent with the accuracy at this stage of investigation of the data reported in the following section.

Several instructive problems were encountered with the initial operation of the system. Both RFI and X-ray noise were extreme and extensive protective measures were necessitated. Nested enclosures were constructed to suppress counting from the innermost, the RFI, X-rays, and RFI again. The innermost enclosure consisted of a copper bellows assembly bolted to the face of the e-gun and grounding through spring contact to the mounting ring supporting the foil window. Blocking the passage in the bellows was a .004" thick Mylar disk placed to protect the face of the e-gun from the possible back ejection of material from the foil window.

Surrounding the HPAC, together with the evacuation tube and valve to the dump chamber was a 1/16" lead enclosure with open ports to allow access to the optical windows and bellows connecting to the e-gun. Additional 0.5" lead plates were positioned in strategic locations to shadow the external instrumentation and operators.

The outermost, and most complete RFI shield consisted of 5 sides of a welded aluminum cube approximately one meter on a side. It could be lowered onto an aluminum base plate lying under the asbestos base of the bakeout oven.

Electrical contact between the case and base was assured by commercially available RFI gasketing. All gas inlets and vacuum lines through the base were grounded to base by sealing them to the base at the point of penetration with RFI gaskets. Contact between the penetrating tapered output end of the e-gun and the case was made with a sliding RFI gasket. The only unprotected openings through the enclosure were the two opposed circular ports centered on the same optical axis as the windows of the HPAC. Since there was no significant asymmetries or conductive penetrations through these holes, RFI radiated from them was at a minimum level and one which was found to be acceptable to the external instrumentation.

For the spectroscopic surveys of the spontaneous emission, three high-aperture systems have been found useful; an f/2 camera-spectrograph with about 300 Å/mm dispersion at the film plane, an f/4, 0.25 meter spectrometer with the exit slit removed to give about 100 Å resolution, and an f/4, 0.25 meter spectrograph coupled to a 4-stage image intensifier system arranged so that the dispersed spectrum of a single discharge could be photographed at a sensitivity where single-photon scintillations could be recorded.

The f/2-spectrograph was employed primarily to obtain the time-integrated spectra of the e-beam afterglow for the purpose of locating features of interest, as well as serving as an impurity monitor. Four pulses at the maximum beam energy were required for a useful exposure on Tri-X film developed to an ASA equivalent index of 2400.

The f/4-spectrograph/intensifier shown schematically in Figure 10 was to extend both sensitivity and resolution of the f/2 survey instrument. By adjustment of the accelerating voltage threshold sensitivity could be varied from the resolution of single photon scintillations to the integral of n successive photon scintillations within the decay time of the phosphor on the output screen.

Figure 10

Schematic representation of the spectrograph-image intensifier combination used to record spectra of single discharges at the level of sensitivity where single photon scintillations could be distinguished.

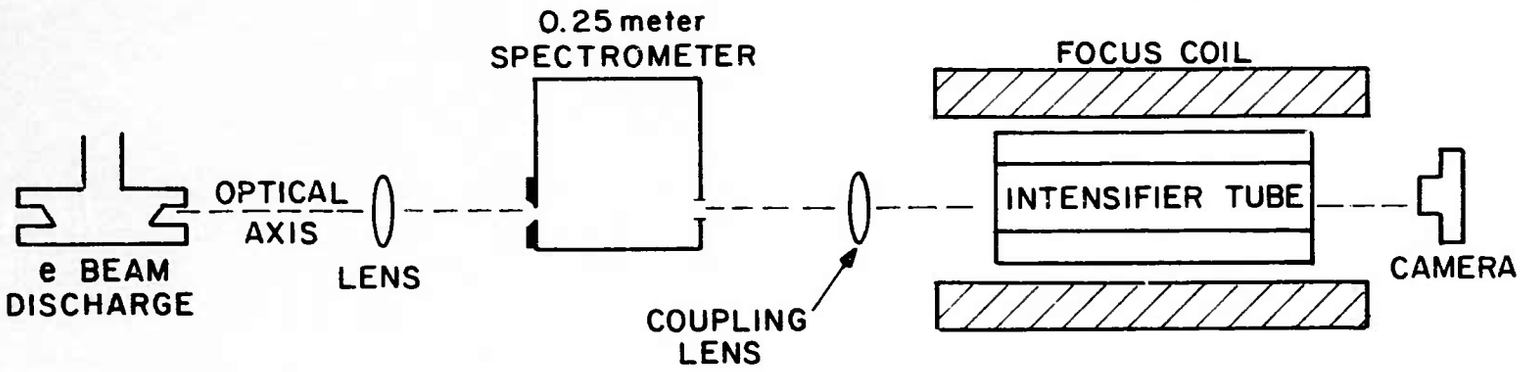
0.25 meter
SPECTROMETER
FOCUS COIL
OPTICAL
AXIS
INTENSIFIER TUBE
e BEAM
DISCHARGE
LENS
CAMERA
COUPLING
LENS

The 0.25 m spectrometer was used with a nine stage RCA-C31025C photomultiplier to obtain the transient intensity response for a particular 100 Å wavelength region. The useable region of sensitivity extended from 3000 Å to 8500 Å. The photomultiplier risetime of 1.5 nanosecond insured the transient intensity could be monitored with nanosecond resolution if adequate recording techniques were used. Intensities were such that typical signals were in the range of 0.1 to 1.0 volts into 50Ω with decay times in the range of a few x 10^{-8} sec. to a few x 10^{-7} sec.

This suggested the use of a Biomation 8100 transient recorder which provides the 8-bit digitization of input signals not less than 0.05 volts for full scale conversion over 2048 time increments of at least 10 nanoseconds each. The device was directly interfaced to the data acquisition computer currently serving the University's Atomic Physics group. Future refinements are under construction to give 300 psec resolution for at least the first 32 points.

Calibration of the 0.25 m spectrometer and detection system was accomplished by comparison to a standard of irradiance traceable to NBS. Detection sensitivities which calibrated the power at the spectrometer entrance slit to voltage at the 8100 input ranged from 20μ watts/volt at 4000 Å. The rather low sensitivity in the violet was primarily a consequence of the 6000 Å blaze wavelength of the grating, chosen to enhance the usually depressed red-sensitivity of most fast detection systems. A consideration of geometrical factors and volume sampled gave an overall calibration depending on wavelength which equated between one and two kilowatt/liter of incoherent power radiated from the e-beam afterglow to 1 volt of detected signal.

The addition to the system of an internal optical cavity contained in the HPAC-1b and having coincident optical axis with it has permitted the preliminary inference of optical gain from measurements of the enhancement of certain spectral features observed in the optical cavity. The cavity support-

ing these measurements is a sub-concentric geometry imposed by the availability of mirrors and the physical dimensions of the shielded system. The measurements discussed in the following section were obtained with multi-layer dielectric mirrors of maximum available reflectivity over the various 1000 Å regions examined.

A more quantitative system for the direct measurement of gain was constructed as shown in Figure 11. Since the lifetimes for the source of molecular emissions ranged from 160 nsec. at 1 atmosphere to 26 nsec. at 7 atmospheres as discussed in Section II, it was necessary to use a rapidly pulsed light source for the measurement of small signal gain or absorption in a particular transition during the afterglow period. A nitrogen laser pumped, tunable dye laser with a FWHM of a few Angstroms was used in the differential path arrangement shown in Figure 11 to measure the attenuation or amplification of the beam reflected through the plasma by the internal dielectric mirror. Use of the optical delay line in the reference path allowed for the detection of both beams with a single photomultiplier and electronics system thus minimizing the drift of the balance of sensitivity between the paths. Resulting system stability was of the order of 6% with timing jitter between the e-beam and the dye laser small in comparison with a recombination lifetime. As accuracy of the timing measurement was around 4 nsec., adequate resolution of the particular phase of the afterglow sampled by the dye laser beam could be established.

The success in the use of this system in the recently reported[1,2] preliminary measurements at 6400 Å and in the detailed re-examination of that band, together with the analogous measurements at 5170 Å discussed in the following section, indicates it will continue to be the primary technique utilized in the measurement of gain at the other wavelengths of importance in the helium afterglow. The dye laser technology is well enough developed to support investigation

Figure 11

Experimental system for the direct measurement of time-resolved gain spectra.

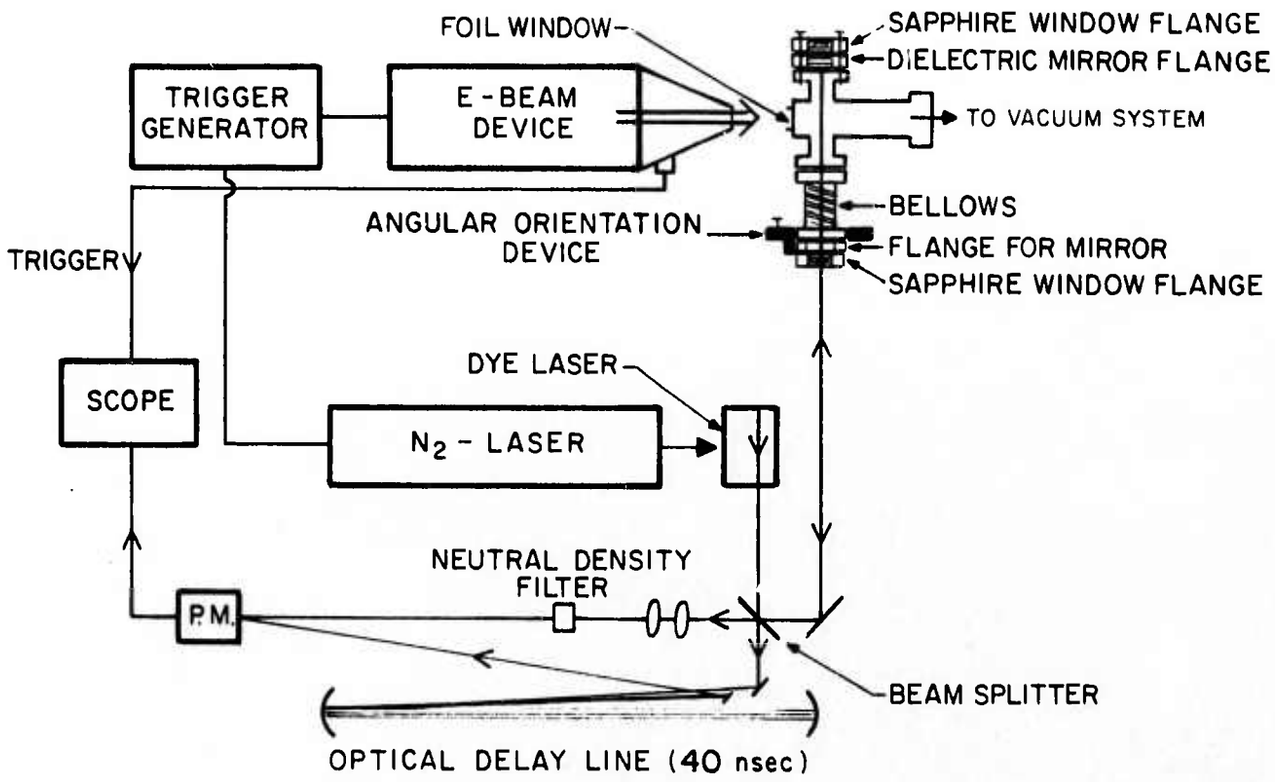
FOIL WINDOW
SAPPHIRE WINDOW FLANGE
DIELECTRIC MIRROR FLANGE
TRIGGER GENERATOR
E-BEAM DEVICE
TO VACUUM SYSTEM
BELLOWS
ANGULAR ORIENTATION DEVICE
FLANGE FOR MIRROR
TRIGGER
SAPPHIRE WINDOW FLANGE
DYE LASER
SCOPE
N_2 - LASER
NEUTRAL DENSITY FILTER
P.M.
BEAM SPLITTER
OPTICAL DELAY LINE (40 nsec)

over the 3500 Å - 7500 Å spectral region; so, it can be reasonably expected that the stimulated emission spectrum and its dependence on experimental parameters can be well characterized by this technique in advance of projected attempts to construct an operating laser device excited by the larger APEX electron beam gun.

IV. TECHNICAL RESULTS

Preliminary values were obtained for the most important diagnostic parameters characterizing the e-beam afterglow excited in 3 atmospheres of helium with the previously described HPAC-1 system.[3] Confirmation and extension[4,16] of these values to cover the one to five atmosphere pressure range was accomplished in the HPAC-1b chamber at greatly improved gas purity. A copy of the resulting Physics Letters appears in Appendix I.

The first report of stimulated emission from a high pressure recombining helium afterglow was made in the previous report[1] on the contract activities and accepted for publication in Applied Physics Letters[2]. A preprint of those preliminary measurements of stimulated emission at 6400 Å appears in Appendix II.

Parameters considered to date in this work have been a) output wavelengths, b) spontaneous emission, energies and peak power levels, c) incoherent output efficiencies, d) stimulated emission, and e) stimulated output efficiencies. Each is considered in the following subsections, and those reported previously are reviewed to the extent that they clarify present results.

a) Output wavelengths

Figure 12 presents a survey spectrum of the spontaneous emission from a single discharge in the HPAC-1b system made with the f/4 spectrograph-image intensifier combination having greatly improved sensitivity and resolution over conventional spectrographic systems. Principal limitation on both quantities have been reduced to the quantum noise imposed by the discrete nature of the photodetection events. All the information available in the spectrum has been recorded. Primary detection occurs with an S-11 photocathode with subsequent acceleration and multiplication of the emitted photoelectrons. In contrast to direct film recordings[1,2], this system has an enhanced sensitivity in the shorter wavelength region and a pronounced cut-off in the red around 6400 Å.

Relative sensitivity of the intensifier tube as a function of wavelength is shown in Figure 13.

Figure 12

Survey spectrum of the visible region made with the f/4 spectograph - image intensifier system. Long wavelengths are to the left. Each spectrum is a time-integrated record of the afterglow from a single discharge of the e-beam gun in helium at 3 atmospheres in the HPAC-1b system. Exposures are for different accelerating voltages corresponding to different values of the number of superimposed photon scintillations required within the decay time of the output phosphor to reach the threshold for photographic detection. From top to bottom, accelerating voltages are 25, 30, 35 and 40 KV, the last two satisfying the requirements for the detection of scintillations from single photoelectrons.

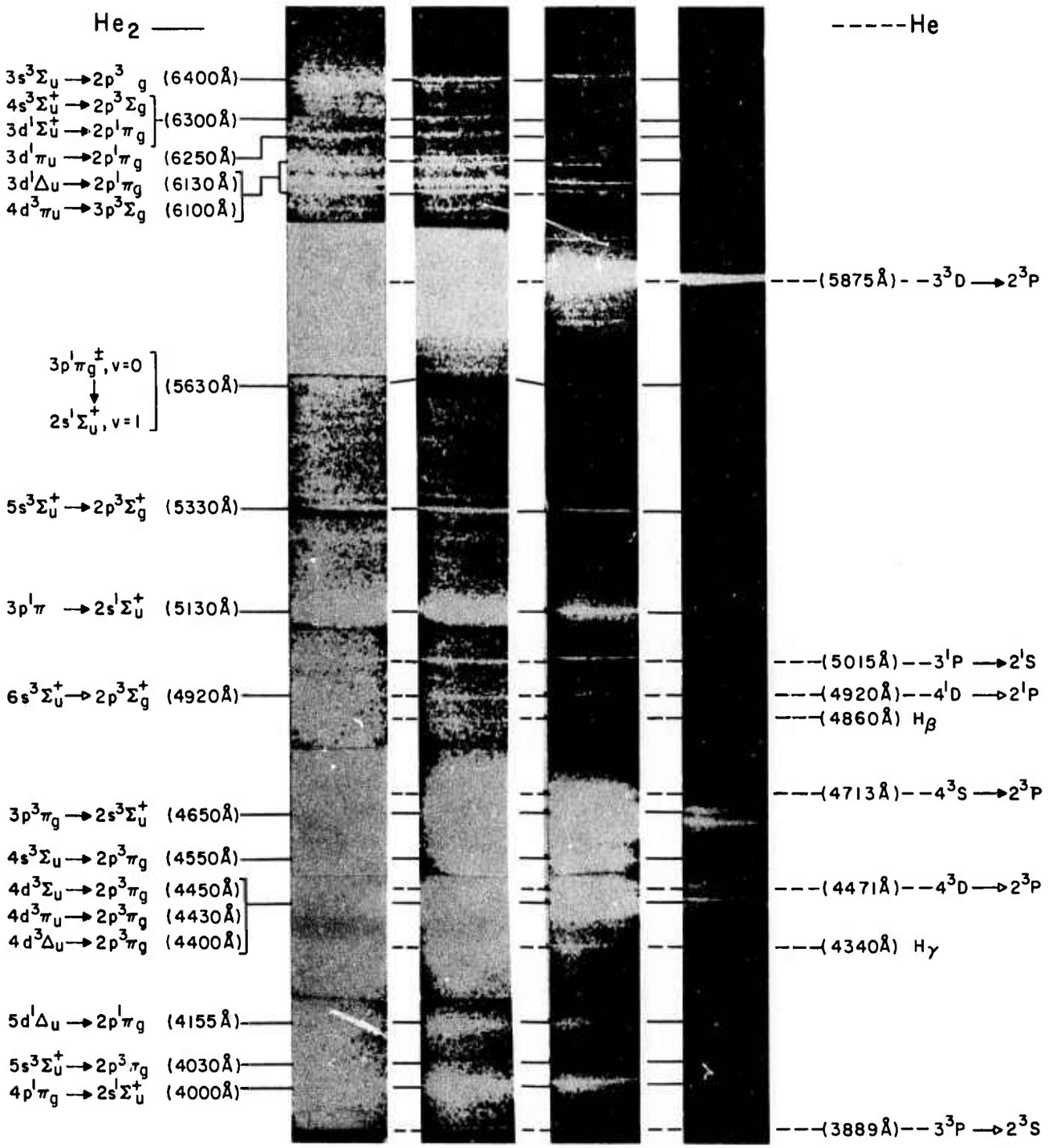
He2
-----He
3s3Σu → 2p3 g (6400Å)
4s3Σu+ → 2p3Σg
3d1Σu+ → 2p1πg (6300Å)
3d1πu → 2p1πg (6250Å)
3d1Δu → 2p1πg (6130Å)
4d3πu → 3p3Σg (6100Å)
---(5875Å)--3³D → 2³P
3p1πg±, v=0
↓
2s1Σu+, v=1 (5630Å)
5s3Σu+ → 2p3Σg+ (5330Å)
3p1π → 2s1Σu+ (5130Å)
---(5015Å)--3¹P → 2¹S
6s3Σu+ → 2p3Σg+ (4920Å)
---(4920Å)--4¹D → 2¹P
---(4860Å) Hβ
---(4713Å)--4³S → 2³P
3p3πg → 2s3Σu+ (4650Å)
4s3Σu → 2p3πg (4550Å)
4d3Σu → 2p3πg (4450Å)
4d3πu → 2p3πg (4430Å)
4d3Δu → 2p3πg (4400Å)
---(4471Å)--4³D → 2³P
---(4340Å) Hγ
5d1Δu → 2p1πg (4155Å)
5s3Σu+ → 2p3πg (4030Å)
4p1πg → 2s1Σu+ (4000Å)
---(3889Å)--3³P → 2³S

Figure 13

Graph as a function of wavelength of the relative sensitivity of the image intensifier system used to obtain the data of Figure 12.

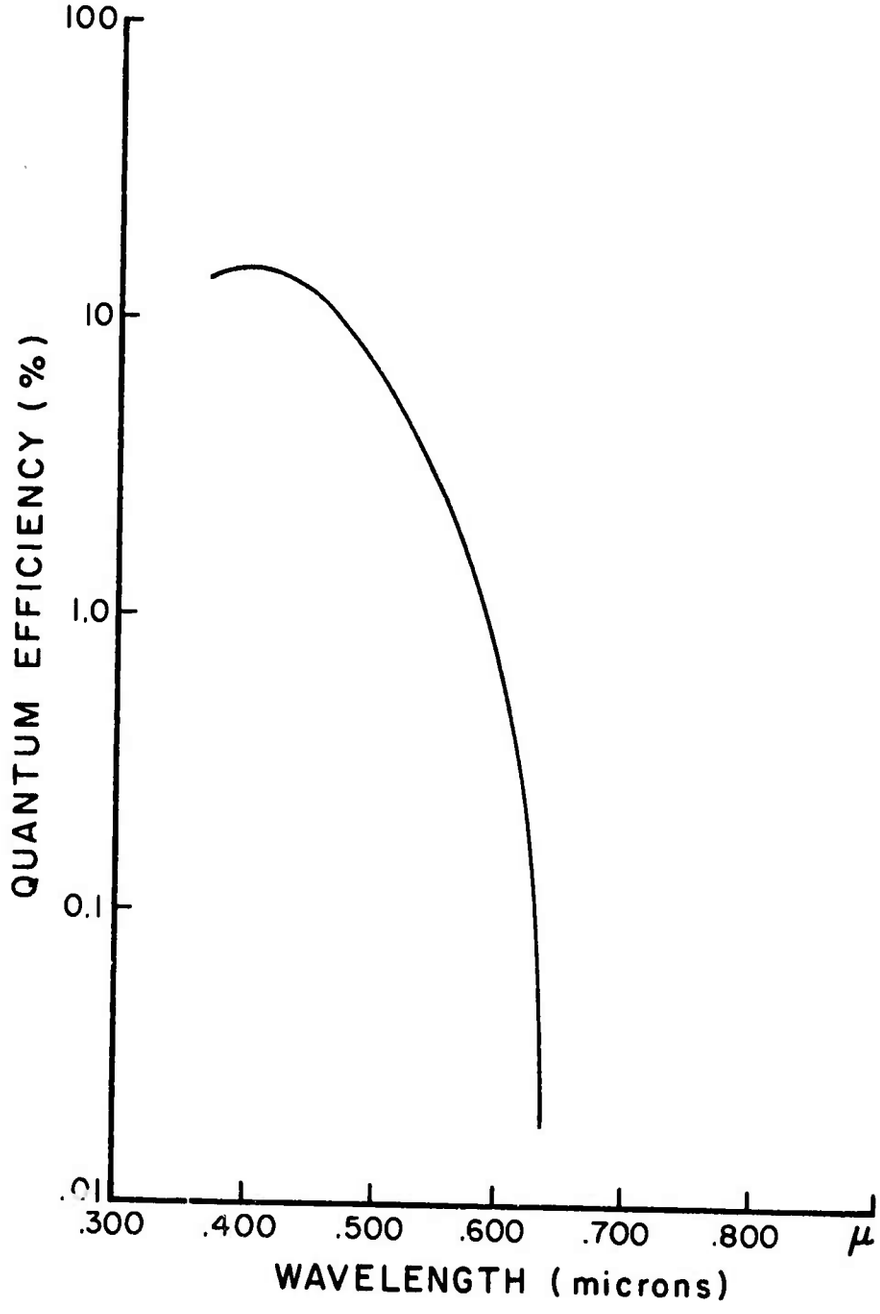
100
10
1.0
0.1
.01
QUANTUM EFFICIENCY (%)
.300
.400
.500
.600
.700
.800
μ
WAVELENGTH (microns)

Several exposures of the spectrum are shown in Figure 12 and correspond to different values of accelerating voltage on the image intensifier tube and, hence, to different values of gain for the photoelectron amplification. Each represents a different value of the number of successively superimposed photon scintillations required within the decay time of the output phosphor to reach the threshold exposure of the recording film. From right to left, the exposures represent increasing accelerating voltage with the last two strips satisfying the requirements for the detection of scintillations from single photoelectons. Values of actual photoelectron gain corresponding to the accelerating voltages shown can be read from Figure 14.

In Figure 12, most of the He_2 spectrum is seen, with principal interest being directed toward the relatively enhanced features in the red. However, it can be seen that the other members of the "favorable" Rydberg-series discussed in the introductory material are present. In particular

1. the $ms^3\Sigma_u^+ \rightarrow 2p^3\Pi g$ series convergent at 3680 Å is represented strongly by the m=3,4 and 5 members at 6400 Å, 4540 Å and 4030 Å, respectively, and
2. the $mp^1\Pi g \rightarrow 2s^1\Sigma_u$ convergent at 3130 Å and terminating on a state optically connected to the $1s\sigma^2 2s\sigma$ repulsive ground state is evidenced by the relatively strong m=3 and 4 components at 5130 Å and 4000 Å, respectively. This latter series is of tangential interest in that, if lasing could be accomplished for one component, the delivery of population to the $2s^1\Sigma_u$ state might occur at a rate sufficient to invert the vacuum - UV transition from this state to the repulsive ground state.

The spectral information of Figure 12 is summarized in Figures 15 and 16 which are energy level diagrams of

Figure 14

A graph of photoelectron gain as a function of accelerating voltage for the image intensifier system used to record the spectra of Figure 12.

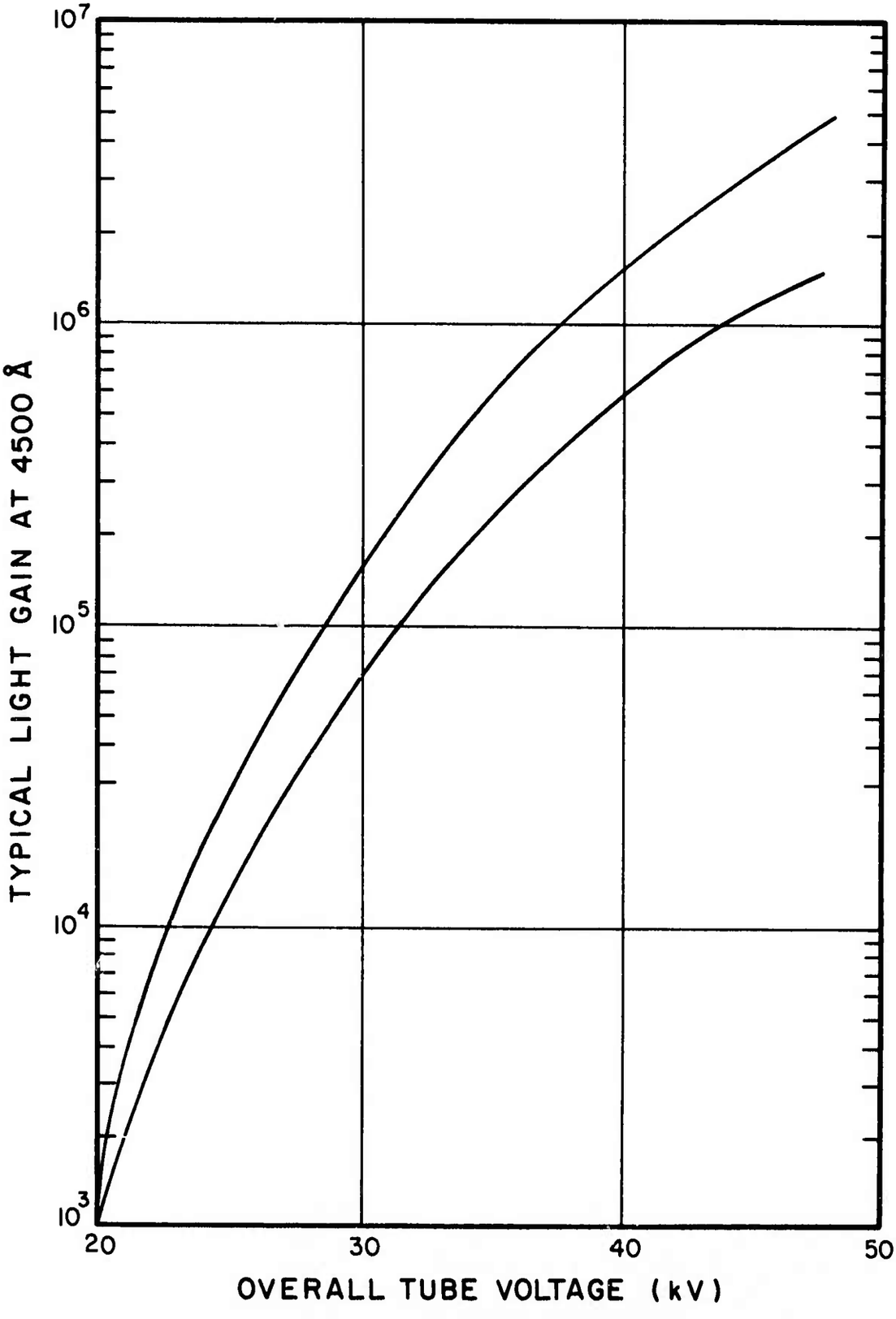
10^7
10^6
10^5
10^4
10^3
TYPICAL LIGHT GAIN AT 4500 Å
20
30
40
50
OVERALL TUBE VOLTAGE (kV)

Figure 15

Energy level diagram of atomic helium showing for clarity only those states participating in transitions observed with appreciable intensity in the afterglow at three atmospheres.

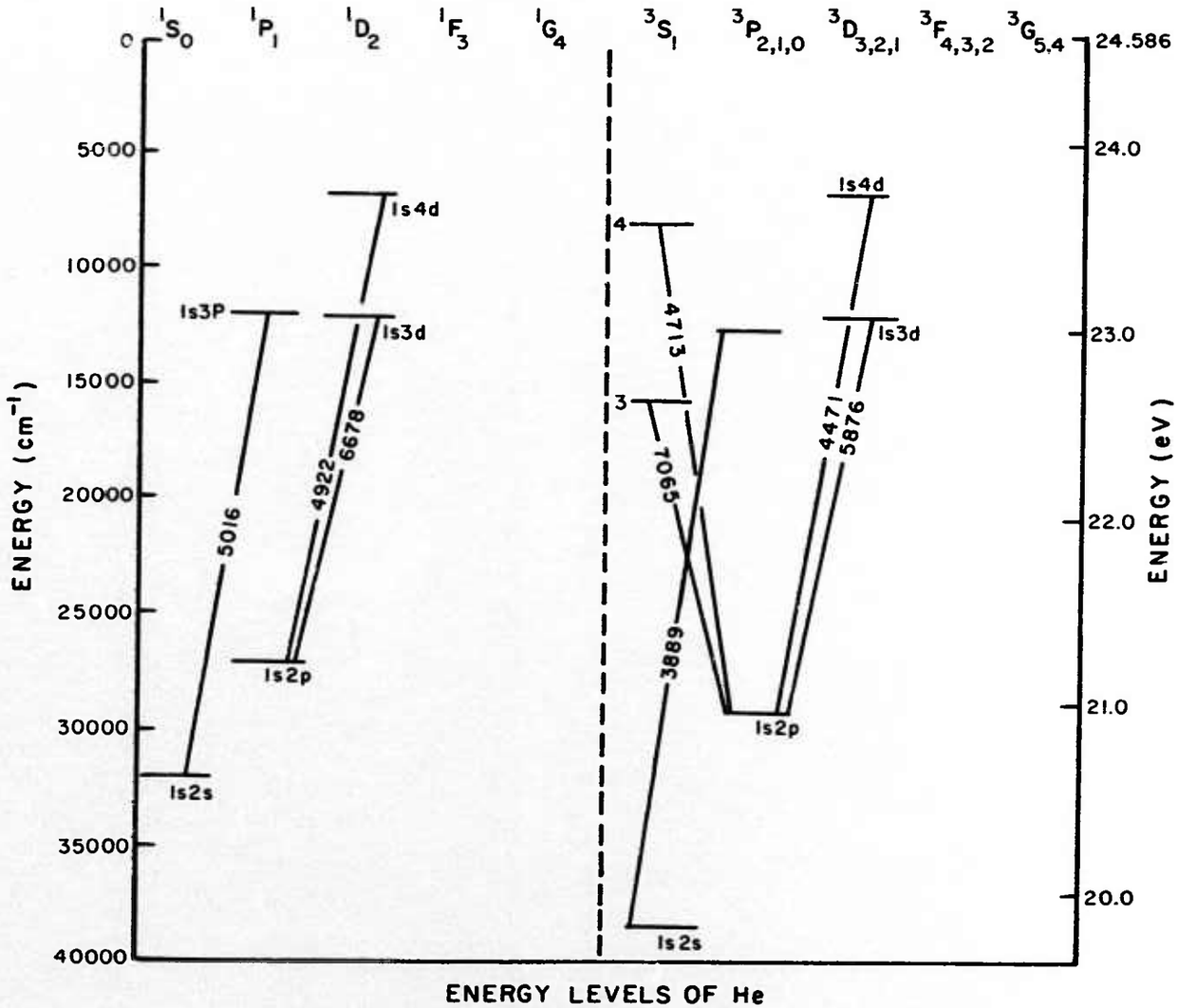

ENERGY LEVELS OF He

Figure 16

Energy level diagram of molecular helium showing for clarity only those states participating in transitions observed with appreciable intensity in the afterglow at three atmospheres.

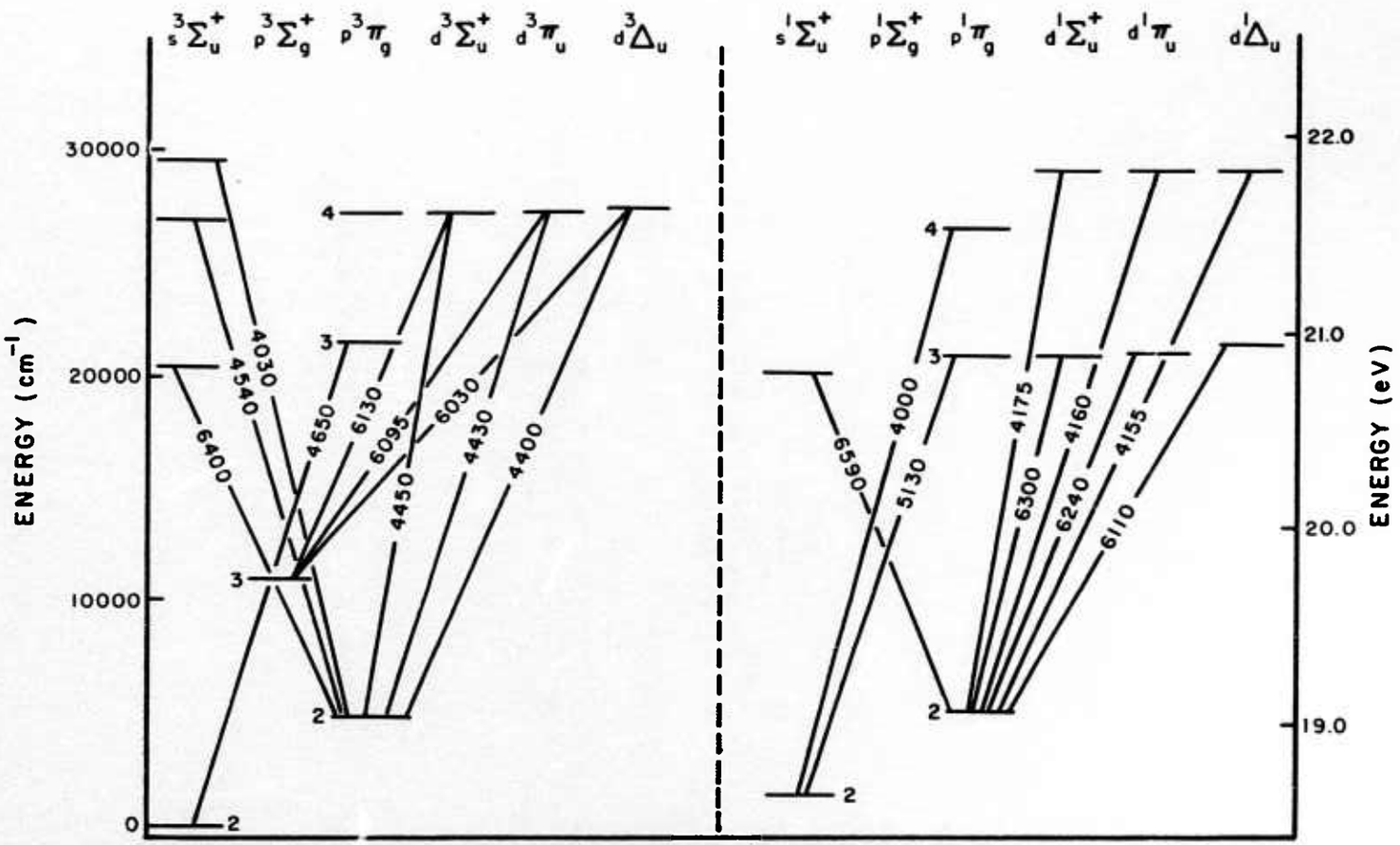

ENERGY LEVELS OF He_2

He and He_2 in which for clarity only those states participating in transitions observed in the afterglow with appreciable intensity are shown. The general observation can be made that the abundance of He_2 levels excited is characteristic of a collisional-radiative recombination origin of the light with good collisional mixing between levels.

The bands generally appear at relative intensities which could be reasonably expected from radiative and collisional cascading in the course of the stabilization of the collisional-radiative recombination of He_2^+. This is the cascading discussed in Section II. Of course, such comparisons are quite qualitative and dependent upon subjective averaging over a considerable variety of low pressure helium recombination spectra. In addition, the following transitions appear anomalously enhanced:

1. the $3s^3\Sigma_u^+ \rightarrow 2p^3\Sigma_g$ at 6400 Å
2. the transitions from the 4d complex to the pσ level at 6130 and 6100 Å.

These represent transitions which, in a sense, compete with the normally intense 3-d complex. As can be seen from Figure 16, the third is equivalent to a short-circuit from principal quantum level 4 to 2 by-passing the "normal" stabilization current which tends to relax captured electrons from one principal quantum level at a step. The first can be rationalized as a transition from a state benefitting from one of the "fine-tuning" effects of collisional stabilization which tend to move bound electron populations back and forth between angular momentum sub-levels corresponding to the same principal quantum number. It is this effect which, as discussed in Section II, would allow a lasing transition to capture virtually all of the stabilizing electron current between principal quantum levels. In the case of

the 6400 Å transition, the particular radiating sublevel lies at a somewhat lower energy, ∿ 0.22eV, than the d-complex and should show a gain of population relative to the d-complex when the electron density is high and such "lateral" collisions are frequent.

The rather restricted excitation summarized in Figure 15 for the atomic spectrum is, conversely, more characteristic of some type of selective excitation and warrants further investigation of the possible kinetic processes which might supply such upper state excitation.

b) Spontaneous emission, energies and peak power levels

Each of the spectral features in the wavelength range of the instrumentation showed one or a combination of three basic transient responses, each correlating with a different excitation mechanism as shown in Figure 17.

A typical example of an emission showing a combination of direct e-beam, and recombination excitation is found in the data of Figure 18. In this figure, the emission of the $3^3S \rightarrow 2^3P$ line of atomic helium at 7065 Å is recorded on a horizontal scale of 200 nanoseconds/division by 81 watts/liter per division vertically. While the upper 3^3S state of this transition is optically forbidden to the ground 1^1S state and hence an unlikely candidate for excitation by the primary electrons, it does have a non-zero cross section for secondary electrons which might be expected to have energies near the threshold for excitation of this system. Most probably the situation here is analogous to the excitation of the N_2 C-state in the e-beam N_2 laser. That state is also optically forbidden to the ground X-state and as a consequence is only weakly excited by the higher energy primary electrons but strongly excited by the secondary electrons whose energy lies only slightly above the excitation threshold.

With the exception of the band at 5130 Å the detailed examination on an expanded time base of the leading edges of the molecular emission, as typified by the one at 6400 Å, showed no evidence of a component of e-beam excitation either by pri-

Figure 17

Time evolution of selected atomic and molecular emissions at 3 atmospheres illustrating the three basic excitation mechanisms observed: 1) 5015 Å atomic transition, direct excitation by primary electrons, 2) 7065 Å atomic transition, excitation by energetic secondary electrons and 3) 6400 Å molecular transition, excitation by recombination of He_2^+ ions and cool secondary electrons.

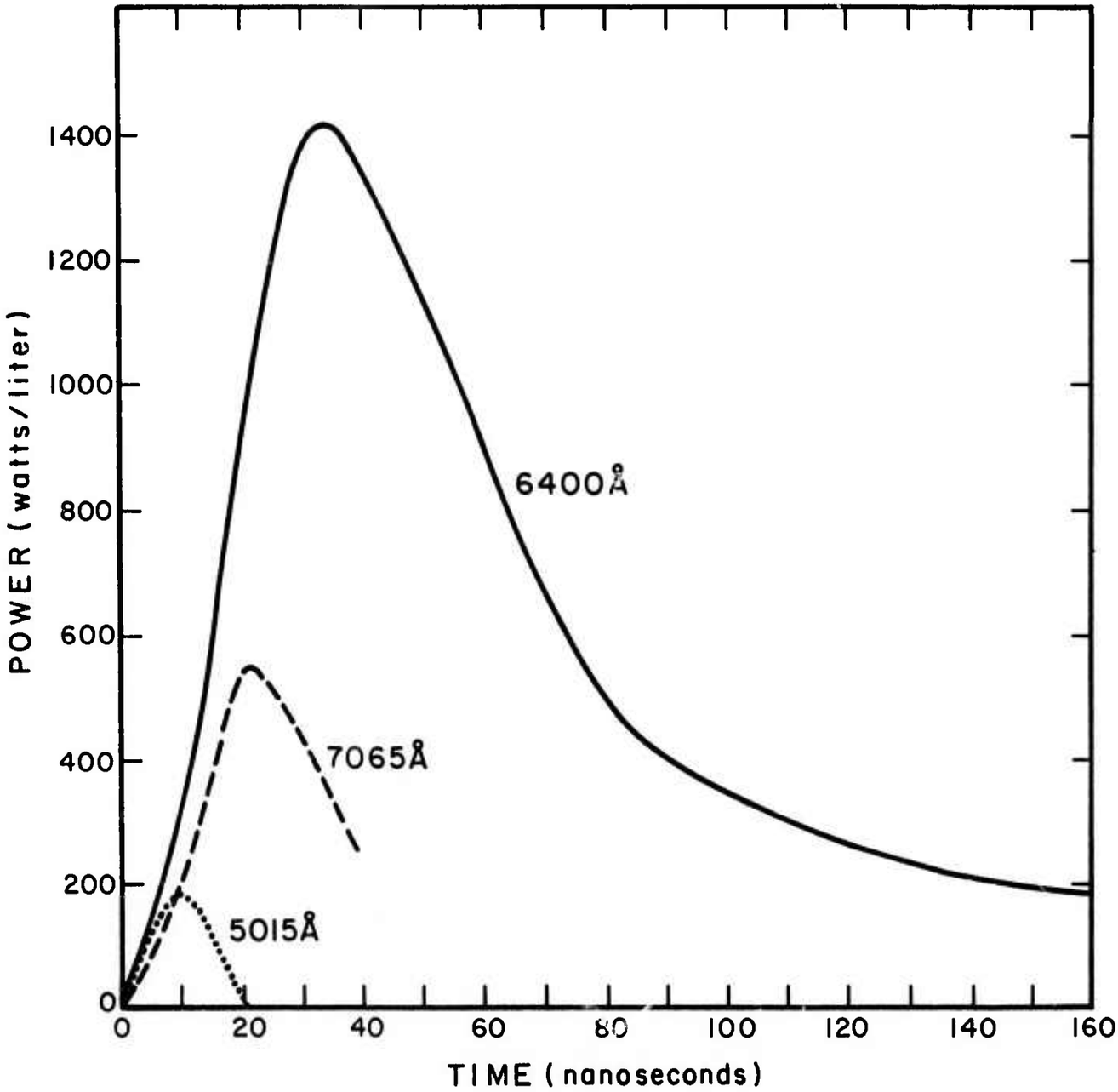
POWER (watts/liter)
1400
1200
1000
800
600
400
200
0
6400Å
7065Å
5015Å
0
20
40
60
80
100
120
140
160
TIME (nanoseconds)

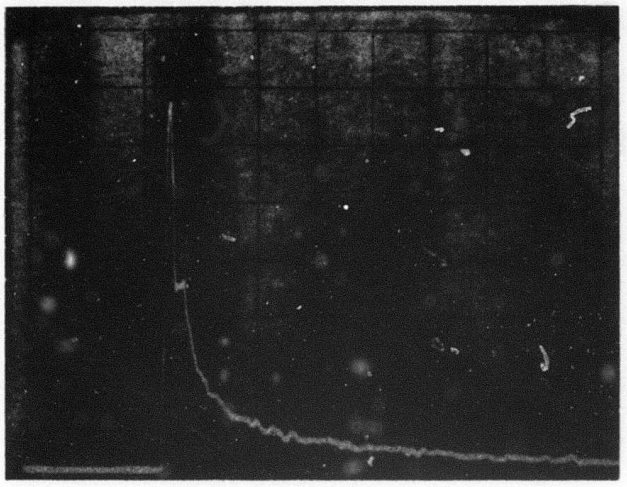

Figure 18 : Time evolution of a single pulsed excitation of the 7065Å line which shows both an early component due to excitation from energetic secondary electrons and a later recombination component. Scales are 200 nanoseconds per horizontal division and 81 watts/liter per vertical division.

mary or secondary electrons. This is what would be expected in the absence of a stable He_2 ground state. The leading edge showed a rise time consistent with the decay of the component of the 7065 Å excitation inferred to be due to the secondary electrons. This also is consistent with the simple model which requires the secondary electrons to cool before they can participate in collisional recombination with the ions. If they are energetic enough to excite the 7065 Å line, they are too hot as a group to recombine with the He_2^+ ions to give the 6400 Å radiation. The exceptional excitation of the $3p^1\pi_g \rightarrow 2s^1\Sigma_u^+$ transition centered at 5130 Å showed an early component in addition to the recombination peak. Since this state dissociates to a 3^1P atom, it is likely this early source of excitation results from the three-body molecular association of ground state atoms with 3^1P atoms produced by the primary electrons in the beam. Stimulated emission peaking at 5170 Å was found in the P-branch of this band for both excitation sources.

From these spontaneous emission data an interesting comparison can be made of the output energies resulting from each of the threc processes. These are summarized in Table IV.

Table IV

Comparison of Measured Output Energies

from Direct Excitation and Recombination

at 3 Atmospheres

Line	Direct e-beam Excitation (micro-Joules/liter)	Recombination (micro-Joules/liter)
5015 Å	∿ 1.8	-
7065 Å	∿ 16	71
6400 Å	< 2.7	110

Table IV serves to underscore the comments made in Seccion II that the potential for recovering much of the e-beam energy "lost" to ionization is quite high in recombination systems.

Implicit in the development of data of the sort presented in Table IV is a knowledge of lifetimes by which the peak powers are multiplied to estimate the output energy per pulse. The particular lifetimes desired are the lifetimes against recombination defined by equation (7), Section II, and tabulated in Table III. The energy output, E, can be written in terms of these quantities as

$$E = \int_0^\infty I(t)dt \quad , \qquad (17)$$

which becomes upon substitution from (10)

$$E = \int \left\{ I_{(0)}^{-\frac{1+\eta}{2+\eta}} + K(1+\eta)(CK)^{-\frac{1+\eta}{2+\eta}} t \right\}^{\frac{2+\eta}{1+\eta}} dt \quad . \qquad (18)$$

Upon integration followed by substitution from (12) and (11), this becomes

$$E = I(0)\tau_0 \quad . \qquad (19)$$

Table V summarizes the resulting energies per pulse radiated spontaneously.

Table V

Summary of the Energies per Pulse of the Principal Spectral Features Emitted Spontaneously

Wavelength	Energy (micro-Joules/liter)			
Pressure (atm.)	1	3	4.2	7
He_2				
6400 Å	104	52.5	35.0	32*
4650 Å	42.5	31.4	25.2	24*
He				
7065 Å	-	54*	59*	92*
6678 Å	38.6*	24.2	12.1*	15.0*
5875 Å	665	905	2200	4400*

*HPAC-2

c) Incoherent Output Efficiencies--From the data of Table V and the input e-beam energy estimated in equation (16), the output efficiency can be obtained for the prominent spectral features examined. Table VI summarizes these results.

Table VI

Efficiencies for the Incoherent Radiation Observed from the Recombination

Wavelength	Efficiency		
Pressure (atm)	1	3	4.2
He_2			
6400 Å	.0057%	.00096%	.00054%
4650 Å	.0023%	.00057%	.00032%
He			
7065 Å	--	.001%	.001%
6678 Å	.002%	.0004%	.00015%
5875 Å	.036%	.016%	.028%

Efficiencies are not particularly impressive, but this is not surprising because in the absence of a stimulated transition, at these electron densities a large fraction of the level to level stabilization should be accomplished by non-radiative transitions. According to theory, if a stimulated transition can be developed, the energy now lost to the collisional channels could be tapped by a competing radiative transition, if strongly induced. This effect is illustrated in part e) of this section for the case of the 6400 Å and 5130 Å bands.

d) Stimulated Emission Spectra--The ability of the helium afterglow to sustain stimulated emission was investigated with the dye laser apparatus of Figure 11. By directly measuring the attenuation or amplification of the probing beam, the coefficient of loss or gain could be directly determined.

As shown, an optical delay line was used to retard the reference beam so that both beams could be detected with the same photomultiplier with a separation in time small compared to the characteristic drift times of the electronics. A charge integrating amplifier detected the signals and displayed them on the screen of an oscilloscope as a step function. The x-position of the first step served to record the interval following the e-beam discharge at which the afterglow was sampled. Time resolution was of the order of 6 nsec, but jitter originally of about 100 nsec rendered the measurement tedious. Recent improvements have reduced jitter to 25 nsec. Long-term stability of the relative intensities between paths was of the order of 6% which determined minimal gain or loss which could be recorded with significance.

Figure 19 shows the topology over the space of parameters indicated of the map of gain resulting from the preliminary measurement reported previously[1,2] for 3 atmospheres pressure. Across the xz plane to the rear of the data has been plotted the time dependence of the spontaneous emission for scale. For comparison on the yz plane to the left edge is shown the normal emission spectrum of the $3s^3\Sigma_u^+ \rightarrow 2p^3\Pi_g$ transition, uncorrected for pressure and Stark broadening. As can be seen, the R-branch appears absorptive while highest gains are found in the Q-branch head and P_4 and P_6 components. Higher members of the P-branch appear absorptive. Units plotted are the gain coefficient per round trip transit of the afterglow, so that the peak gain of 0.23 measured at the head of the Q-branch corresponds to a value of 0.04 cm^{-1} at 6400 Å.

Through reconstruction of the N_2-laser used to pump the dyes, improvement in trigger generation, and operational experience the reduction in system jitter mentioned above was accomplished during the current reporting period. This permitted the re-examination of the stimulated emission spectrum in the 6400 Å region with much greater detail in both time and wavelength. Agreement

Figure 19

Fractional gain per round trip transit as a function of wavelength and time for the afterglow of a 3 atmosphere helium discharge as directly measured fr the enhancement of a probing dye laser beam. Regions of stimulated emission lie above the x,y plane; absorption below. Across the x,z plane to the rear of the data has been plotted the time dependence of the spontaneous emission for scale and on the plane to the left edge is shown the normal emission spectrum of the $3s^3\Sigma_u^+ \rightarrow 2p^3\Pi_g$ transition of the He_2 uncorrected for broadening mechanisms.

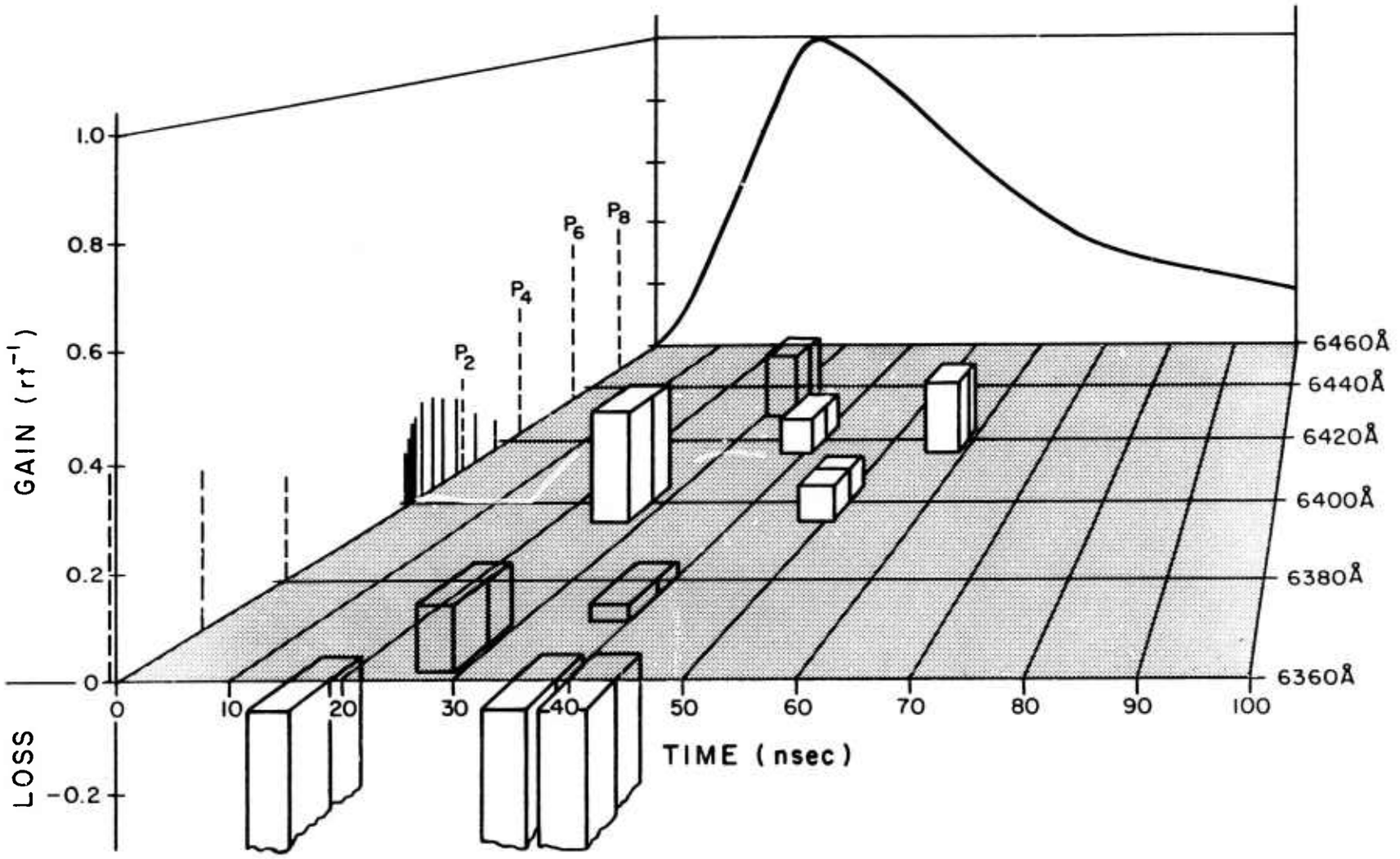
1.0
0.8
0.6
0.4
0.2
0
-0.2
GAIN (rt⁻¹)
LOSS
P2
P4
P6
P8
0
10
20
30
40
50
60
70
80
90
100
TIME (nsec)
6460Å
6440Å
6420Å
6400Å
6380Å
6360Å

with the preliminary spectrum was generally good with both showing an "island" of gain peaking around 6400 Å and 30 nanoseconds. A pronounced difference occurred in the disappearance of the absorptive edges in the tails of the band at higher and lower wavelength. Coincidentally, this change in the spectrum was realized after an extensive reconstruction of the electron beam gun to correct a failing Marx generator, so that the interpretation of the change is unclear. Data taken with the upgraded dye laser system has proven to be clearly reproduceable to within statistical error as seen in the following figures. While the dependence of spectra upon initial beam conditions is to be ultimately investigated, the current assignment of priorities has emphasized completion of the ongoing spectral survey under the optimal conditions for this gun and what limited exploration of other discharge conditions that has been done peripherially has not served to reproduce the original conditions.

Figure 20 shows the best available map of the gain resulting from the remeasurement in extensive detail over the 6400 Å region of a 3 atmosphere helium afterglow. Orientation of the view is that of Figure 19 rotated 90° about the Z axis. As in Figure 19, data is plotted in units of fractional gain per round trip transit of the afterglow. Intensity and focus of the probing dye laser beam were such as to investigate stimulated emission at the 0.4 megawatt/liter power level. Each datum is plotted as a small shaded horizontal plane spanning the appropriate range of times and wavelength. Vertical lines serve to locate data elements over the corresponding parameter values on the co-ordinate plane. Time resolution was a uniform 10 nanoseconds and data planes appearing anomalously long result from the overlap of contiguous measurements. The extent of statistical scatter is clearly indicated by the occurrence of two or more planes at differing levels of gain covering a common overlap of domains on the co-ordinate plane.

Figure 20

Time resolved stimulated emission spectrum for the 6360-6460 Å region of the afterglow of a 3 atmosphere helium plasma. Data is plotted in units of fractional gain per round trip transit as directly measured from the amplification or attenuation of a dye laser beam reflected thrcugh the afterglow. Time resolution was a uniform 10 nanoseconds and shaded data planes appearing anomalously long result from the overlap of contiguous measurements. The observed gain maximum corresponds to the peak of the P-branch of the $3s\,^3\Sigma_u^+ \rightarrow 2p\,^3\Pi_g$ transition of He_2.

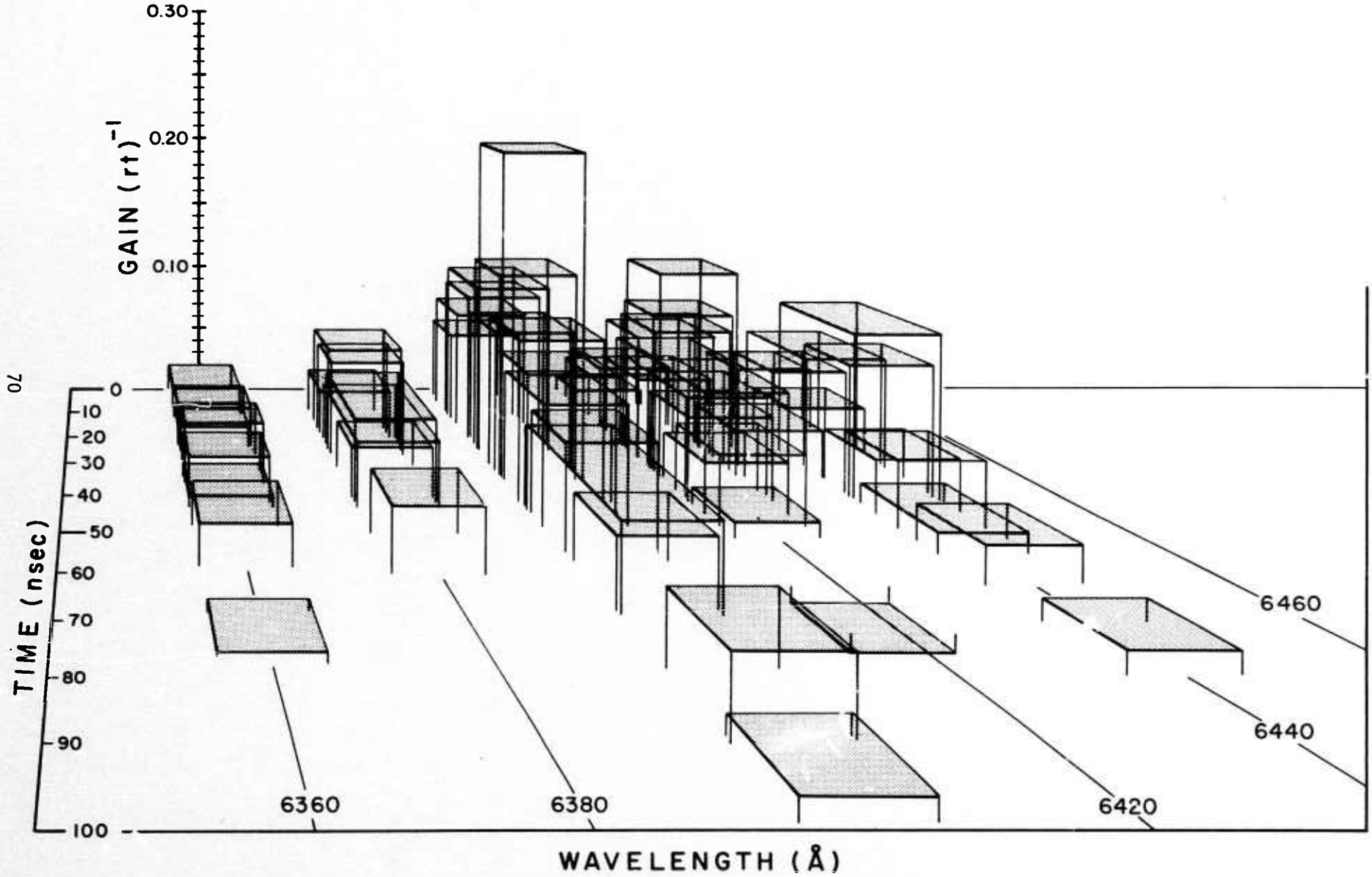
0.30
0.20
0.10
GAIN (rt)$^{-1}$
0
10
20
30
40
50
60
70
80
90
100
TIME (nsec)
6360
6380
6420
6440
6460
WAVELENGTH (Å)

Crossections along (λ,z) planes of Figure 20 give more precisely quantitative representations of the time-dependence of the stimulated emission at each of the wavelengths examined. These are reproduced in Figures 21, a through e, and again are plotted in units of fractional gain per round trip transit at the 0.4 megawatt/liter level of power density. Each elementary measurement appears as a rectangle and the composite nature of the anomalously long data planes of Figure 20 is clearly seen. Conversion of the ordinates to power densities requires only multiplication by the peak dye laser power density of 0.4 megawatts/liter in the sampled volume.

For reference the spectrum of spontaneous emission expected from the same transition in the absence of broadening mechanisms is reproduced in Figure 22 together with its measured time dependence. The peak in gain can be seen, then to correspond to the unresolved Q-branch and lower members of the P-branch of the transition and generally follows the time-dependence of the spontaneous emission. Such observations suggest that the time dependence of stimulation emission in this band reflects almost completely the time-dependent evolution of the general excited state population and not a significant time-dependent change of the pair inversion ratio of the two states involved.

A similar behavior is found to be in the second band in which stimulated emission was observed, that of the $3p\,^1\Pi_g \rightarrow 2s\,^1\Sigma_u^+$ transition at 5130 Å. Topology of the resulting map of gain in the 5100 - 5200 Å wavelength region is shown in Figure 23. Orientation and scale of the view is the same as in Figure 19 but in this case for the blue-green region of the spectrum. For these measurements the power density of the dye laser beam in the probed volume of afterglow was 1.4 megawatts/liter. Time resolution of the data was again 10 nanoseconds and anomalously long data result from the overlap of contiguous measurements.

A peak in gain, broader than that in the 6400 Å band, can be seen to occur around 5170 Å and 30 nanoseconds. A second, earlier peak is also seen

Figure 21

Graphs of the time resolved stimulated emission observed at various wavelengths in the $3s^3\Sigma_u^+ \rightarrow 2p^3\Pi_g$ transition of He_2 formed in the recombination afterglow of an electron beam discharge into three atmospheres of helium. Data is plotted in units of fractional gain per round trip transit as directly measured from the amplification of a dye laser beam reflected through the afterglow. Each measurement appears as a rectangle of width consistent with the time resolution of the measurement system.

a) λ = 6360 Å

b) λ = 6380 Å

c) λ = 6400 Å

d) λ = 6420 Å

e) λ = 6440 Å

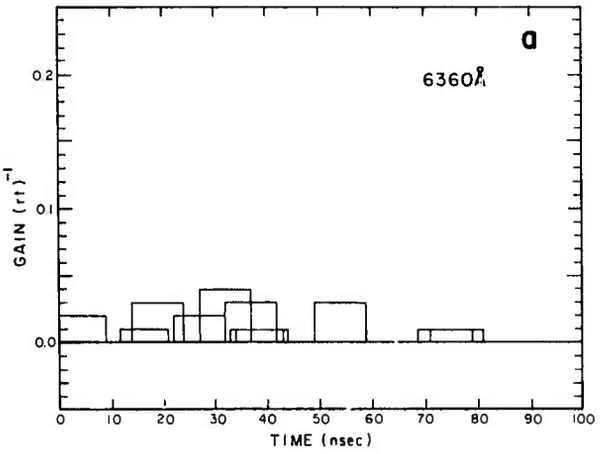
a
6360Å
GAIN (rt)$^{-1}$
0.2
0.1
0.0
0 10 20 30 40 50 60 70 80 90 100
TIME (nsec)

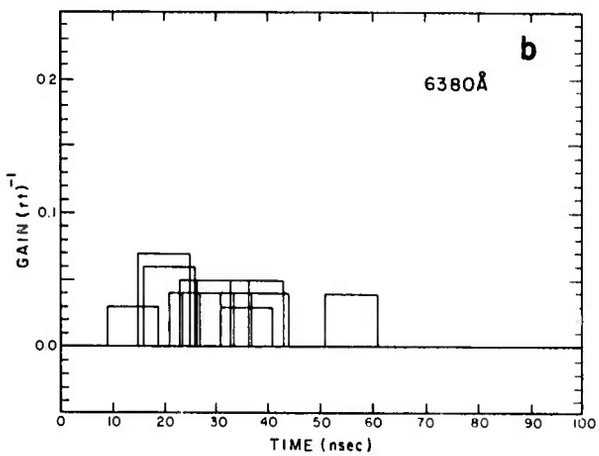
b
6380Å
GAIN (rt)$^{-1}$
0.2
0.1
0.0
0 10 20 30 40 50 60 70 80 90 100
TIME (nsec)

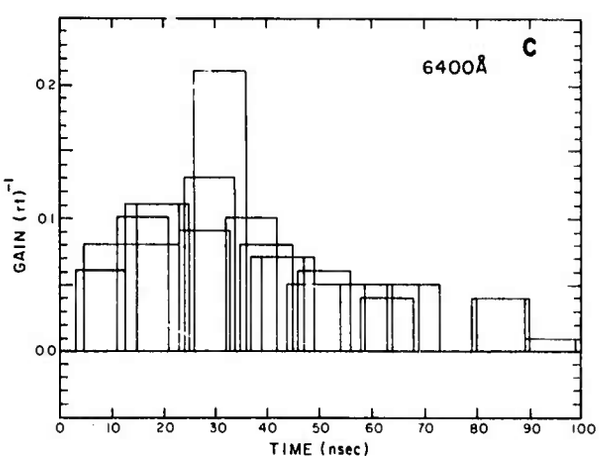
c
6400Å
GAIN (rt)$^{-1}$
0.2
0.1
0.0
0 10 20 30 40 50 60 70 80 90 100
TIME (nsec)

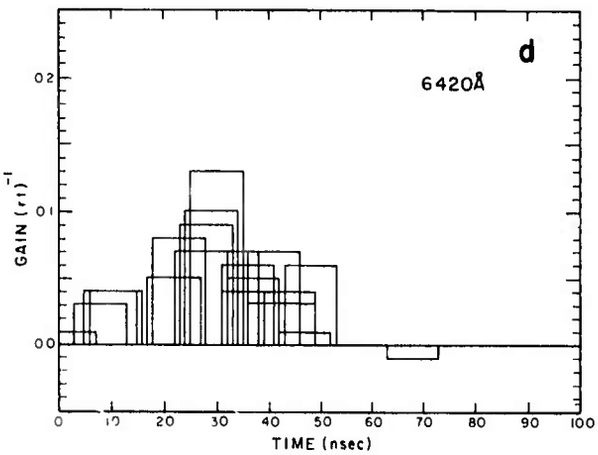
d
6420Å
GAIN (rt)$^{-1}$
0.2
0.1
0.0
0 10 20 30 40 50 60 70 80 90 100
TIME (nsec)

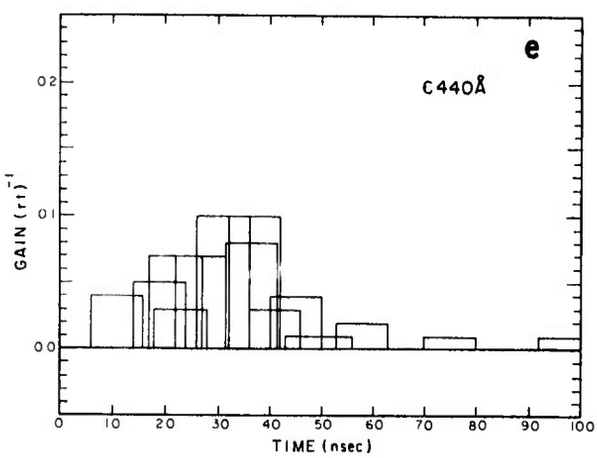
e
6440Å
GAIN (rt)$^{-1}$
0.2
0.1
0.0
0 10 20 30 40 50 60 70 80 90 100
TIME (nsec)

Figures 22

Upper: Typical spectrum expected for spontaneous emission of the $3s^3\Sigma_u^+ \rightarrow 2p^3\Pi_g$ band of He_2, uncorrected for broadening mechanisms. P and R branch members are indicated by the dashed lines to the right and left, respectively, and Q-branch elements are shown by solid lines. Ordinates indicate relative intensities generally expected in spontaneous emission and integers give corresponding J-values of the lower state.

Lower: Comparison of stimulated and spontaneous emissions as functions of time at 6400 Å for excitation conditions corresponding to those giving ——— stimulated emission; - - - spontaneous emission.

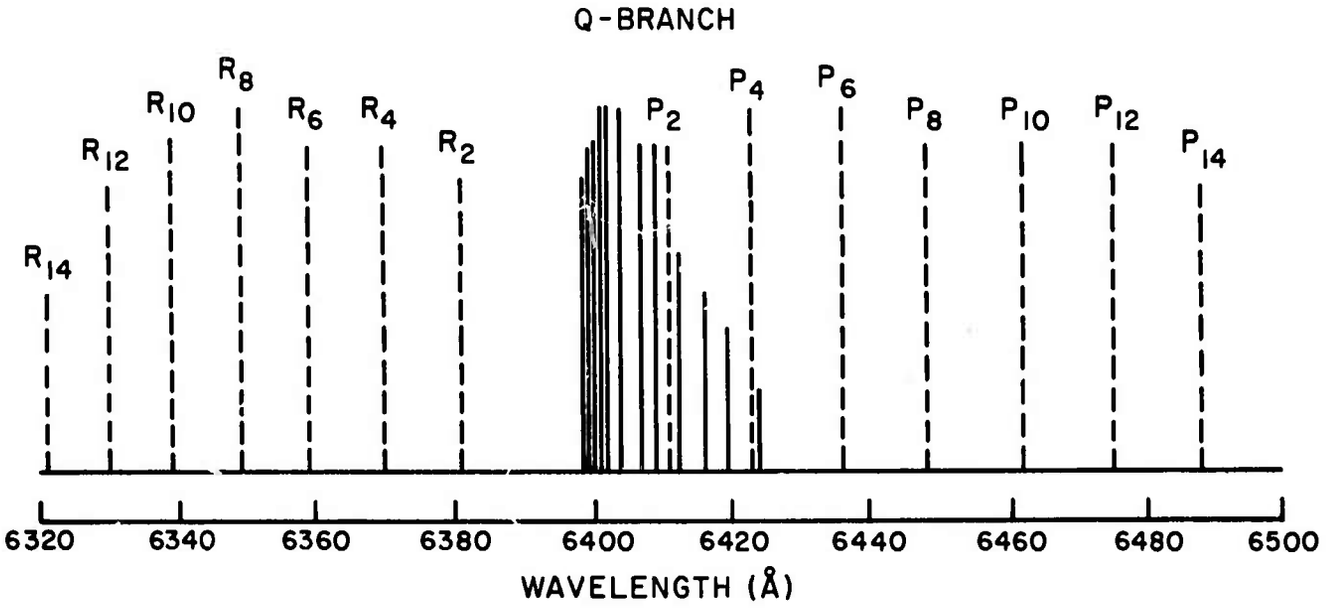
Q-BRANCH
R14
R12
R10
R8
R6
R4
R2
P2
P4
P6
P8
P10
P12
P14
6320
6340
6360
6380
6400
6420
6440
6460
6480
6500
WAVELENGTH (Å)

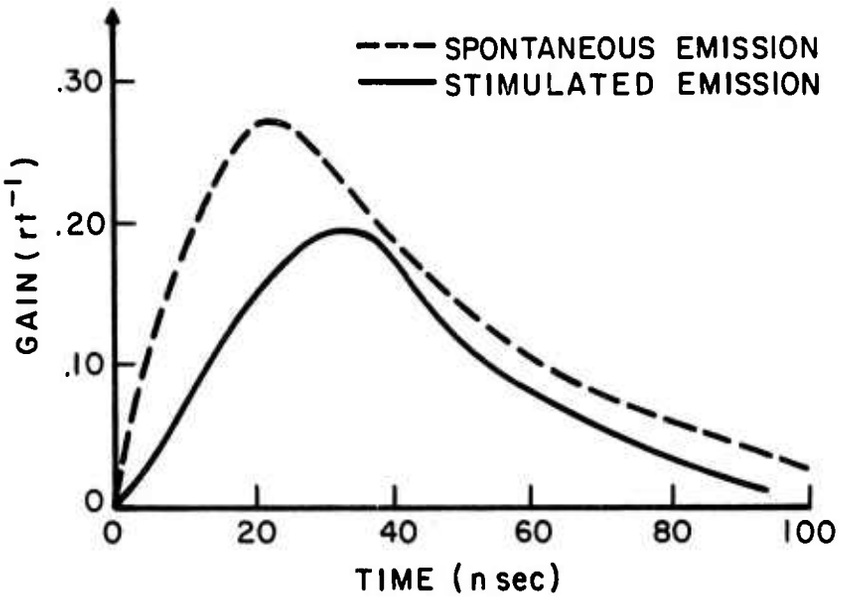
SPONTANEOUS EMISSION
STIMULATED EMISSION
GAIN (rt⁻¹)
.30
.20
.10
0
0
20
40
60
80
100
TIME (n sec)

Figure 23

Time resolved stimulated emission spectrum for the 5100 - 5200 Å wavelength region of the afterglow of a 3 atmosphere helium plasma. Data is plotted in units of fractional gain per round trip transit as directly measured from the amplification or attenuation of a dye laser beam reflected through the afterglow. Time resolution was a uniform 10 nanoseconds and shaded data planes appearing anomalously long result from the overlap of contiguous measurements. The observed gain maximum corresponds to the peak of the P-branch of the $3p\,^1\Pi_g \rightarrow 2s\,^1\Sigma_u^+$ transition of He_2.

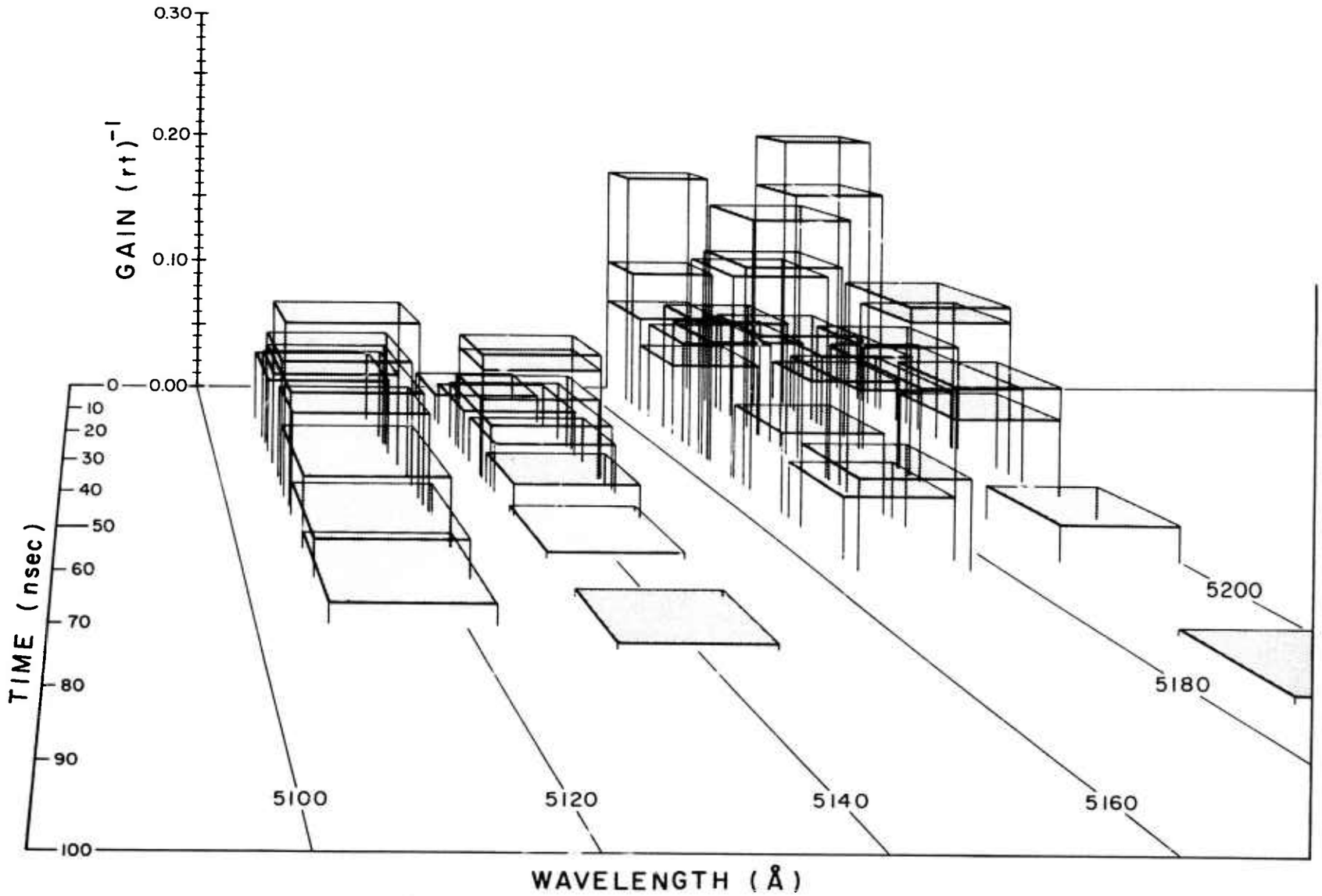
0.30
0.20
0.10
0.00
GAIN (rt)$^{-1}$
0
10
20
30
40
50
60
70
80
90
100
TIME (nsec)
5100
5120
5140
5160
5180
5200
WAVELENGTH (Å)

and it appears that the maximum lies at some time less than the basic 10 nanosecond unit of resolution used in these measurements. As mentioned in Section b previously, this early excitation of the $3p\,^1\Pi_g$ state most probably occurs as a result of the three-body associative reaction of a ground state atom with a $3\,^1P$ atom produced by the primary electron beam,

$$He(3\,^1P) + 2He \rightarrow He_2{}^*(3p\,^1\Pi_g) + He \quad . \qquad (20)$$

Since the normal dissociation limit of the $3p\,^1\Pi_g$ molecular state yields a $3\,^1P$ atom, reaction (20) would require no *ad hoc* potential curve crossings or intermediate collisional relaxation steps. In the absence of long-range "potential humps", the cross section for (20) should be reasonably large; thus, rendering plausible this explanation for the early source of excited He_2 population.

Four sections along (λ,z) planes of Figure 23 are shown in Figures 24. Both in Figures 23 and 24 conversion of the ordinates to power densities of stimulated emission requires only multiplication by the peak dye laser power density of 1.4 megawatts/liter focused into the probed volume of afterglow.

The reference spectrum of the spontaneous emission expected from the same transition in the absence of broadening is shown in Figure 25 together with its measured time-dependence. As can be seen the peak in gain at 5170 Å corresponds to the P(7) component of the spectrum and is not unreasonable in view of the statistical weights and spacings of the rotational levels of the upper $3p\,^1\Pi_g$ state. As in the case of the 6400 Å band, the correspondence between stimulated and spontaneous emission as functions of time suggests that the evolution of the gain parameter is primarily an effect of the change in total excited state population produced by the continuing recombination and collisional relaxation processes.

Figures 24

Graphs of the time resolved stimulated emission observed at various wavelengths in the $3p\,^1\Pi_g \rightarrow 2s\,^1\Sigma_u^+$ transition of He_2 formed in the recombining afterglow of an electron beam discharge into 3 atmospheres of helium. Data is plotted in units of fractional gain per round trip transit as directly measured from the amplification of a dye laser beam reflected through the afterglow. Probing laser power densities were calibrated to be 1.4 megawatts/liter. Each measurement appears as a rectangle of width consistent with the time resolution of the measurement system.

a) λ = 5115 Å

b) λ = 5140 Å

c) λ = 5170 Å

d) λ = 5194 Å

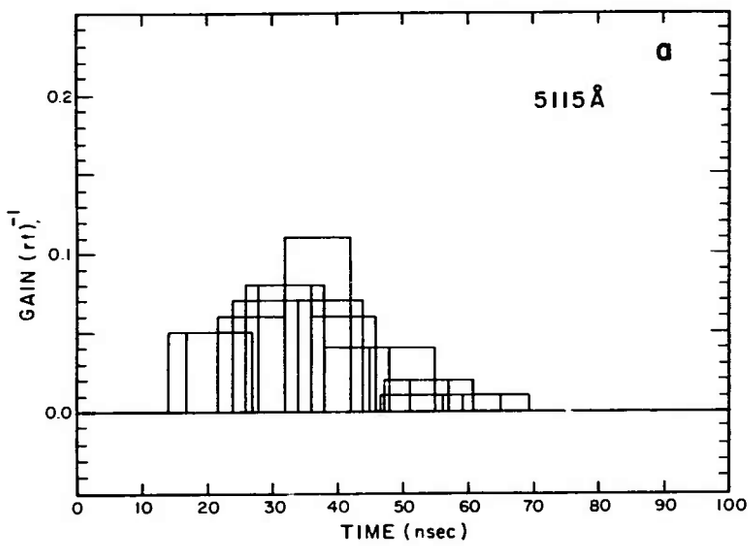
a
5115Å
GAIN (rt)$^{-1}$
0.2
0.1
0.0
0 10 20 30 40 50 60 70 80 90 100
TIME (nsec)

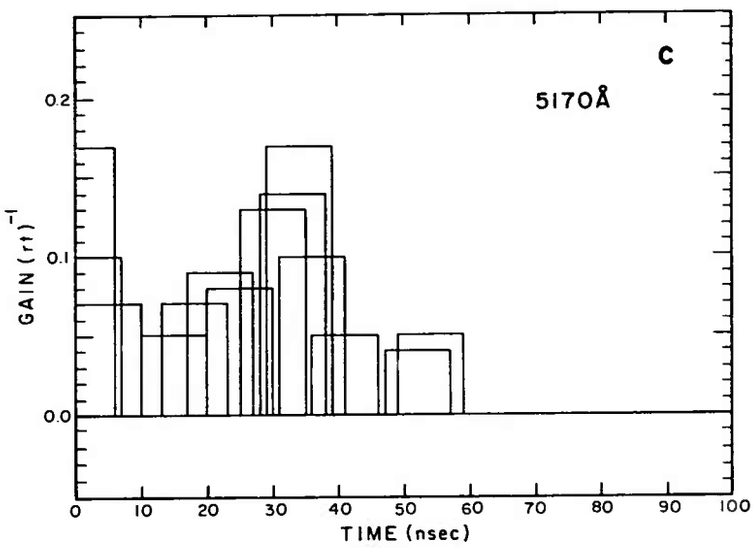
c
5170Å
GAIN (rt)$^{-1}$
0.2
0.1
0.0
0 10 20 30 40 50 60 70 80 90 100
TIME (nsec)

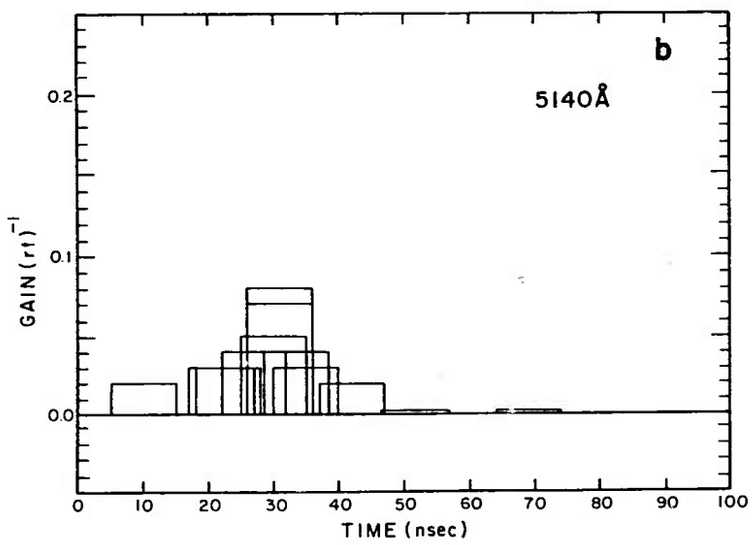
b
5140Å
GAIN (rt)$^{-1}$
0.2
0.1
0.0
0 10 20 30 40 50 60 70 80 90 100
TIME (nsec)

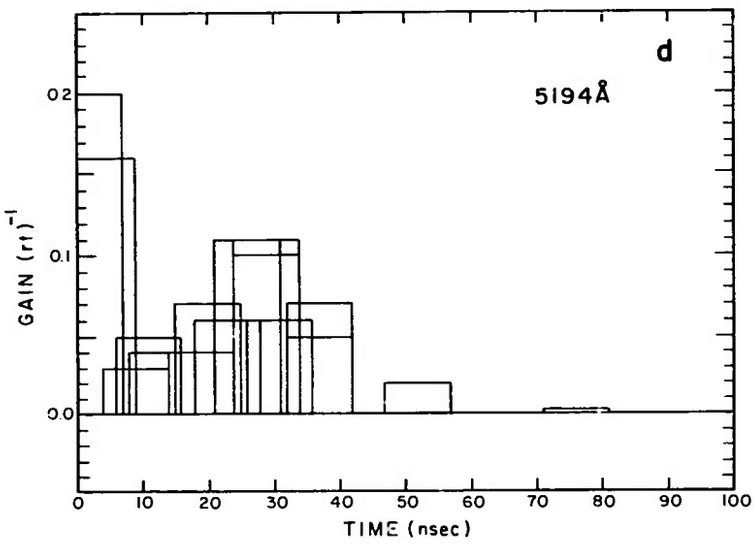
d
5194Å
GAIN (rt)$^{-1}$
0.2
0.1
0.0
0 10 20 30 40 50 60 70 80 90 100
TIME (nsec)

Figures 25

Upper: Typical spectrum expected for spontaneous emission of the $3p\,^1\Pi_g \rightarrow 2s\,^1\Sigma_u^+$ band of He_2, uncorrected for broadening mechanisms. P and R branch members are indicated by the dashed lines to the right and left, respectively, and Q-branch elements are shown by solid lines. Ordinates are proportional to relative intensities generally expected in spontaneous emission and integers give corresponding J-values of the lower state.

Lower: Comparison of stimulated and spontaneous emissions at 5170 Å as functions of time for excitation conditions corresponding to those giving the data of Figures 23 and 24. ——— stimulated emission; --- spontaneous emission.

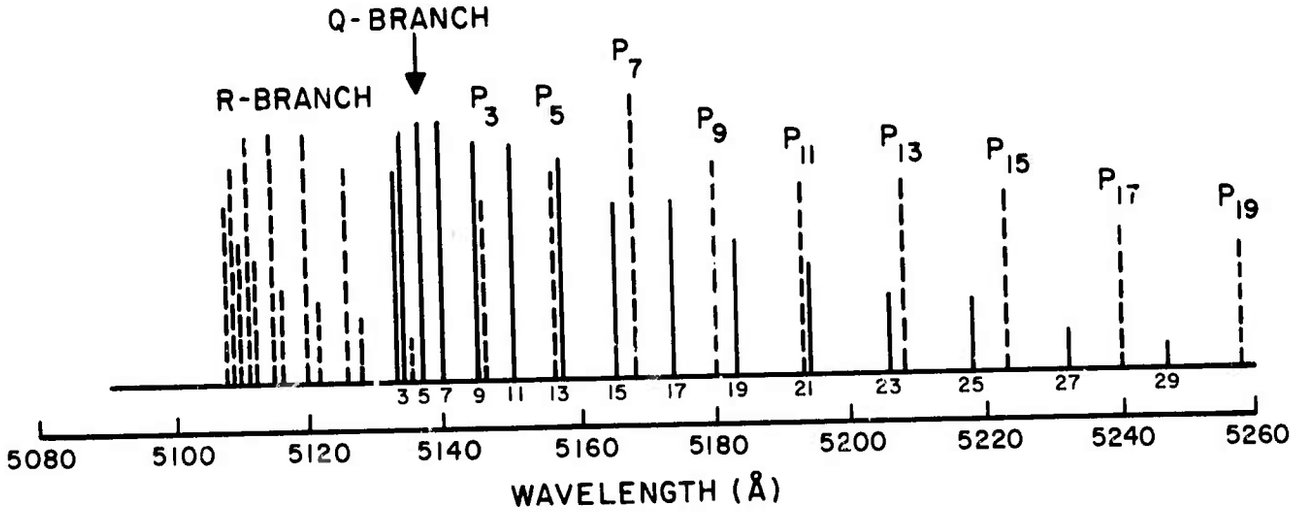
Q-BRANCH
R-BRANCH
P3
P5
P7
P9
P11
P13
P15
P17
P19
3 5 7 9 11 13 15 17 19 21 23 25 27 29
5080 5100 5120 5140 5160 5180 5200 5220 5240 5260
WAVELENGTH (Å)

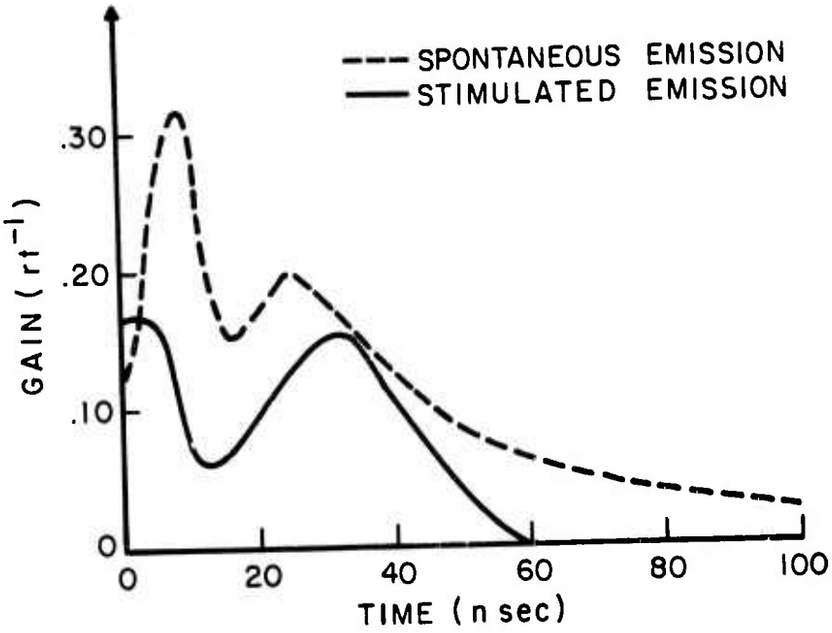
SPONTANEOUS EMISSION
STIMULATED EMISSION
GAIN (rl⁻¹)
.30
.20
.10
0
0 20 40 60 80 100
TIME (n sec)

The absence of an early peak in Figures 24 a and b is not significant, and is only a consequence of the paucity of data at those wavelengths, 5115 and 5140 Å. Extrapolating from the above comments it can be reasonably expected that such a maximum will be found when the data becomes available for those domains of (t,λ).

Further confirmation of the magnitude of the gain in the 6400 Å band was obtained from quantitative observations of the axial intensity emitted from a resonant cavity containing the plasma as a function of cavity length. Cavities were used in which the mean lifetime of a photon in the cavity considerably exceeded the lifetime of the amplifying medium. For these measurements, the dye laser was removed and a dielectric mirror of 99% reflectance at 6400 Å was added. Optics were used having solid angles of acceptance small compared to the solid angle spanned by the forward lobe of the radiation pattern from the cavity. Under these conditions, there is no geometric effect and the axial intensity is simply a function of the number of transits of the plasma a photon can make before the plasma decays and the gain or loss occurring during each transit.

If it is assumed that the small signal extinction coefficient, K, is proportional to the population of the excited states, then after n transits of the afterglow, it will be given approximately by

$$K = K_o e^{-\frac{2n\ell}{c\tau}} , \qquad (21)$$

where ℓ is the length of the resonant cavity and τ is the recombination lifetime. Considering discrete intervals of time equal to the duration of a complete round trip transit the energy, E, in the cavity resulting om the spontaneous emission during the first of these, will after n transits have been attenuated (or amplified) to

$$E(n) = I_o \frac{2\ell}{c} e^{-2K_o\ell \frac{c\tau}{2\ell}(1-e^{-\frac{2n\ell}{c\tau}}) - nL} \qquad (22)$$

where I_o is the initial spontaneous intensity and L is the passive cavity loss per round trip. During the n^{th} pass, the energy emitted axially from the cavity is approximately, $L \cdot E(n)$, assuming losses are primarily due to transmission. Then integrating over all transits, the energy emitted from the cavity as a result of the first increment of spontaneous emission $I_o(2\ell/C)$, is

$$E = \int_o^\infty \frac{\tau}{Q} \; LI_o e^{-2K_o \ell Q(1-e^{-n/Q})-nL} \; dn \quad , \tag{23}$$

where now the parameters have been collected in terms of Q, the probable number of photon transits in a recombination lifetime, and

$$Q = \frac{c\tau}{2\ell} \quad . \tag{24}$$

Through transformation of variables, this becomes

$$E = I_o \tau L e^{-\alpha} \int_o^1 \frac{}{z} \; (QL-1) \; e^{\alpha z} dz, \quad , \tag{25}$$

where $\alpha = 2K_o \ell Q$ the mean fractional intensity decrease, and this is

$$E = I_o \tau L e^{-\alpha} (QL)^{-1} M(QL, QL+1, \alpha) \tag{26}$$

where M is the confluent hypergeometric function.

For gain $\alpha = |\alpha|$ so letting $\beta = -|\alpha|$ and recognizing for each time increment there is an additional emission of spontaneous energy, then the substitutions.

$$I_o \rightarrow I_o e^{-p/Q} \tag{27a}$$

$$K_o \rightarrow K_o e^{-p/Q} \tag{27b}$$

must be made in (26). The resulting total energy emitted axially per pulse then becomes

$$\varepsilon = \int_0^\infty E dp = I_o \tau / Q \int_{\beta_o e^{-p/Q}}^\infty e^{-p/Q} M(QL, QL+1, -\beta e^{-p/Q}) \, dp \qquad (28)$$

Transforming variables, this becomes

$$\varepsilon = I_o \tau \beta_o^{-1} \int_o^{\beta_o} M(1, QL+1, x) dx \quad . \qquad (29)$$

Expanding in terms of the usual infinite series for M(a,b,z) and factoring terms having useful limiting properties gives

$$\varepsilon = \varepsilon_o F(\beta_o, LQ) \qquad (30)$$

where

$$\varepsilon_o = I_o \tau (\beta_o)^{-1} (e^{\beta_o} - 1) \quad , \qquad (31)$$

represents an emitted energy, characteristic of a simplified equivalent plasma of constant spontaneous intensity I_o, and gain per round trip (β_o/Q), (both decreasing discontinuously to zero after a lifetime τ) and a lossless cavity of length allowing Q complete transits during τ. The multiplicative correction function F is given by

$$F(\beta_o, LQ) = (e^{\beta_o} - 1)^{-1} \left\{ \beta_o + \sum_{m=1}^{\infty} \frac{1}{m+1} \frac{(\beta_o)^{m+1}}{(LQ+1)\ldots(LQ+m)} \right\} \quad , \qquad (32)$$

where F is of order unity for small gains and losses.

Data suitable for the evaluation of eq. (30) is shown in Figure 26. In this figure are shown the intensity emitted axially at 6400 Å from the cavity together with the spontaneous emission.

Figure 27 shows a plot of the axial intensity from which the passive

Figure 26

Time resolved enhancements of the intensity at 6400 Å observed in the resonant cavity during single e-beam excitations at three atmospheres of helium. In each photograph the uppermost curve is the enhanced intensity, the center curve is the normal afterglow emission, and the lower curve the background noise. Two different cavity lengths are shown at 46 cm and 29 cm. The horizontal time scale is 40 nanoseconds/division in each case.

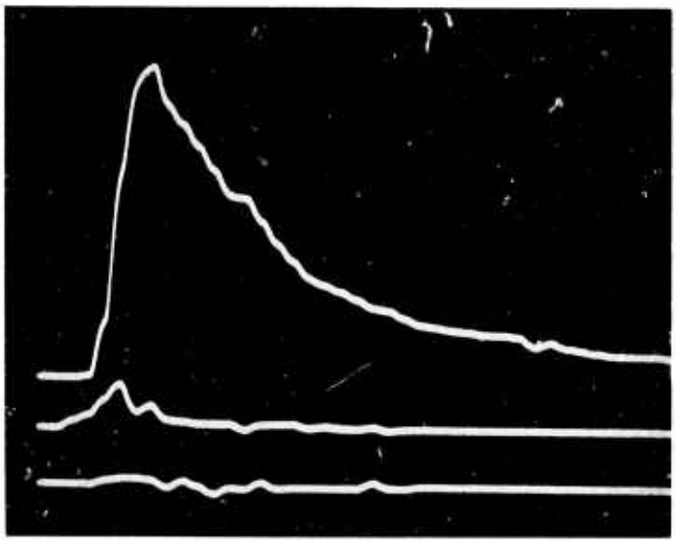

CAVITY
LENGTH
46 cm
RATIO
21:1

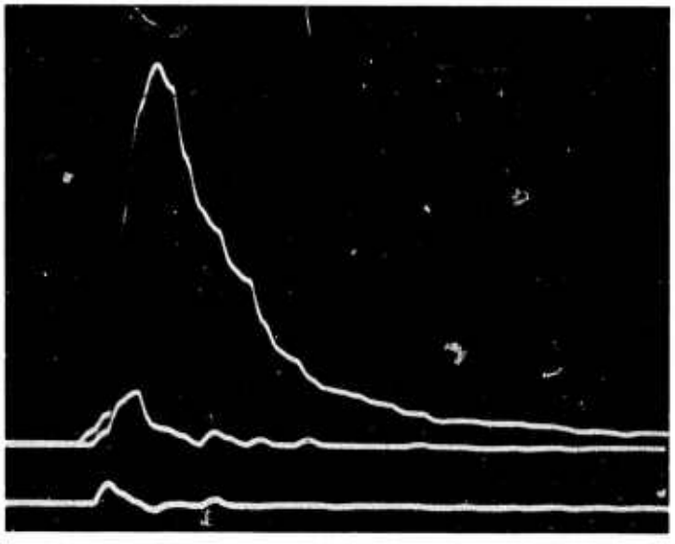

CAVITY
LENGTH
29 cm
RATIO
60:1

Figure 27

Logarithmic plot as a function of time of the intensity emitted axially at 6400 Å for a cavity of 53.3 cm. length. The straight line slope corresponding to a passive loss of 3.0% per round trip is shown.

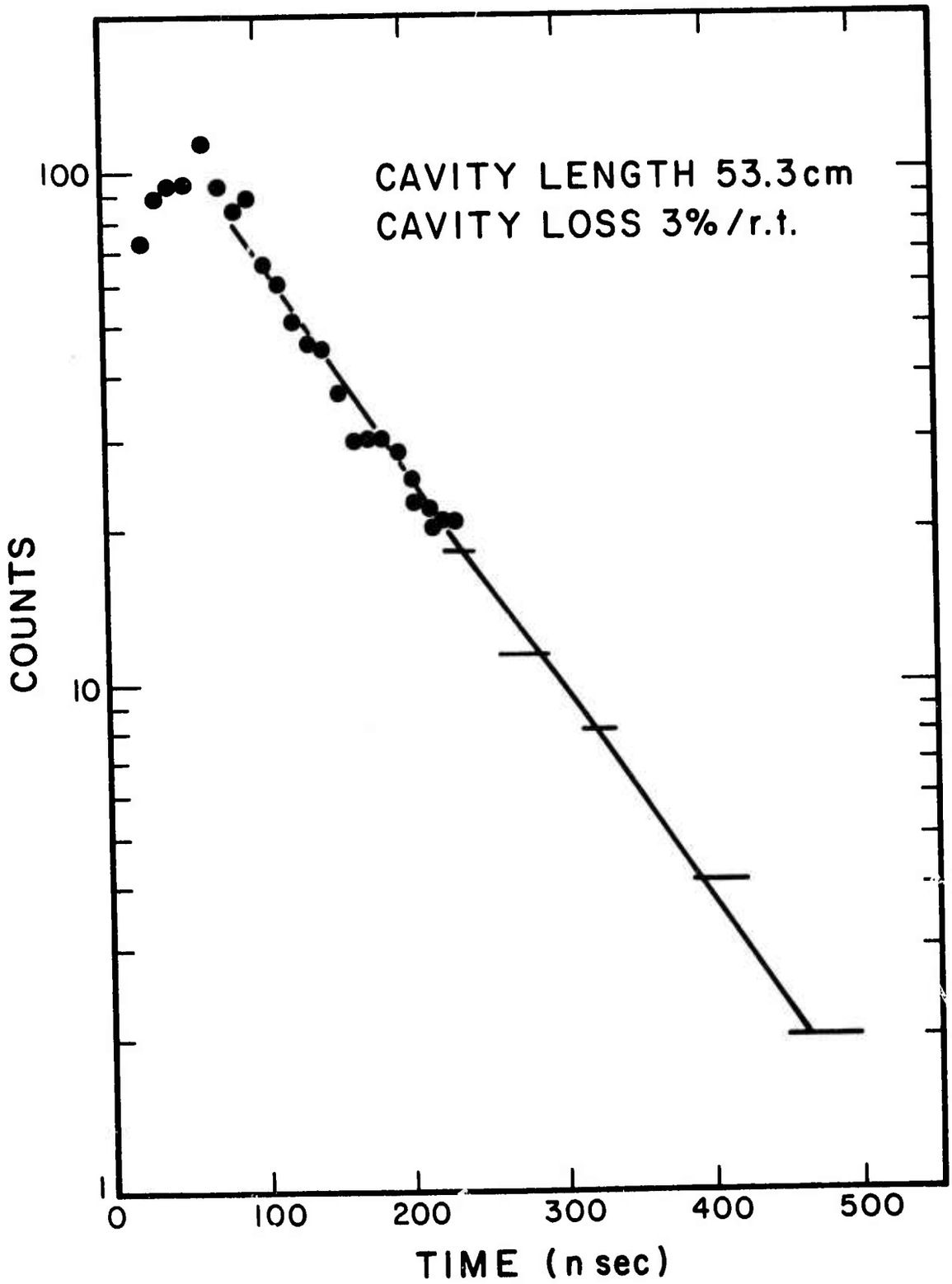
CAVITY LENGTH 53.3cm
CAVITY LOSS 3%/r.t.
COUNTS
100
10
1
0
100
200
300
400
500
TIME (n sec)

cavity loss can be determined. Correlation for various cavity lengths of the exponential decay times for the loss of intensity from the cavity following termination of the discharge afterglow gave a passive cavity loss of 3% per round trip. With this calibration equations (30) through (32) can be evaluated.

Figure 28 summarizes the resulting energy per pulse emitted axially at 6400 Å and normalized to the isotropic incoherent emission from the afterglow for cavities of four different lengths. Shown for comparison are curves modeling the expected growth of pulsed energy from the particular cavity according to (30) when containing an amplifying medium of 0.104, 0.124 and 0.144 (round trip)$^{-1}$ peak gain and corrected according to (32) for a time-dependence of the gain proportional to that observed for the spontaneous emission. The best value at this pressure of 3 atmospheres appears to be 0.124 and corresponds to an average over the 45 Å FWHM bandpass of the 6413 Å interference filter used in the measurement. Comparison with Figure 20 identifies this as the average gain over the Q-branch and lower P-components and provides the agreement with the higher peak values resolved for certain of those components.

It appears the close correlation in the 6400 Å band between the different measurement approaches confirms the existance of significant gain in the He_2 system. Research in progress now is expected to extend this type of direct measurement to the other bands of He_2 at 4400 Å and 4000 Å for other values of pressure.

e) Stimulated Output Efficiencies--The measurements of the previous part d) serve to give the first rough estimates of the efficiency of the stimulated emission observed. At the present time, characterization of the dye laser is incomplete, but the importance of even crude approximations to the output efficiency warrants

Figure 28

Functional dependence on the number of round-trip transits of the cavity made by a photon during the lifetime, τ, of the plasma, of the energy emitted axially per pulse from a resonant cavity enclosing the plasma and normalized to the energy of the spontaneous incoherent radiation. Wavelength was selected by an interference filter centered at 6413 Å with a FWHM of 45 Å and passive cavity losses were 0.03 per round trip. X - experimental date; solid curves--theoretical models given by equations(31) and(32) for values of fractional gain per round trip of 0.104, 0.124, and 0.144 as marked.

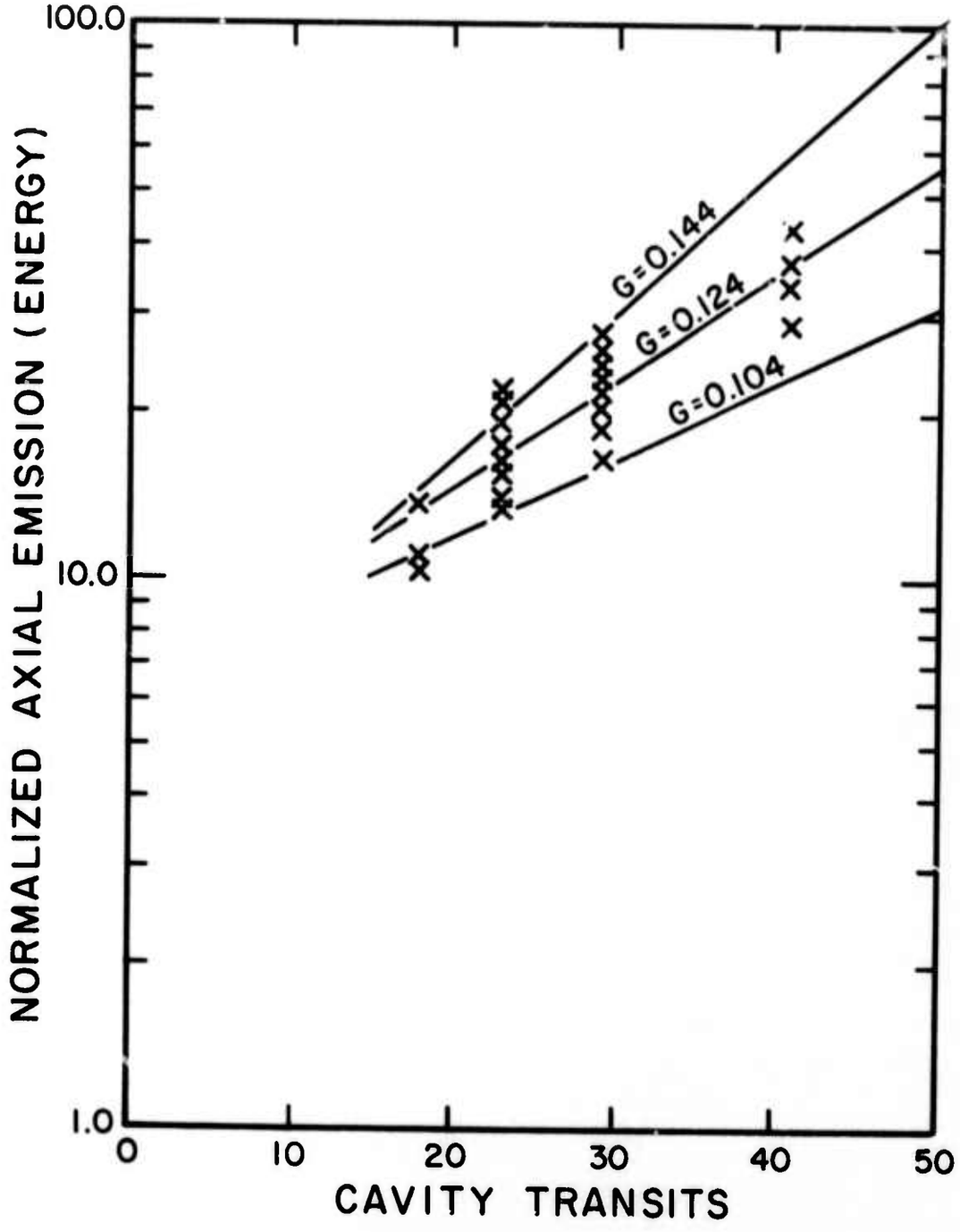
100.0
10.0
1.0
NORMALIZED AXIAL EMISSION (ENERGY)
G=0.144
G=0.124
G=0.104
0
10
20
30
40
50
CAVITY TRANSITS

their tentative use. Collecting the peak fractional gains from Figures 19, 21, and 24, and the probing dye laser power densities (dye laser power/illuminated volume per round trip transit) the data of Table VII was compiled. The theoretical limit shown was obtained from (15b) and the assumption of one photon per ion originally produced by the electron beam. For comparison the energy per pulse emitted spontaneously at 6400 Å is found in Table V to be .052 mJ/liter. The corresponding value from Table VII of 35 mJ/liter for stimulated emission clearly indicates that the energy normally lost during the recombination to non-radiative channels of stabilization can be returned to an induced channel as stimulated emission. Whether values of stimulated emission can be finally raised to the theoretical limit of one photon per ion shown in Table VII will be determined by probing at higher power densities. Although this has not been done yet, recent comparative measurements at lower powers are encouraging as they indicate no evidence of saturation of the transition at the higher powers. Figures 29 illustrate this point for the 5170 Å band. Two graphs of gain are shown as functions of time for probing powers differing by a factor of 100. This data was obtained by repeating the measurements shown in Figure 24 c with a calibrated neutral density filter in the probing beam. To within statistical error no difference is seen in the fractional gains. The situation is summarized in Figure 30 where the energy of stimulated emission is shown as a function of probing power density together with the horizontal line indicating the maximum energy theoretically available. The dashed line connects the measurements with unit slope and re-emphasizes the absence of any evidence of saturation of the transition at these power levels.

Considering finally the indicated system efficiencies, from Table VI, it can be seen the increased energy of stimulated emission raises those efficiencies to

$$\varepsilon(6400\ \text{Å}) \geq 0.6\% \qquad (33)$$

TABLE VII

Energy and Peak Power

Extracted from the 3 Atmosphere

Recombining Helium Afterglow

Wavelength Å	Probing Power (Megawatts/liter)	Power Extracted (Megawatts/liter)	Energy Extracted (mJ/liter)	Theoretical Limit (mJ/liter)
6400 (preliminary)	25 (est)	5.8	35	527
6400	0.4	0.092	0.55	527
5170	1.4	0.25	1.5	652

Figures 29

Graphs of time-resolved stimulated emission at 5170 Å from a 3 atmosphere helium afterglow. Data is plotted in units of fractional gain per round trip transit as directly measured from the amplification of a dye laser beam reflected through the afterglow at two different probing power densities.

Upper Curve: Probing power density = 1.4 megawatts/liter

Lower Curve: Probing power density = 0.014 megawatts/liter

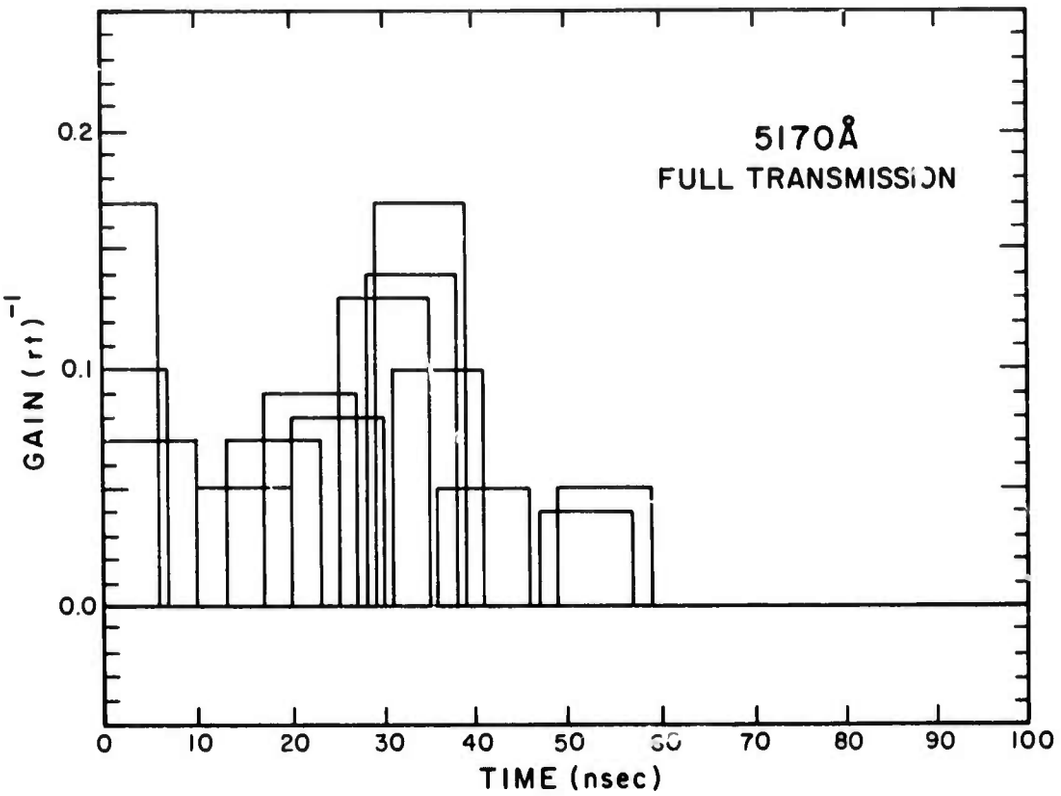
5170Å
FULL TRANSMISSION
GAIN (rt)$^{-1}$
0.2
0.1
0.0
0
10
20
30
40
50
60
70
80
90
100
TIME (nsec)

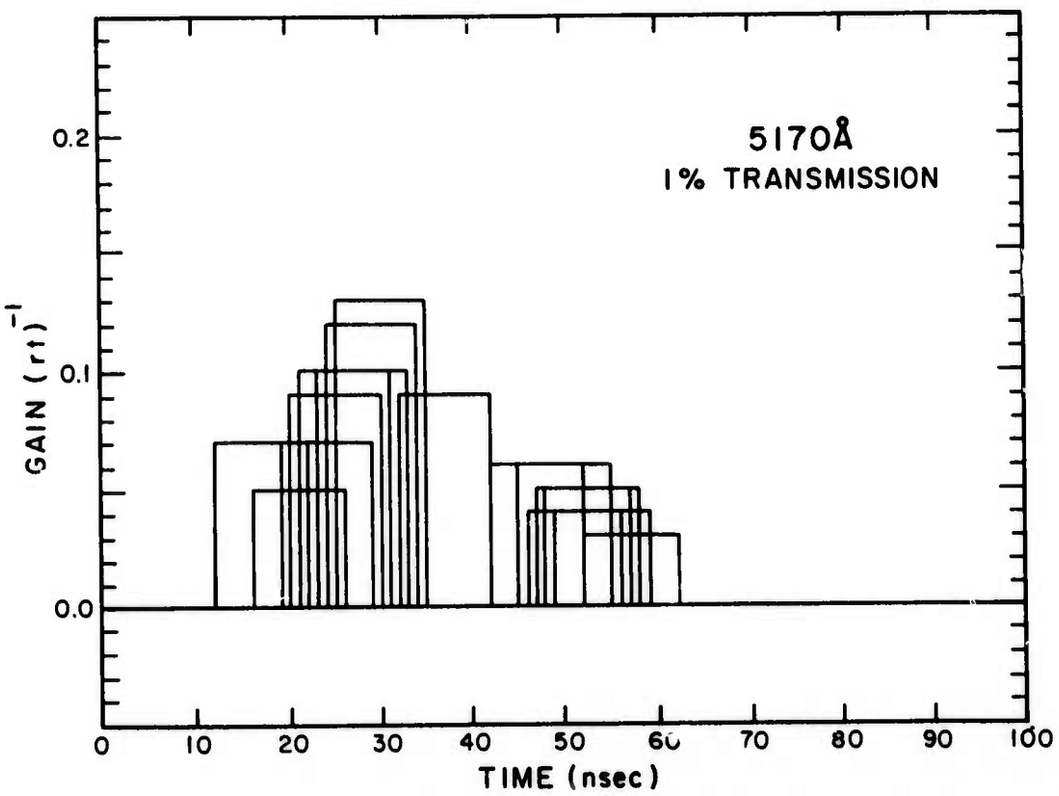
5170Å
1% TRANSMISSION
GAIN (rt)$^{-1}$
0.2
0.1
0.0
0
10
20
30
40
50
60
70
80
90
100
TIME (nsec)

Figure 30

Logarithmic graph of the energy per pulse extracted from the 3 atmosphere helium afterglow at 5170 Å as a function of power density focused into the plasma by the probing laser beam. The horizontal line at the top indicates the maximum energy theoretically available to the transition under these experimental conditions. The dashed line provides a reference slope of 1.

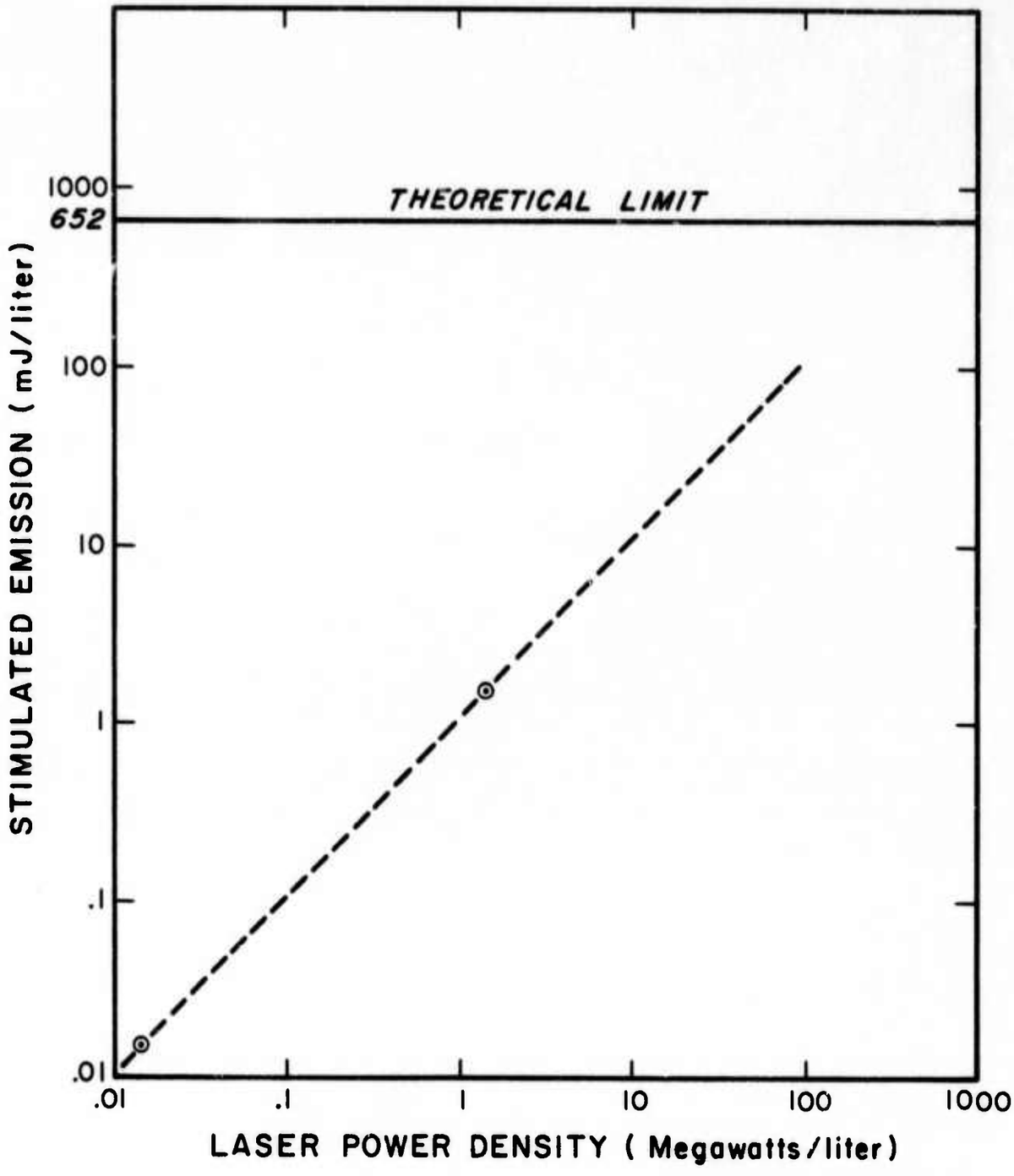
THEORETICAL LIMIT
652
1000
100
10
1
.1
.01
STIMULATED EMISSION (mJ/liter)
.01
.1
1
10
100
1000
LASER POWER DENSITY (Megawatts/liter)

for the best overall value of efficiency of stimulated emission at 6400 Å obtained to date. As in the case of the data of Figure 30 for 5170 Å, the real limit to efficiency will only be determined when data is available at high enough power to show a bending of curve from which an asymptote can be estimated. As there is no evidence saturation is occurring yet, it can be expected that a further reduction in the cross-section of the probing beam will raise efficiencies close to the theoretical values of Table I. The implications of these results are discussed in the following section.

V. IMPLICATIONS

The most evident implication of the technical results presented in the previous section is that since stimulated emission has been observed with a significant extraction of energy, the feasibility of a recombination laser has been demonstrated. Had a longer gain-path length been available for the duration of the afterglow lifetime, a laser would have been realized for each of the two wavelengths examined, 6400 and 5170 Å. The more subtle implications are, perhaps, even more important. In particular:

(1) The results summarized in Table IV suggest that in helium collisional recombination does in fact offer a mechanism for optically recovering the majority of the excitation energy lost to ionization and wasted in analogous N_2 and H_2 e-beam laser systems.

(2) The relatively short lifetimes summarized for the He_2 system in Table III indicate that these are in fact recombination lifetimes, and the possibility of unrealized higher order terms slowing the recombination has not yet become a problem at 7 atmospheres. This is of considerable significance, as is indicated in Figure 6, because now the range of parameters spanned by extrapolations to the objective lifetime of a nanosecond is small compared to the range over which measurements are available.

Neither the reheating of the electrons by the stabilizing processes nor an unexpected saturation of the sequence has become a problem. As can be seen, the experimental points on the 1 to 7 atmosphere interval are consistent with theoretical calculations at an electron temperature of 1000°K. This temperature is in turn consistent with the extrapolations of the thermal economy calculations[14,15] which predict the degree of temperature rise produced by the superelastic stabilizing collisions.

Clearly there is a much stronger basis for extrapolating the results of both experiments at 0.1 atmosphere and 3.0 atmospheres to a lifetime of a few nanoseconds at 20 atmospheres than there was initially on the basis of the first measurement alone. In fact, the recombination rate coefficient corresponding to the 75 nanosecond lifetime and electron density

$$[e] = 5 \times 10^{14} \text{ cm}^{-3} \tag{36}$$

is

$$\alpha = 2.7 \times 10^{-8} \text{ cm}^{3} \text{ sec}^{-1}$$

and represents one of the largest values measured for collisional recombination in the absence of dissociative recombination. It is confirming evidence that the parametric forms such as (4) can indeed be considered valid to such large values.

(3) The implication of the rather low efficiencies for the incoherent emission of radiation from the recombination as shown in Table VI is that much of the stabilization is carried by non-radiative collisional channels. However, in this case, the prospect for reducing the importance of such channels by the competition from a lasing channel is good in view of the high preliminary values of gain and the much higher efficiency, 0.6%, for the extraction of stimulated emission. Figure 31 presents the comparison of experiment and theory as a guide to potential extrapolation of energy available in the 6400 Å band. In the present experiment spontaneous emission is about three orders of magnitude below the energy corresponding to the quantum efficiency of the transition. The improvement introduced by stimulating the transition is seen to be substantial and in the rough approximations of Section IV e) appear to bring the energy extracted to within 20% of that theoretically

Figure 31

Energy/liter per pulse as a function of gas pressure calculated to be available to the 6400 Å transition in He_2 in the afterglow of the recombining e-beam discharge. The experimental points reported in this paper for spontaneous emission are shown by the open circles. The plus mark records the comparable value for the stimulated emission.

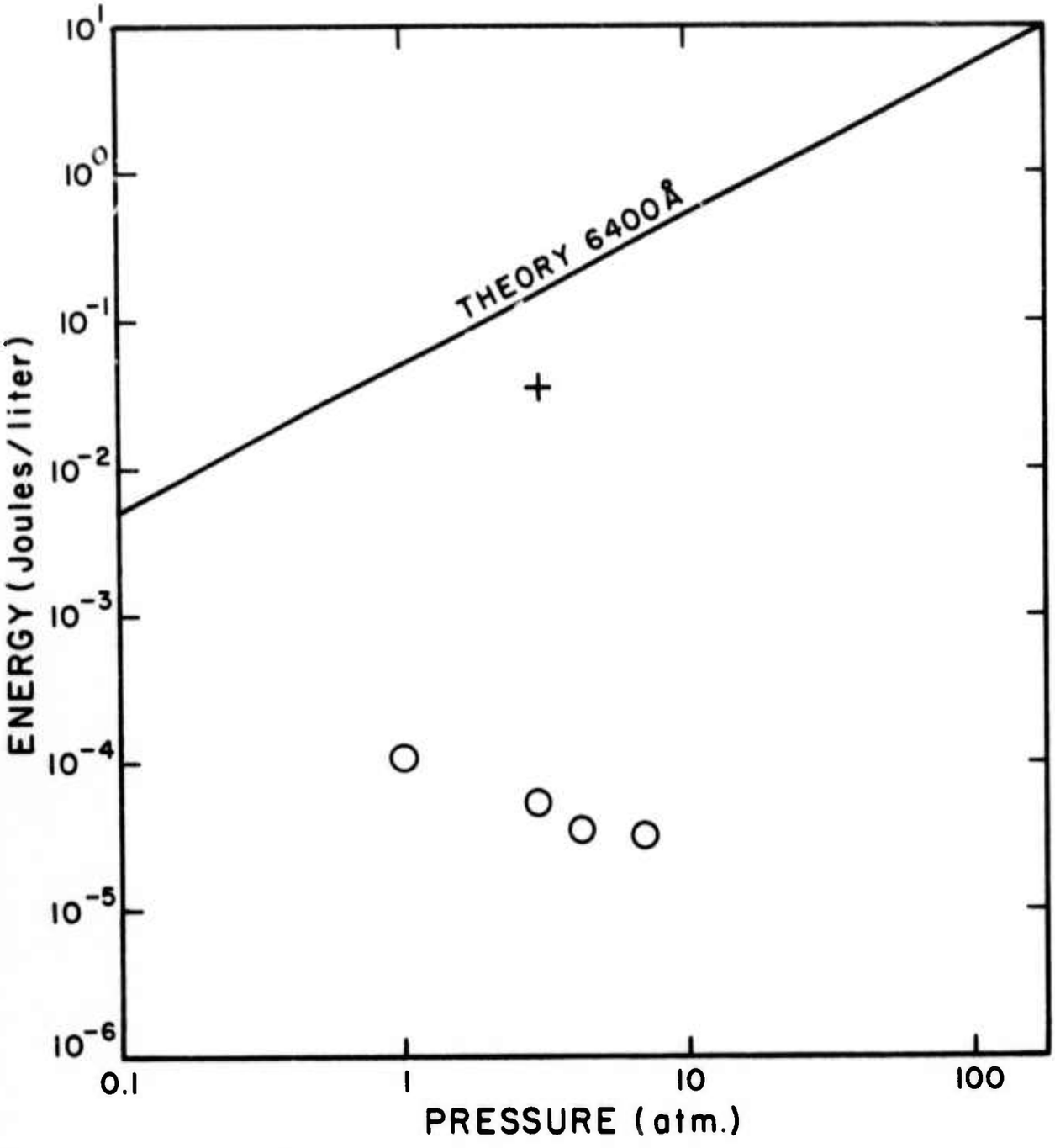
10^{1}
10^{0}
10^{-1}
10^{-2}
10^{-3}
10^{-4}
10^{-5}
10^{-6}
ENERGY (Joules/liter)
THEORY 6400Å
0.1
1
10
100
PRESSURE (atm.)

available. The further confirmation of these indications carries the highest priority as does their extension to shorter wavelength regions.

In summary it appears that the stimulated emission observed in this work confirms the importance of the collisionally stabilized mechanism as a source of population inversion of significance to the development of new types of high energy lasers depending upon electron beam excitation at high gas densities.

REFERENCES

1. C. B. Collins, A. J. Cunningham, and B. W. Johnson, Recombination Laser, Report No. UTDP A002-3,ONR Contract No. N00014-67-A-0310-0007, 1973.

2. C. B. Collins, A. J. Cunningham, S. M. Curry, B. W. Johnson, and M. Stockton, Appl. Phys. Lett. (publication pending).

3. C. B. Collins, Recombination Laser, Report No. UTDP A002-1, ONR Contract No. N00014-67-A-0310-0007, 1973

4. C. B. Collins, A. J. Cunningham, and B. W. Johnson, Recombination Laser, Report No. UTDP A003-1, ONR Contract No. N00014-67-A-0310-0007, 1973.

5. D. R. Bates, A. E. Kingston, and R. W. P. McWhirter, Proc. Roy. Soc. (London) A267, 297 (1962).

6. D. R. Bates and S. P. Khare, Proc. Phys. Soc. (London) 85, 231 (1965).

7. C. B. Collins, Phys. Rev. 177, 254 (1969).

8. C. B. Collins, Phys. Rev. 186, 113 (1969).

9. D. R. Bates and A. E. Kingston, Planet. Space Sci. 11, 1 (1963).

10. J. Berlande, M. Cheret, R. Deloche, A. Gonfalone, and C. Manus, Phys. Rev. A1, 887 (1970).

11. E. Hinnov and J. G. Hirschberg, Phys. Rev. 125, 795 (1962).

12. C. B. Collins, H. S. Hicks, W. E. Wells, and R. Burton, Phys.Rev. 6, 1545 (1972).

13. C. B. Collins, H. S. Hicks, and W. E. Wells, Phys. Rev. A2, 797 (1970).

14. D. R. Bates and A. E. Kingston, Proc. Roy. Soc. A279, 10 (1964).

15. D. R. Bates and A. E. Kingston, Proc. Roy. Soc. A279, 32 (1964).

16. A. J. Cunningham, B. W. Johnson, and C. B. Collins, Phys. Lett. 45A, 473 (1973).

APPENDIX I
Reprint of Phys. Lett. 45A, 473 (1973)

AFTERGLOW OF AN E-BEAM DISCHARGE IN SEVERAL ATMOSPHERES OF HELIUM☆

A.J. CUNNINGHAM, B.W. JOHNSON and C.B. COLLINS
The University of Texas at Dallas, Dallas, Texas 75230, USA

Received 18 July 1973

Spectral observations of recombining helium afterglows at neutral pressures in the range 1 to 7 atmospheres and initial electron densities of 5×10^{14} cm^{-3} are presented.

The possibility [1] of obtaining population inversion through collisional-radiative recombination of hydrogenic ions with electrons emphasizes the importance of the basic study of this recombination process in dense afterglows. We report the preliminary characterization of the spectra emitted from a recombining helium afterglow at neutral pressures from 1 to 7 atmospheres and an initial electron density of 5×10^{14} cm^{-3}. In contrast to previous studies [2, 3] this work provides the first direct observation of radiation, consistent with a recombination origin, emitted from a dense helium afterglow.

A Febetron 706 electron beam gun was used to create the primary ionization in the test gas. Single pulses of 500 keV peak energy, 8 kA peak current, and 3 nsec duration were projected through a titanium foil window into a rectangular tests cell of standard UHV grade construction. Quartz windows on opposite side faces allowed spectroscopic observations from a lamina of plasma, transverse to the e-beam excited, by the primary electrons.

Fig. 1 shows the spectra obtained. Peak incoherent energy occurred at 5875 Å and peak incoherent power at 6400 Å. The transient intensity dependence for 100 Å regions of the spectrum was monitored using an *f*/4 spectrograph together with a photomultiplier of 1.5 nsec rise time. Each of the spectral features observed showed at least one of three basic transient responses corresponding to different excitation mechanisms, as summarized in fig. 2. Decay times for all molecular transitions were equivalent to within experimental precision, but atomic decay times varied from the molecular value to much longer times.

☆ This research was supported by the U.S. Advanced Research Projects Agency of the Department of Defence and monitored by ONR under Contract No. N00014-67-A-0310-0007.

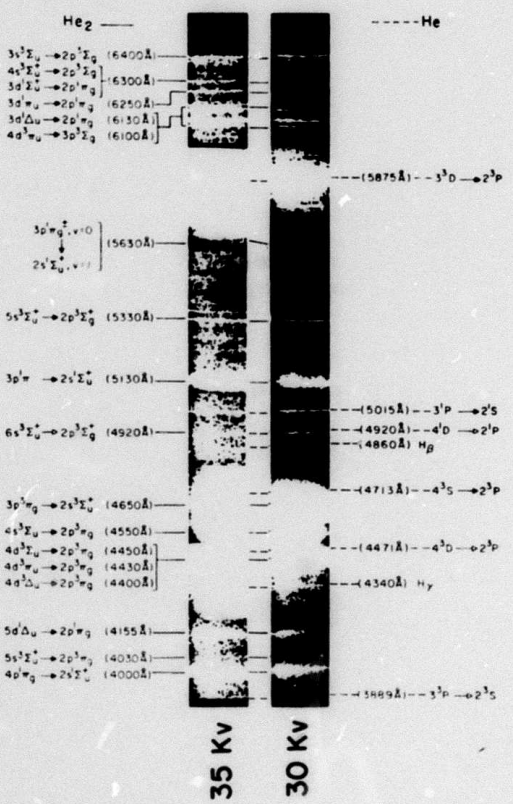

Fig. 1. Survey spectrum recorded with an *f*/4 spectrograph-image intensifier combination at two different image intensifier accelerating voltages of 30 and 35 kV. Each spectrum is a time integrated record of the afterglow from a single discharge of the e-beam gun in helium at three atmospheres pressure.

The decay times attributed to ion-electron recombination can be compared by starting from the general

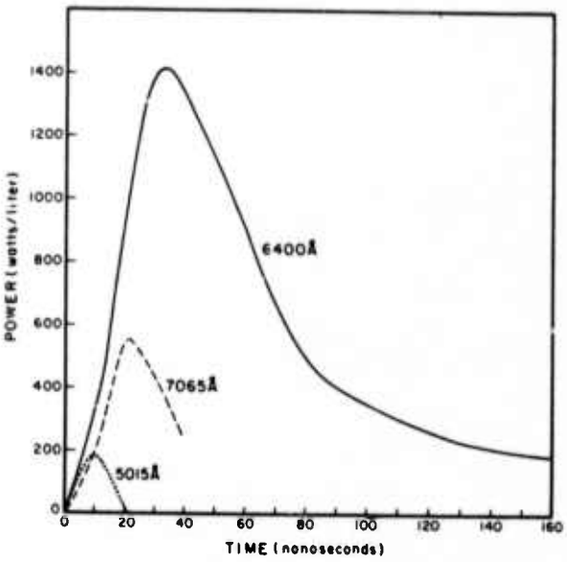

Fig. 2. Time evolution of selected atomic and molecular emissions illustrating the three basic excitation mechanisms observed: 1) 5015 A atomic transition, direct excitation by primary electrons; 2) 7065 A atomic transition, excitation energetic secondary electrons and 3) 6400 A molecular transition, excitation via recombination of He_2^+ ions and cool secondary electrons.

parametrization [4] for the effective recombination rate coefficient, α,

$$\alpha = K[e]^{\eta}(T_e/300)^{-9/2} \qquad (1)$$

where $[e]$ is the free electron concentration, T_e the electron temperature, and η an exponent between 0.0 and 1.0 which reflects the two or three body character of the recombination, respectively. This gives the intensity model

$$\frac{d}{dt}\left[I - \frac{1+\eta}{2+\eta}\right] = (1+\eta)\left[I_0 - \frac{1+\eta}{2+\eta}\right]\tau^{-1} \qquad (2)$$

Table 1
Lifetimes (nanoseconds) against recombination of the principal spectral features of the high pressure helium afterglow.

Wavelength			Pressure (atm.)			
			1	3	4.2	7
6400 A	He_2		160	82	59	26
4650 A	He_2		130	82	53	34
7065 A	He		–	267	350	93
6678 A	He		208	100	45	29
5875 A	He	Early	880	490	425	300
		Late	2800	3800	2700	2320

where I is the time-varying intensity with initial value I_0 and τ^{-1} is the inverse of the effective lifetime against recombination at the time corresponding to I_0. Effective lifetimes are then determined from the linear portion of graphs of the inverse intensity to a single power as a function of decay time and are shown in table 1.

These results demonstrate the importance of the afterglow period to the radiative economy of such high density, electron beam discharges. They also confirm the significance of the recombination mechanism as a source of excited state population, leading to the potential of much high system efficiencies for high energy gas lasers.

References

[1] C.B. Collins, A.J. Cunningham and B.W. Johnson, Abstracts 25th Gaseous electronics Conf., London, Ont. Canada, 1972, p. 153.
[2] F. Robben and E. Hagberg, Aktibolaget Atomenergi, Stockholm, Report No. TDM-FFA-762, 1967 (unpublished).
[3] M. Bourène and J. LeCalvé, J. de Phys. 32 (1971) 29.
[4] C.B. Collins, H.S. Hicks and W.E. Wells, Phys. Rev. A2 (1970) 797.

Appendix II

Preprint for Appl. Phys. Lett. (pending)

Stimulated emission from the recombining afterglow of an electron-beam discharge in several atmospheres of helium*

C. B. Collins, A. J. Cunningham, S. M. Curry, B. W. Johnson, and M. Stockton

The University of Texas at Dallas, Dallas, Texas 75230
(Received 9 November 1973)

Stimulated emission from excited states of He_2 has been observed as a consequence of the collisionally stabilized recombination of He_2^+ ions with electrons in the afterglow of a pulsed gigawatt electron-beam discharge into 3 atm of helium. Peak gains of the order of 0.04 cm^{-1} were found in components of the $3s\,^3\Sigma_u^+ - 2p\,^3\Pi_g$ transition of He_2 in the 6400-Å region by directly measuring the time-resolved gain spectra using a tunable dye laser.

Because of the possibility[1] of obtaining population inversion as a consequence of the collisionally stabilized recombination of hydrogenic ions with electrons, a considerable importance has been attached to the basic study of this recombination process in very dense high-pressure afterglows. A preliminary characterization of the time-dependence spectra emitted from an electron beam-excited helium afterglow at atmospheric pressures has been reported.[2] Observations of the incoherent spontaneous emission showed general agreement with an extrapolated collisional-radiative recombination model which had been found adequate to describe[3-5] the recombination of He_2^+ ions with electrons in the afterglows of conventional low-pressure helium discharges.

Recombination lifetimes leading to the production of excited states of He_2 were determined to be 160, 80, and 26 nsec at 1, 3, and 7 atm.[2] At 3 atm for an electron density of 5×10^{14} cm^{-3} and an electron temperature of 1000 °K the effective two-body rate coefficient was 2.7×10^{-8} cm^{-3} sec^{-1}. Under these conditions the resulting populations of several pairs of levels of He_2 are found to be inverted and stimulated emission is observed. Gains of the order of 0.04 cm^{-1} for the unresolved head of the Q branch and the P_4 and P_6 components of the $3s^3\Sigma_u^+ - 2p^3\Pi_g$ transition of He_2 are reported here.

In this experiment the primary ionization of the high-pressure helium was produced by a 3-nsec electron beam of 8-kA peak current at 500 kV. It was discharged by a Febetron 706 into a stainless steel cell through a titanium foil window of 0.001-in. thickness welded to one end face of the cell. The experimental cell was of standard UHV construction and could be evacuated to 10^{-11} Torr and baked to 400 °C. It was fitted with sapphire windows on opposite faces, with the optical axis perpendicular to the e-beam. This geometry allowed for the probing of a lamina of plasma excited by primary electrons which have penetrated equal distances into the cell. The optical axis was terminated on one side of the plasma with a dielectric mirror fixed immediately inside the cell from the sapphire window to provide for the return of a probing laser beam.

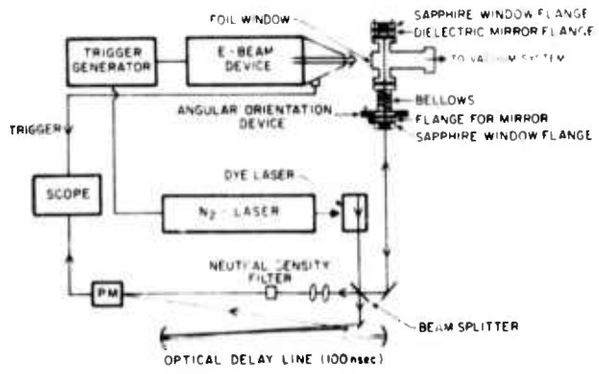

FIG. 1. Experimental system for the direct measurement of gain spectra.

Since the lifetimes for the source of molecular emissions ranged from 160 nsec at 1 atm to 26 nsec at 7 atm, it was necessary to use a rapidly pulsed light source for the measurement of small-signal gain or absorption in a particular transition during the afterglow period. A nitrogen-laser-pumped tunable dye laser with a FWHM of a few angstroms was used in the differential path arrangement shown in Fig. 1 to measure the attenuation or amplification of the beam reflected through the plasma by the internal dielectric mirror. Use of the optical delay line in the reference path allowed for the detection of both beams with a single photomultiplier and electronics system, thus minimizing the drift of the balance of sensitivity between the paths. The resulting system stability was of the order of 6% with timing jitter between the e-beam and the dye laser being of the order of a recombination lifetime. However, as the accuracy of the timing measurement was around 4 nsec, adequate resolution of the particular phase of the afterglow sampled by the dye laser beam could be established.

Figure 2 shows the topology of the map of gain resulting from measurement at 3 atm pressure over the space of parameters indicated. Across the xz plane to the rear of the data has been plotted the time dependence of the spontaneous emission for scale. For comparison on the yz plane to the left edge is shown the normal emission spectrum of the $3s^3\Sigma_u^+ - 2p^3\Pi_g$ transition, uncorrected for pressure and Stark broadening. As can be seen the R branch is absorptive while highest gains are found in the Q-branch head and P_4 and P_6 components. Higher members of the P branch appear absorptive. Units plotted are the gain coefficient per round-trip transit of the afterglow, so that the peak gain of 0.23 measured at the head of the Q branch corresponds to a value of 0.04 cm^{-1} at 6400 Å.

Further confirmation of the magnitude of the gain was obtained from observation of the axial intensity emitted from a resonant cavity containing the plasma as a func-

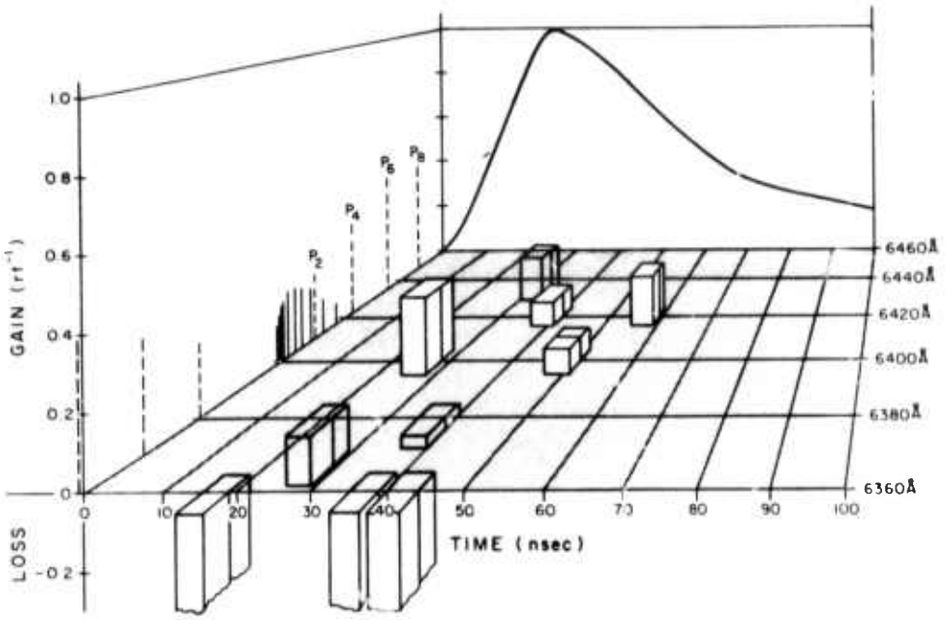

FIG. 2. Fractional gain per round-trip transit of the plasma as a function of wavelength and time for the afterglow of a 3-atm helium discharge. Regions of stimulated emission lie above the xy plane; absorption, below. Across the xz plane to the rear of the data has been plotted the time dependence of the spontaneous emission for scale and on the plane to the left edge is shown the normal emission spectrum of the $3s^3\Sigma_u^+ \rightarrow 2p^3\Pi_g$ transition, uncorrected for broadening mechanisms.

tion of cavity length. Cavities were used in which the mean lifetime of a photon in the cavity considerably exceeded the lifetime of the amplifying medium. For these measurements the dye laser was removed and a dielectric mirror of 99% reflectance at 6400 Å was added. Optics were used having solid angles of acceptance small compared to the solid angle spanned by the forward lobe of the radiation pattern from the cavity. Under these conditions there is no geometric effect and the axial intensity is simply a function of the number of transits of the plasma a photon can make before the plasma decays and the gain or loss occurring during each transit.

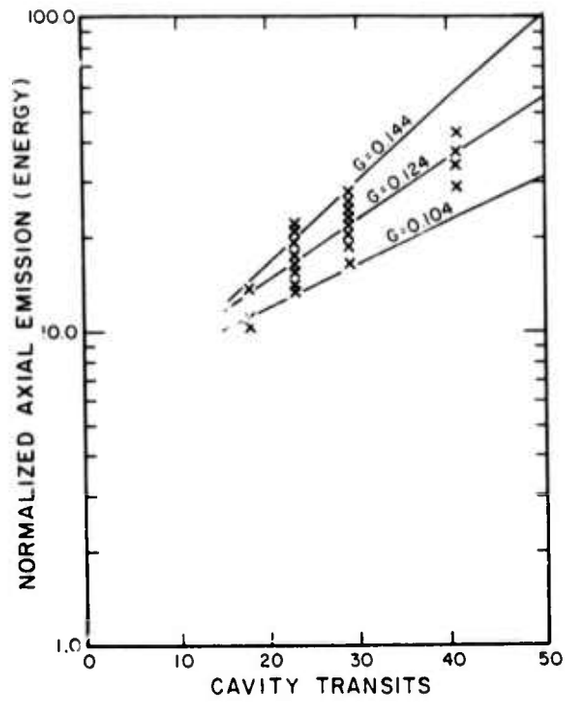

FIG. 3. Functional dependence on the number of round-trip transits of the cavity made by a photon during the lifetime τ of the plasma, of the energy emitted axially per pulse from a resonant cavity enclosing the plasma and normalized to the energy of the spontaneous incoherent radiation. Wavelength was selected by an interference filter centered at 6413 Å with a FWHM of 45 Å and passive cavity losses were 0.03 per round trip. ×—experimental data; solid curves—theoretical models given by Eqs. (1) and (2) for values of fractional gain per round trip of 0.104, 0.124, and 0.144 as marked.

Figure 3 summarizes the resulting energy per pulse emitted axially at 6400 Å and normalized to the isotropic incoherent emission from the afterglow for cavities of four different lengths. The passive loss of the cavity was determined to be 3% per round trip from the exponential decay of the axial intensity following the termination of the afterglow. Shown for comparison are curves modeling the expected growth of pulsed energy from the particular cavity when containing an amplifying medium of 0.104, 0.124, and 0.144 (round-trip)$^{-1}$ peak gain and corrected[6] for a time dependence of the gain proportional to that observed for the spontaneous emission. The best value appears to be 0.124 and corresponds to an average over the 45-Å FWHM bandpass of the 6413-Å interference filter used in the measurement. Comparison with Fig. 2 identifies this as the average gain over the Q branch and lower P components and provides agreement with the higher peak values resolved for certain of those components.

It appears that the stimulated emission observed in this work confirms the importance of the collisionally stabilized recombination mechanism as a source of population inversion of significance to the development of new types of high-energy lasers depending upon electron-beam excitation at high gas densities.

*Research supported by the U. S. Advanced Research Projects Agency of the Department of Defense and monitored by ONR under Contract No. N00014-67-A-0310-0007.

[1]C. B. Collins, A. J. Cunningham, and B. W. Johnson, Abstracts of the 25th Gaseous Electronics Conference, London, Ontario, Canada, 1972, p. 153 (unpublished).
[2]A. J. Cunningham, B. W. Johnson, and C. B. Collins, Phys. Lett. A 45, 473 (1973).
[3]E. Hinnov and J. G. Hirschberg, Phys. Rev. 125, 795 (1962).
[4]J. Berlande, M. Cheret, R. Deloche, A. Gonfalone, and C. Manus, Phys. Rev. A 1, 887 (1970).
[5]C. B. Collins, H. S. Hicks, and W. E. Wells, Phys. Rev. A 2, 797 (1970).
[6]This correction modifies the formula for the total emitted energy ϵ_0 from the value

$$\epsilon_0 \propto I_0 \tau (GN)^{-1} (l^{GN} - 1) , \tag{1}$$

characteristic of a simplified equivalent plasma of constant spontaneous intensity I_0, and gain per round trip, G, both decreasing discontinuously to zero after a lifetime τ, and a lossless cavity of a length allowing N complete transits during the plasma lifetime. The consideration of a time dependence of $\exp(-t/\tau)$ for both I_0 and G, and a passive loss L per round trip introduces a multiplicative correction function

$$F(GN, LN) = (l^{GN} - 1)^{-1} \left(GN + \sum_{m=1}^{\infty} \frac{1}{m+1} \frac{(GN)^{m+1}}{(LN+1)\cdots(LN+m)} \right) , \tag{2}$$

where F is of order unity for small gains and losses.